INFORMATION TO USERS

This manuscript has been reproduced from the microfilm master. UMI films the text directly from the original or copy submitted. Thus, some thesis and dissertation copies are in typewriter face, while others may be from any type of computer printer.

The quality of this reproduction is dependent upon the quality of the copy submitted. Broken or indistinct print, colored or poor quality illustrations and photographs, print bleedthrough, substandard margins, and improper alignment can adversely affect reproduction.

In the unlikely event that the author did not send UMI a complete manuscript and there are missing pages, these will be noted. Also, if unauthorized copyright material had to be removed, a note will indicate the deletion.

Oversize materials (e.g., maps, drawings, charts) are reproduced by sectioning the original, beginning at the upper left-hand corner and continuing from left to right in equal sections with small overlaps. Each original is also photographed in one exposure and is included in reduced form at the back of the book.

Photographs included in the original manuscript have been reproduced xerographically in this copy. Higher quality 6" x 9" black and white photographic prints are available for any photographs or illustrations appearing in this copy for an additional charge. Contact UMI directly to order.

U·M·I
University Microfilms International
A Bell & Howell Information Company
300 North Zeeb Road Ann Arbor MI 48106-1346 USA
313 761-4700 800 521-0600

Order Number 9304658

Photophysical processes and photoinduced electron transfer reactions of tris(2,2′-bipyridine)ruthenium(II) or $Ru(bpy)_3{}^{2+}$ adsorbed onto porous Vycor glass and modified porous Vycor glass

Fan, Jianwei, Ph.D.

City University of New York, 1992

U·M·I
300 N. Zeeb Rd.
Ann Arbor, MI 48106

PHOTOPHYSICAL PROCESSES AND PHOTOINDUCED ELECTRON TRANSFER REACTIONS OF TRIS(2,2'-BIPYRIDINE)RUTHENIUM(II) OR RU(BPY)3 2+ ADSORBED ONTO POROUS VYCOR GLASS AND MODIFIED POROUS VYCOR GLASS

by

JIANWEI FAN

A dissertation submitted to the Graduate Faculty
in Chemistry in partial fulfillment of the
requirements for the degree of Doctor of Philosophy,
The City University of New York.

1992

This manuscript has been read and accepted for the Graduate Faculty in Chemistry in satisfaction of the dissertation requirement for the degree of Doctor of Philosophy.

6|20|92

date

Chairman of Examining Committee

8/20/92

date

Executive Officer

A.D. Baker

Supervisory Committee

The City University of New York

ABSTRACT

Photophysical Processes and Photoinduced Electron Transfer Reactions of Tris(2,2'-bipyridine)ruthenium(II) or Ru(bpy)3 2+ Adsorbed onto Porous Vycor Glass and Modified Porous Vycor Glass

by

Jianwei Fan

Advisor: Professor Harry D. Gafney

In the 5 to 90 °C range, the photophysical and photochemical properties of $Ru(bpy)_3^{2+}$ cation exchanged onto porous Vycor glass, $Ru(bpy)_3^{2+}$(ads), have been investigated and compared with the similar measurements in aqueous solution. In contrast to fluid solution behavior, measurements of emission quantum yield, Φ_{em}, and lifetime, τ, reveal that the Φ_{em}/τ ratio, which is equal to the product of $k_r\eta_{isc}$, declines by 42%. Since spectroscopic data offer no indication that the intrinsic parameters which govern the radiative decay rate constant, k_r, change when temperature changes, the temperature dependence of Φ_{em}/τ ratio is attributed to the intersystem crossing yield, η_{isc}. Fitting the temperature dependent lifetime data for $Ru(bpy)_3^{2+}$(ads) reveals a decay channel through a level lying 1168±160 cm^{-1} above the emissive ^{3}MLCT state. Photochemical evidence indicates that it is another MLCT state, rather than a dd state. The change of

the excited state decay channel is attributed to a "matrix effect", where the rigidity of the glass curtails the molecular vibration required to access the dd state, which is located 3600 cm^{-1} above the emissive state in aqueous solution. As a result, nonradiative decay is thought to occur via the less energy demanding population of the MLCT state. The temperature dependent emission quantum yield data for $Ru(bpy)_3^{2+}$(ads) also reveal a higher energy level located 1117±70 cm^{-1} above the ^{1}MLCT state. Thermal population of this state from the ^{1}MLCT state and subsequent decay to the ground state nonradiatively competes with intersystem crossing to the ^{3}MLCT state. As a result, η_{isc} decreases as temperature increases. The appearance of these additional decay channels is attributed to the reduction of the symmetry of the complex upon the adsorption. Cation exchanging of $Ru(bpy)_3^{2+}$ onto the glass reduces the molecular symmetry from D_3 to C_{2v} or C_s. The negatively charged glass surface differentiates the three equivalent bpy ligands according to their distance from the surface. As a result, it removes the degeneracy of the corresponding metal to ligand change transfer (MLCT) excited states. A model of the excited state dynamics of $Ru(bpy)_3^{2+}$(ads) consistent with both lifetime and emission quantum yield data is presented.

The photoinduced disproportionation of $Ru(bpy)_3^{2+}$(ads) occurs among a fixed array of immobilized adsorbates by means of a mobile photodetached electron. Electron migration on the glass surface is thought to occur via population of surface acceptor sites. One possible surface acceptor site is the surface Lewis acid B_2O_3 sites. The role of these sites has been examined by a selective reaction with NH_3. Photochemical data obtained with NH_3 treated and untreated samples reveal that an equivalent reaction occurs in the presence or absence of NH_3. Measurements of quantum yield as a function of initial loading indicate that the maximum yield in the presence of NH_3 occurs at loading of ca.1.7×10^{-6} moles of $Ru(bpy)_3^{2+}$/g, which corresponds to a separation between the adsorbates of 57 Å. Since this is equivalent to that obtained in the absence of NH_3, the data indicate that the B_2O_3 sites are not involved in the electron migration process. In fact, since the rate of the disproportionation reaction increases in the presence of NH_3, it suggests that the B_2O_3 sites actually hinder electron migration on the glass surface.

ACKNOWLEDGEMENTS

I would like to express my sincere appreciation to my research advisor, Professor Harry D. Gafney, for his assistance and patience in directing this thesis work, and for his support and encouragement which have given me so much confidence and strength in the pursuit of my Ph.D degree.

I would also like to express my gratitude to Professor Richard Pizer, Professor A. D. Baker and Professor Gerald Koeppl for the generous help they have readily provided me over the years. Thanks to Professor Thomas Strekas, Professor Raymond Disch and Professor Jerome Schulman for their beneficial advise and suggestions. Thanks to Steven Tysoe, Edgar Mendoza and other fellow students in my research group for their useful discussions and friendly help during my stay at Queens College.

Most of all, I would like to express my thanks to my dear parents, who have done every thing they can for me ever since I was born, and to my dear husband, who has been so understanding, supportive and self-sacrificing throughout the years of my graduate study.

TABLE OF CONTENTS

EXPERIMENTAL

LIST OF FIGURES

LIST OF TABLES

INTRODUCTION

The photophysics and photochemistry of Ru(II) and Os(II) polypyridine complexes have been the focus of numerous studies during the past twenty years.[1-5] Interest in these complexes stems from both theoretical and practical points of view. Theoretically, their unusual combination of well defined optical absorption, chemical stability, luminescence, and excited state redox properties offers unique insights into the excited state dynamics of transition metal complexes.[2-8] As a result, the complexes have been applied in fields as diverse as photocatalysis, electrochemistry, photoelectrochemistry, chemi-and electrochemi-luminescence, and electron and energy transfer.[9-13] Further, their unique room temperature luminescence and excited state lifetime and redox properties have led to their use as spectroscopic probes of new environments[14-17] and in solar energy conversion.[18-27] $Ru(bpy)_3^{2+}$ (bpy = 2,2'-bipyridine), regarded as the parent ion, has received the most attention and played a key role in the development of this research area.[1-8] Extensive investigations of $Ru(bpy)_3^{2+}$ in aqueous solution have produced a detailed model of its excited state properties, which generally serves as the basis for the analysis of other Ru(II) and Os(II) polypyridine complexes.[8] The light-induced processes for $Ru(bpy)_3^{2+}$ are summarized in Figure 1.[4,5] The species formed by light absorption is a high-energy excited state that must undergo some type of deactivation. Deactivation processes include (a) luminescence, (b) degradation of electronic energy into heat, (c) photochemical reactions leading to the disappearance of the original molecule, and (d) quenching by

Figure 1. Schematic representation of light induced processes of $Ru(bpy)_3^{2+}$.

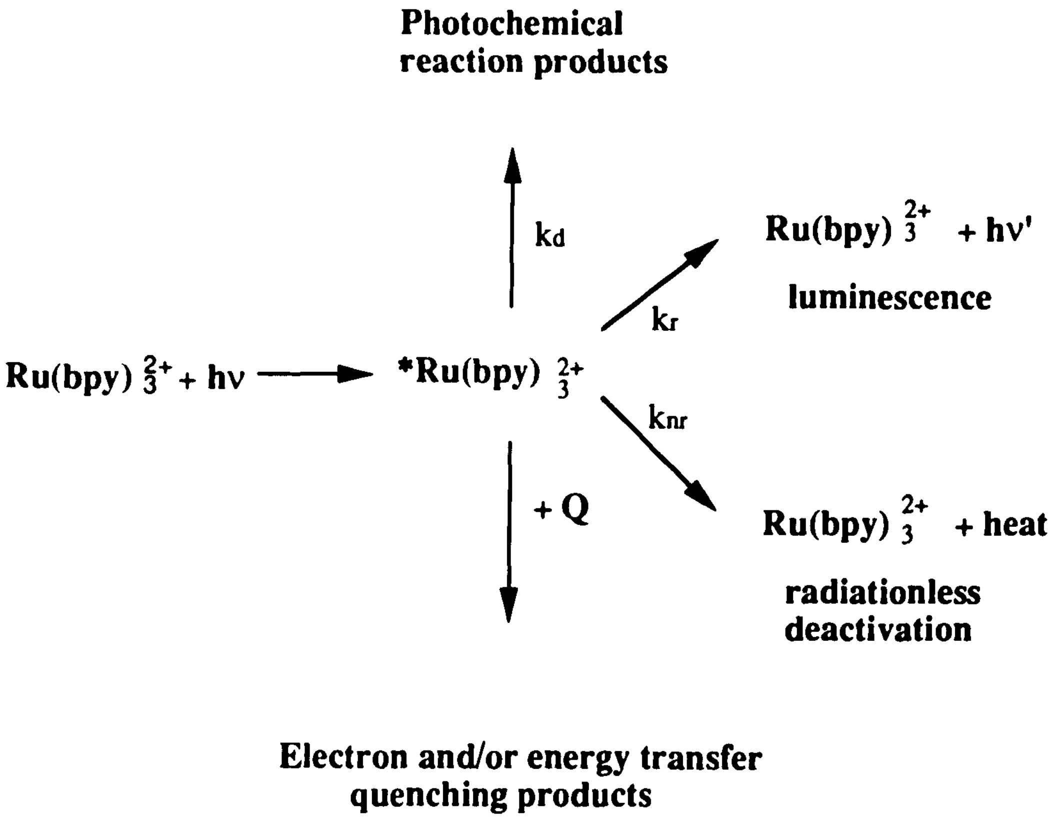
Photochemical reaction products
kd
Ru(bpy) $_3^{2+}$ + hν'
luminescence
kr
Ru(bpy) $_3^{2+}$ + hν
*Ru(bpy) $_3^{2+}$
knr
+ Q
Ru(bpy) $_3^{2+}$ + heat
radiationless deactivation
Electron and/or energy transfer quenching products

other species. The last includes electron- and energy-transfer processes. The following sections will discuss these decay processes in detail from both photophysical and photochemical aspects.

I. Photophysical Processes of Ru(bpy)$_3^{2+}$

(i) Characterization of the Excited States

Ru^{2+} is a d^6 metal ion, while the polypyridine ligands are usually colorless molecules possessing σ-donor orbitals localized on the nitrogen atoms and π donor and π^* acceptor orbitals more or less delocalized on aromatic rings.[3-5] Figure 2 shows a simplified molecular orbital representation of the electronic structure of Ru(bpy)$_3^{2+}$.[3] The molecular symmetry of the complex is D$_3$, but in octahedral microsymmetry, the metal d-orbitals are split into t$_{2g}$ (stabilized) and e$_g$ (destabilized) orbitals, and the ground state is (t$_{2g}$)^6 with $^1A_1$ symmetry. One electron excitation from occupied to empty orbitals can take place in four possible ways: (a) d-->d*, giving rise to metal-centered excited states, (b) d-->π_L*, giving rise to metal-to-ligand charge-transfer MLCT excited states, (c) π_L->d*, giving rise to ligand-to-metal charge-transfer LMCT excited states, and (d) π_L--> π_L*, giving rise to ligand-centered LL excited states. All these states could have both singlet and triplet multiplicity. Figure 3 shows the currently known relative energies of the excited states.[5] In addition, in suitable cases, there can be interactions with the solvent molecules leading to charge transfer to solvent (CTTS) transitions as well.

Figure 2. A simplified molecular orbital representation of the electronic structure of $Ru(bpy)_3^{2+}$.

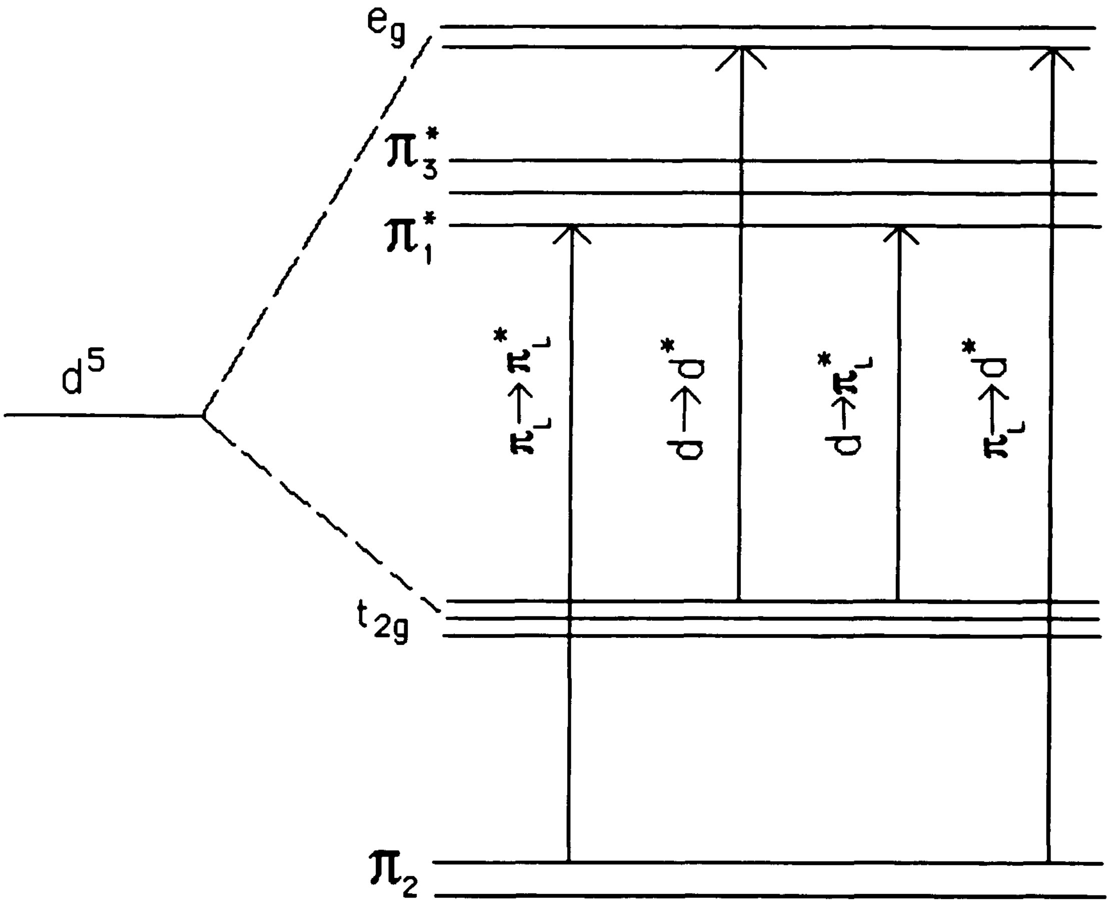
e_g
π_3^*
π_1^*
d^5
$\pi_L \rightarrow \pi_L^*$
$d \rightarrow d^*$
$d \rightarrow \pi_L^*$
$\pi_L \rightarrow d^*$
t_{2g}
π_2

Figure 3. Energy ordering of the excited states of $Ru(bpy)_3^{2+}$.

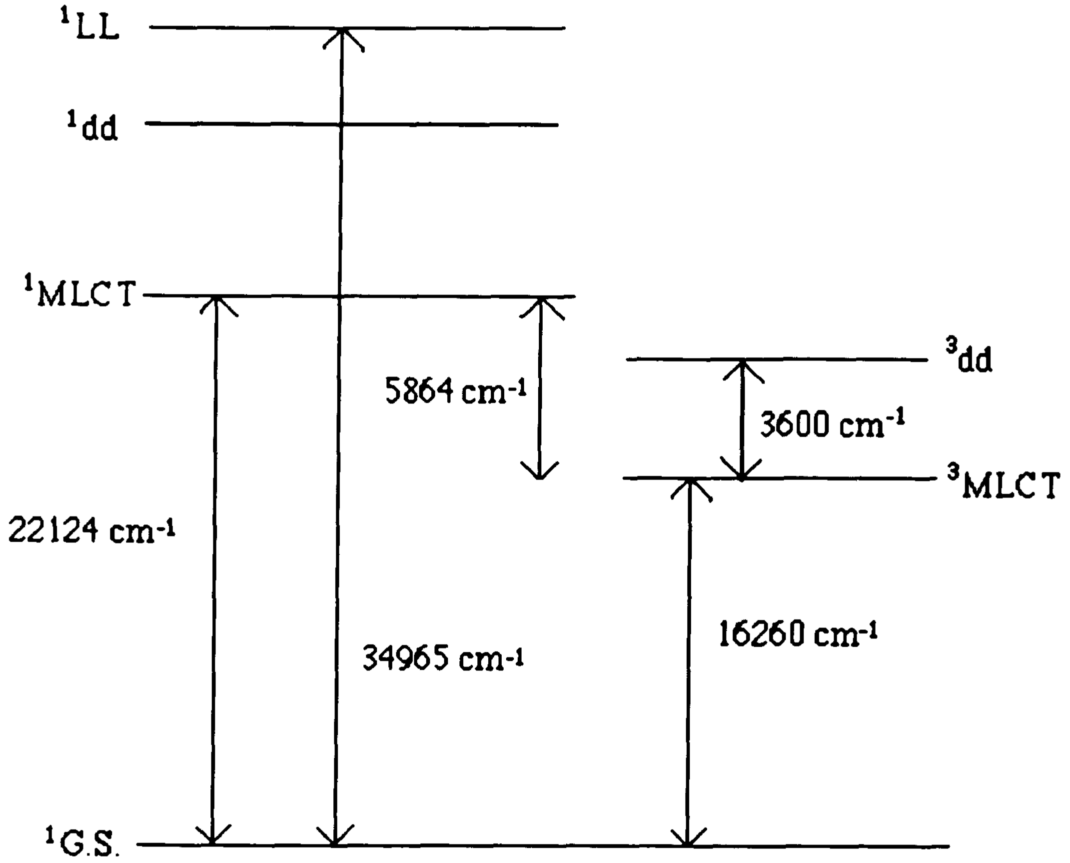

^{1}LL
^{1}dd
^{1}MLCT
^{3}dd
^{3}MLCT
^{1}G.S.
5864 cm^{-1}
3600 cm^{-1}
22124 cm^{-1}
34965 cm^{-1}
16260 cm^{-1}

Figure 4 presents the absorption spectrum of the $Ru(bpy)_3^{2+}$ complex in aqueous solution at room temperature. Indicated therein are the currently accepted assignments of the various absorption bands.[2-5] The intense UV band at 285 nm ($\varepsilon = 87000\ M^{-1}cm^{-1}$) is assigned as a ligand centered LL (π_L-->π_L*) transition by comparison with the spectrum of the protonated bipyridine ligand. In the visible region, the intense band at 452 nm ($\varepsilon = 14600\ M^{-1}cm^{-1}$) is assigned to a MLCT transition (d-->π_L*). The shoulders at 322 nm and 344 nm might be metal centered dd transitions (d-->d*), which give rise to weak (Laporte forbidden) absorption bands (ε = ca.100 $M^{-1}cm^{-1}$). In the long wavelength tail of the absorption spectrum, a shoulder (not shown here) is present at about 550 nm (ε = ca. 600 $M^{-1}cm^{-1}$) in the absorption spectrum of $Ru(bpy)_3^{2+}$ in an ethanol-methanol glass at 77K. This absorption feature is thought to correspond to a spin-forbidden MLCT transition.

On excitation into any of its absorption bands, $Ru(bpy)_3^{2+}$ shows a broad, structureless orange-yellow emission in solution at room temperature with a maximum around 610 nm. In glassy solvents at 77 K, however, the emission band is well resolved with the band origin at 580 nm and a vibrational progression of ca.1350 cm^{-1}, as shown in Figure 5.[4,5]

The orbital nature of the emitting state, long a center of controversy, has now been firmly established to be essentially of a charge transfer type, spin-forbidden in character.[3] However, the spin-orbit interaction is sufficiently strong that the spin labels are only a formal designation. Low temperature luminescence measurements of $Ru(bpy)_3^{2+}$ and $Ru(phen)_3^{2+}$ in

Figure 4. Electronic absorption spectrum of $Ru(bpy)_3^{2+}$ in aqueous solution.

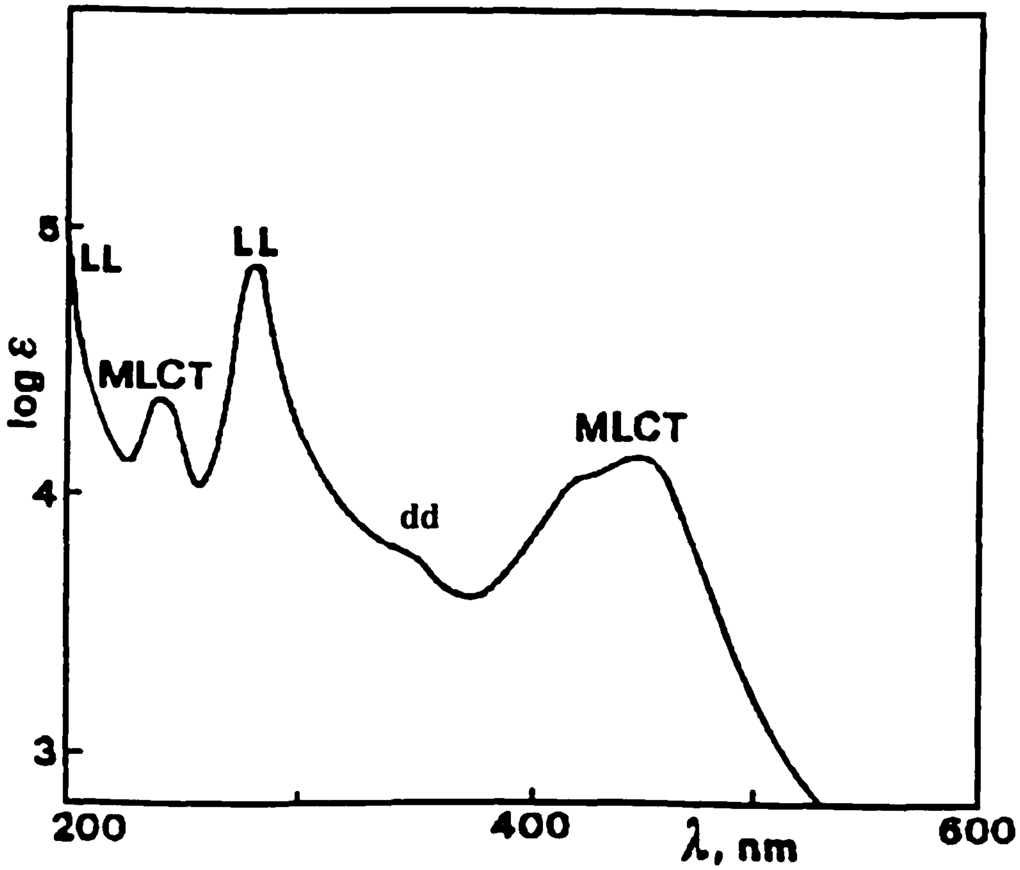
5
4
3
log ε
LL
MLCT
LL
dd
MLCT
200
400
600
λ, nm

Figure 5. Emission spectrum of $Ru(bpy)_3^{2+}$ in alcoholic solution (a) at 77 K; (b) at room temperature.

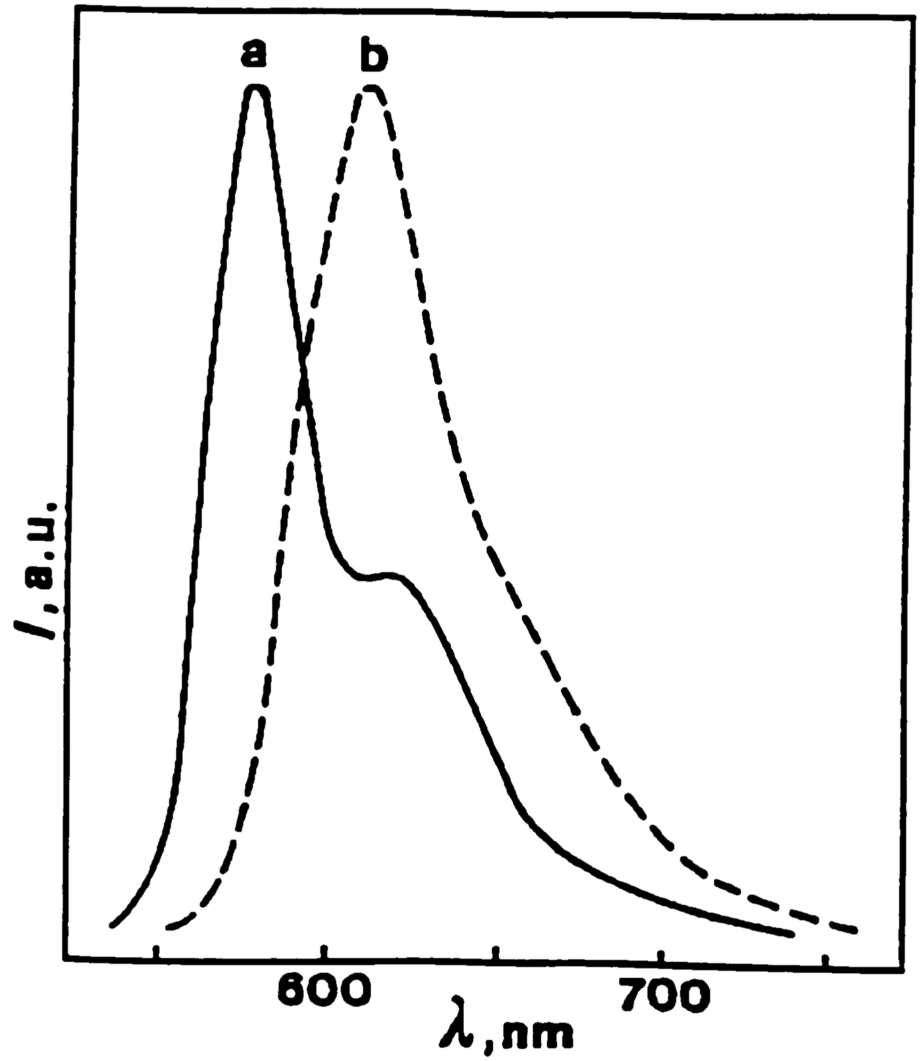
a
b
I, a.u.
600
700
λ, nm

polymethylmethacrylate (PMMA) matrix have established that the emission originates from a manifold of three closely spaced levels.[6,7]

(ii) The Excited State Dynamics

The direct absorption of 452-nm light produces the singlet ^{1}MLCT excited state. The initially produced ^{1}MLCT excited state rapidly undergoes intersystem crossing to the corresponding triplet states, ^{3}MLCT, with a rate constant, k_{isc}, larger than 10^{10} sec^{-1} and an intersystem crossing yield, η_{isc}, of unity.[28] The emissive ^{3}MLCT states decay to ground state via radiative (giving out light) and nonradiative (giving out heat) pathways. Much of the information about the excited state dynamics has been derived from temperature dependent luminescence lifetime and quantum yield measurements. Based on these measurements, several models have been presented to explain the excited state dynamics of $Ru(bpy)_3^{2+}$ within different temperature ranges.

(1) Low Temperature Model - Crosby's Model

In the low temperature range (2-77K), luminescence lifetimes, τ, and quantum yields, Φ_{em}, of $Ru(bpy)_3^{2+}$, $Ru(phen)_3^{2+}$ and their derivatives in polymethylmethacrylate (PMM) matrix were measured by Crosby and coworkers.[6,7] To explain the temperature dependence, these investigators presented a phenomenological model[7] based on the following physical assumptions: (a) The luminescence in these D_3 complexes is a superposition of the emissions of three closely spaced electronic levels; (b) Each of the sublevels is capable of coupling with the ground state either radiatively or nonradiatively, and these pathways are controlled by first order kinetics with associated rate constants k_r and k_{nr} which are independent of temperature; (c) Boltzmann equilibrium is established and maintained in time domains much shorter than the characteristic lifetimes of any of the sublevels, and the observed temperature dependence of lifetime and emission quantum yield is due to the variation of the population distribution among these states at different temperatures.

It was found that the temperature dependence of Φ_{em} and τ, between 2 to 77 K, could be fit very well by this three-level model, which gives the following two analytical expressions for Φ_{em} and τ, respectively[7]

$$\tau = (1 + 2\,e^{-\Delta E_1/kT} + e^{-\Delta E_2/kT})/(k_1 + 2\,k_2\,e^{-\Delta E_1/kT} + k_3\,e^{-\Delta E_2/kT}) \qquad [1]$$

$$\Phi_{em} = (k_{1r} + 2\,k_{2r}\,e^{-\Delta E_1/kT} + k_{3r}\,e^{-\Delta E_2/kT})/(k_1 + 2\,k_2\,e^{-\Delta E_1/kT} + k_3\,e^{-\Delta E_2/kT}) \qquad [2]$$

where k_i and k_{ir} represent the rate constants for total decay and radiative decay from ith level, respectively, and ΔE_i represents the energy separation between ith state (i>1) and the lowest state. These parameters are depicted in Figure 6, and their values were obtained from a simultaneous computer fit of both τ and Φ_{em} equations to the measured data points.[6,7] The energy differences generated from the fitting are ca.10 and 60 cm^{-1}, respectively (Figure 6).

A model based on group theoretical considerations was also proposed

Figure 6. Schematic diagram of three emitting charge transfer states of $Ru(bpy)_3^{2+}$. k_{ir}: rate constant of radiative decay (—>); k_{inr}: rate constant of nonradiative decay (⇝) of the ith level to ground state.

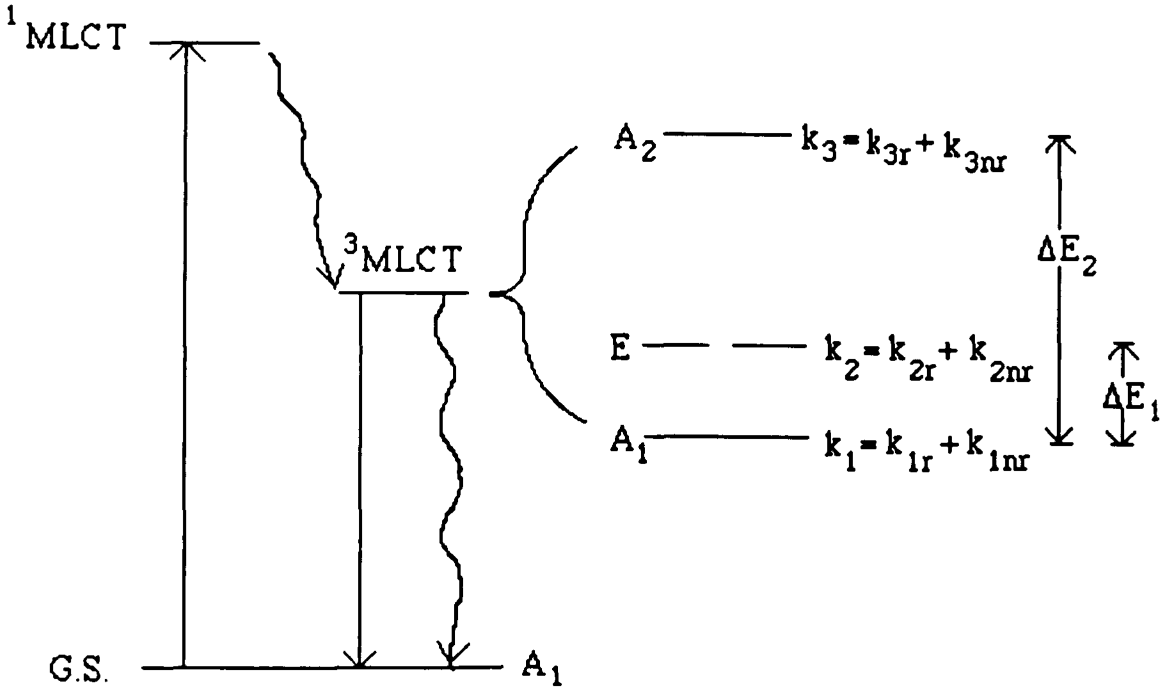
^{1}MLCT
^{3}MLCT
G.S.
A_1
A_2
E
A_1
$k_3 = k_{3r} + k_{3nr}$
$k_2 = k_{2r} + k_{2nr}$
$k_1 = k_{1r} + k_{1nr}$
ΔE_2
ΔE_1

by Crosby and coworker to rationalize the measured data.[29] This model treats the luminescent excited state in terms of a $4d^5$ Ru core and three bpy ligands with one transferred electron in the lowest antibonding $\pi*$ orbital of the coupled ligands, which belong to the a_2 representation in the D_3 point group. This model allows the assignment of the symmetry of the manifold of states with A_1, E and A_2 in order of increasing energy (Figure 6).

Recently there has been some debate about the above model which treated the symmetry of the emissive excited state as D_3. Considerable evidence suggests that, in the emissive MLCT state, the transferred electron is localized on one of the three bpy ligands, rather than delocalized throughout the ring systems of the three equivalent ligands. This was originally proposed by Hipps to account for the observed emission polarization ratio which far exceeds the possible value for a D_3 symmetry molecule.[30] Other experimental evidence comes from EPR[31] and flash photolysis studies.[32] Excited state resonance Raman spectroscopy studies later provided the most direct evidence for the localized model. These studies showed that, in the emissive MLCT state, the complex is best described as $*Ru(bpy)_2(bpy^-)^{2+}$.[33,34] However, more recent studies of time resolved luminescence and magnetic circular polarized luminescence suggest that charge localization in the excited state is not an intrinsic property of the complex but is induced by solvent relaxation processes, or environmentally induced localization.[35-38] Such a conclusion is consistent with the results derived from polarized emission studies[39] on single-crystal $[Ru(bpy)_3](PF_6)_2$

as well as from time-resolved resonance Raman spectroscopy.[40]

(2) Aqueous Solution Model-Van Houten-Watts' Model

The temperature dependence of emission quantum yield and lifetime of $Ru(bpy)_3^{2+}$ in aqueous solution between 0 to 100 °C has been measured by Van Houten and Watts.[8] However, since kT is much larger than the energy difference between the three emissive states (~ 61 cm^{-1}) in this temperature range, an invariant thermal equilibrium distribution among the three states in the luminescence manifold is achieved. In other words, the 0-100 °C temperature range is in the high-temperature limit of the Crosby three-level model,[7] and very little temperature dependence can be predicted from it. Therefore, Van Houten and Watts have proposed another model in which a new decay channel is introduced.[8] In this model, three emissive ^{3}MLCT states are treated as an average state which decays via three pathways: the temperature independent radiative and nonradiative pathways, and a thermal population of a higher energy, metal-centered, dd manifold with the dd state subsequently undergoing nonradiative decay or ligand loss photochemistry. It is the population of this dd state that causes the observed temperature dependence of luminescence.

The model presented by Watts and Van Houten is described in Figure 7. According to this model, the following expressions can be derived for Φ_{em} and τ, respectively[8]

Figure 7. Schematic representation of Watts' model used to interpret the temperature dependence of the luminescence lifetime and quantum yield of $Ru(bpy)_3^{2+}$ in aqueous solution between 0 and 100 °C.

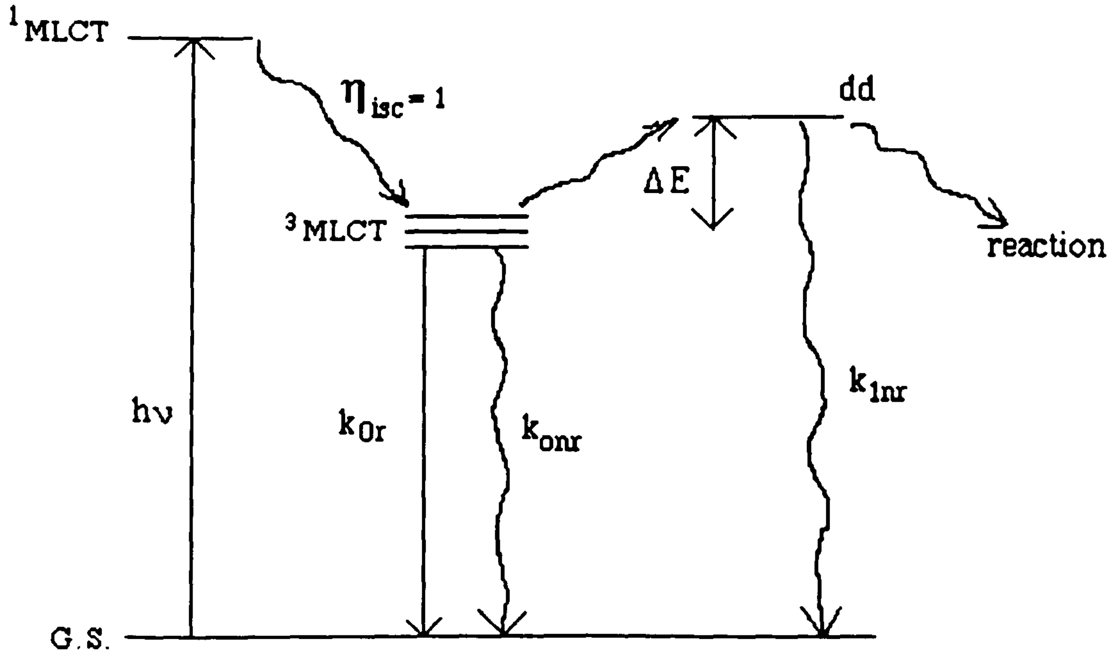
^{1}MLCT
$\eta_{isc}=1$
dd
^{3}MLCT
ΔE
reaction
hν
k_{0r}
k_{onr}
k_{1nr}
G.S.

$$\tau = (k_{0r} + k_{0nr} + k_{1nr}e^{-\Delta E/kT})^{-1} \qquad [3]$$

$$\Phi_{em} = k_{0r}\tau \qquad [4]$$

where k_{0r} and k_{0nr} are the Boltzmann-averaged values of the radiative and nonradiative decay rate constants from the three lower lying ^{3}MLCT states. ΔE is the energy difference between the dd state and the ^{3}MLCT manifold, and k_{1nr} represents the rate constant of the sum of all photophysical and photochemical radiationless processes from dd state.

The values of these kinetic parameters are obtained from a simultaneous computer fit of both τ and Φ_{em} equations to the measured data points. The dd state is found to lie ca. 3600 cm^{-1} above the ^{3}MLCT manifold. Since kT is only ~ 300 cm^{-1} at room temperature, a relative small Boltzmann population of this level is predicted. Nevertheless, the unfavorable Boltzmann factor is offset by the extremely large value of the decay rate constant from this level (~10^{13} s^{-1}), which is roughly seven orders of magnitude larger than the nonratiative decay rate constant from ^{3}MLCT states (~10^6 s^{-1}). Thus, although the steady-state population of this level is extremely small, 90%-95% of the excited state energy is dissipated through this pathway at 100 °C.

The complex is photoinert at room temperature; however, the photolabilization of a bpy ligand in water solution is observed at high temperature in 0.1 M HCl with 436-nm irradiation[8]

$$Ru(bpy)_3^{2+} \xrightarrow[H^+]{h\nu} [Ru(bpy)_2(H_2O)_2]^{2+} + Hbpy^+ \qquad [5]$$

It is believed that the population of dd state at high temperature is responsible for the observed photolabilization reaction.

Solvents can also influence luminescence decay process. Although the radiative decay rate constant is not very sensitive to the nature of the solvent,[41] the nonradiative decay which involves energy transfer to solvent molecules depends strongly on the viscosity of the solvent and the efficiency of vibrational coupling of the solvent molecules to the complex.[41-44] The latter can be illustrated by the isotope effect on the emission quantum yield and lifetime observed for $Ru(bpy)_3^{2+}$.[8] The larger values of lifetime and quantum yield obtained in deaerated D_2O solution at room temperature (1020 ns and 0.07 respectively) than in deaerated H_2O solution (600 ns and 0.042 respectively) indicate a slower non-radiative deactivation due to the relatively inefficient coupling between D_2O and the complex.

In summary, the excited state dynamics of $Ru(bpy)_3^{2+}$ in aqueous solution[8], as well as in other fluid solutions[44], can be described by following scheme, Scheme 1

$$
\begin{array}{llll}
G.S. & \text{----->} & {}^1MLCT & \text{(absorption)} \\
{}^1MLCT & \text{----->} & {}^3MLCT & \text{(intersystem crossing)} \\
{}^3MLCT & \text{----->} & G.S. + h\nu & \text{(emission)} \\
{}^3MLCT & \text{----->} & G.S. + heat & \text{(nonradiative decay)}
\end{array}
$$

^{3}MLCT -----> ^{3}dd (thermal activated internal conversion)
^{3}dd -----> G.S.+ heat (nonradiative decay)
^{3}dd -----> photoproducts (photoinduced ligand labilization)

(3) Wider Temperature Ranges

(a) Phase Transition

Over much wider temperature ranges, phase transition of the solvent affects the $Ru(bpy)_3^{2+}$ decay dynamics. The temperature dependence of the luminescence decay of $Ru(bpy)_3^{2+}$ in propionitrile/butyronitrile solution between 77-333 K is shown in Figure 8.[4,5] The essential features are (a) an Arrhenius-type behavior of the luminescence decay in the rigid glass region (84-100 K), (b) a discontinuity in the glass-fluid transition region (~100-150 K), (c) an Arrhenius-type behavior in the 150-250 K temperature range with essentially the same parameters (same slope) as in the rigid glass; and (d) another steeper Arrhenius-type region for $T > 250$ K. This complex behavior is accounted for by following equation[4]

$$1/\tau = k_0' + B/[\,1+e^{-C(1/T-1/T_B)}\,] + A_1\,e^{-\Delta E_1/kT} + A_2\,e^{-\Delta E_2/kT} \qquad [6]$$

where k_0' is a temperature-independent term, which represents the total decay rate constants from the lowest emissive ^{3}MLCT state. The second term empirically accounts for the behavior in the glass-fluid transition region, while the two exponential terms account for the Arrhenius behavior at low

Figure 8. Temperature dependence of emission lifetime for $Ru(bpy)_3^{2+}$ in propionitrile/butyronitrile solution.

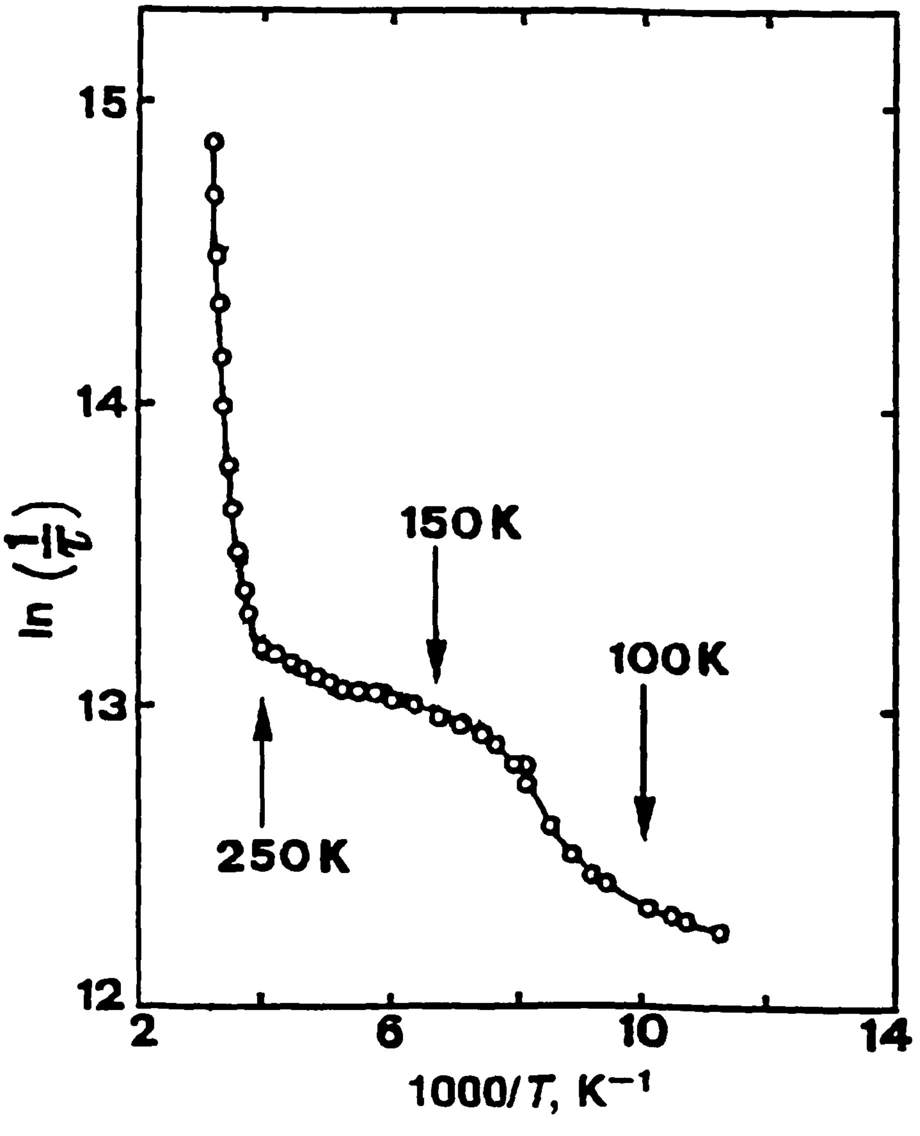
15
14
13
12
ln $\left(\frac{1}{\tau}\right)$
150 K
100 K
250 K
2
6
10
14
1000/T, K^{-1}

and high temperatures.

In the glass region ($T \leq 100$ K), the temperature dependence originates from the thermal equilibrium between three ^{3}MLCT states (~ 60 cm^{-1}). When the matrix melts, large amplitude (low-frequency) vibrational modes come into play which enhance the rate of radiationless deactivation processes with a consequent decrease in excited state lifetime. Once the glass is completely melted, the slightly activated Arrhenius behavior continues because the emission always originates from the same cluster of ^{3}MLCT excited states. At higher temperature, the dd excited state which lies about 3600 cm^{-1} above the emitting levels becomes accessible and very fast radiationless decay occurs through this level.

(b) Kemp's Model

If the experimental temperature is above the phase transition point, Equation 6 becomes[45]

$$1/\tau = k_0 + A_1\, e^{-\Delta E_1/kT} + A_2\, e^{-\Delta E_2/kT} \qquad [7]$$

where again, k_0 is the total decay rate constant from the lowest emissive ^{3}MLCT state. ΔE_1 is the energy gap between the lowest and highest ^{3}MLCT states, and ΔE_2 is the activation barrier for thermal activation from the highest ^{3}MLCT state to the dd state. Kemp and coworkers measured the lifetime of $Ru(bpy)_3^{2+}$ adsorbed onto a cellulose acetate film between 77-333 K, and in organic solvents, such as EtOH, CH_3CN, DMSO and DMF, between

220-400 K. They found that their data were better fit with this two-exponential equation than with the Watts equation (equation 3).[45] Obviously, this equation is a combination of both Crosby's and Watts' models[7,8], which describe the excited state behavior at low and high temperatures, respectively. When the experimental temperature range is wide enough to cover both temperature ranges, Kemp's two-exponential equation[45] is superior to Watts' equation[8], while at room temperature, equations 3 and 7 are equivalent to each other.

In different solvents, the values of kinetic parameters for equation 7, generated from lifetime data fitting, fall in the following ranges: $\Delta E_1 \leq 148$ cm^{-1}, $\Delta E_2 = 3300$ cm^{-1} - 4100 cm^{-1}, and $A_2 = 10^{12}$-10^{14} sec^{-1}.[45] ΔE_2 and A_2 can be explained as the activation energy of population of dd state, and the total decay rate constant from dd state, respectively. However, large reductions in the values of ΔE_2 and A_2 are obtained for $Ru(bpy)_3^{2+}$ on cellulose acetate films, where it is found that $\Delta E_2 = 800$ cm^{-1}, and A_2 is 10^7 sec^{-1}.[45]

(4) Evidence for Participation of Another MLCT State

Although Scheme 1 is very successful in explaining the excited state dynamics of $Ru(bpy)_3^{2+}$ and most of the other Ru(II) polypyridyl complexes in fluid solution, more and more experimental evidence suggests that the combination of a series of three low-lying MLCT states and a thermally activated MLCT --> dd transition is not adequate to account for the temperature dependence in all cases.[46] For polypyridyl complexes of Os(II) in fluid solution,[47,48] for a few mixed chelate complexes of Ru(II) in fluid solution,[49-51] and for Ru(II) complexes in rigid matrices at ambient temperature,[45] although the temperature-dependent lifetime data can be adequately fit by equation 3 or its short form [46]

$$\tau = (k_0 + k_1 e^{-\Delta E/kT})^{-1} \qquad [8]$$

the kinetic parameters obtained from the fits are very different from values that are typically found for the MLCT to dd state conversion. A typical activation barrier for a thermally activated MLCT --> dd transition, ΔE, is within 2500-4500 cm^{-1}, and the nonradiative decay rate constant k_1 from the dd state is within 10^{12}-10^{14} s^{-1}. For these three situations mentioned above, the typical kinetic parameters are ΔE = 300-800 cm^{-1} and k_1 = 10^6-10^8 s^{-1}.[46] An example is $Ru(bpy)_3^{2+}$ incorporated onto cellulose acetate film, as mentioned above.[45] Furthermore, ligand loss photochemistry which occurs via the population of the dd state is not observed for these systems. Based on this information, Meyer and coworkers suggested that the temperature dependence in these systems arises from a thermal population of an additional MLCT state, not a dd state.[46] Direct evidence for such a state occurs in the polarized emission spectra of $[Ru(bpy)_3](PF_6)_2$ single crystals, where a low lying MLCT state, designated $2A_2'$, lies 650±130 cm^{-1} above the lowest energy E' state.[39]

It has been suggested that for those systems which show quite different values of ΔE and k_1, dd states are not thermally accessible even at room temperature.[46] Typically, dd states in complexes of Os(II) lie 30% higher in energy than in their Ru analogues,[52] and the lowest dd state for $Os(bpy)_3^{2+}$ is expected to lie ~ 21000 cm^{-1} above the ground state. Since emission from $Os(bpy)_3^{2+*}$ occurs at 13500 cm^{-1}, it can be predicted that a large energy gap should exist between the MLCT and dd states for Os(II). The values of kinetic decay parameters observed for $Os(bpy)_3^{2+}$ in ethanol/methanol solution ($\Delta E = 312\ cm^{-1}$ and $k_1 = 7.2x10^7\ s^{-1}$) are consistent with the population of another MLCT state, not a dd state.[46]

The effect of substituents on the ligands is also important. An example is $Ru(bpy)_2(dhcb)^{2+}$(dhcb=4,4'-dicarboxy-2,2'-bipyridine), where the electron-withdrawing 4,4'-dicarboxylic acid substituents lower the energies of the π^*-(4,4'-$(CO_2)_2$-bpy) acceptor levels. This ligand becomes the acceptor ligand, and the resulting MLCT excited state is sufficiently stabilized that dd states are not thermally accessible at room temperature. The kinetic decay parameters observed for this complex also correspond to the population of another MLCT state.[46]

In a rigid medium, the appearance of "matrix effects" is also important. When the complexes are adsorbed onto a cellulose acetate film, the rigidity of the matrix curtails the molecular distortions required to access the dd manifold. As a result, nonradiative decay in the more rigid medium is thought to occur via the less energy demanding population of the MLCT state.[46]

(5) Temperature Dependence of Φ_{em}/τ Ratio

Among all the models described above, only those of Crosby (2 - 77 K) and Watts (0 - 100 °C) give both expressions for emission quantum yield and lifetime as functions of temperature.[7,8] In fact, because the emissive ^{3}MLCT state(s) is not populated by absorption directly (spin forbidden), the emission quantum yield also depends on the intersystem crossing yield η_{isc}, which determines the population of the emissive state from relaxation of a higher energy singlet state[4,42], i.e.,

$$\Phi_{em} = \eta_{isc} k_r \tau \qquad [9]$$

Based on the invariance of the luminescent quantum yield with wavelength for $Ru(bpy)_3^{2+}$ at 77 K and room temperature, Demas and Crosby assumed that the efficiency of populating the emissive ^{3}MLCT states from photoinduced ^{1}MLCT states, η_{isc}, is unity and temperature independent.[28b] This is generally accepted to be true for many Ru(II) and Os(II) polypyridyl complexes[2-8,53] and is implied in both models described above.

As a consequence, both models predict that the ratio of Φ_{em}/τ is equal to k_r, assuming $\eta_{isc} = 1$ in equation 9. k_r represents the total radiative decay from three emissive states. By its nature, an individual radiative decay rate constant is temperature independent. However, the total radiative decay rate constant may change with temperature due to the change of population among these three emissive states. This can be predicted from Crosby's low temperature model (equations 1 and 2). However, as long as the temperature exceeds the high temperature limit of Crosy's model (2-77 K), an invariant population distribution among these three emissive states is achieved. As a result, k_r is reasonably treated as an average radiative decay rate constant from three emissive states. k_r is temperature independent, and the ratio of Φ_{em}/τ is also temperature independent. Thus, Watts' model, which treats k_r as an average radiative decay rate constant, requires the ratio of Φ_{em}/τ to be temperature independent.

In H_2O and D_2O solutions, at temperatures between 0 and 100 °C, the measured ratio of Φ_{em}/τ for $Ru(bpy)_3^{2+}$ does not vary with temperature.[8] However some mixed-ligand complexes of Ru(II) show that the measured ratio of Φ_{em}/τ is temperature dependent, although the experimental temperature is above the high temperature limit of Crosby's model. The emission lifetimes and quantum yields of $Ru(bpy)_2(diaz)^{2+}$ (diaz = 4,5-diazafluorene), for example, suggest that Φ_{em}/τ ratio approximately doubles as temperature rises from ca. 200 K to 236 K.[54] Nakamura reports that this ratio for $Ru(bpy)_2(dmby)^{2+}$ (dmby = 3,3'-dimethyl-2,2'-bipyridine) at 77K is ca. 10^2 times larger than that at 298 K, and he attributed it to η_{isc} rather than to k_r.[55] Also, for the compounds $Ru(bpy)_2(diaz)^{2+}$, $Ru(bpy)_2(py)_2^{2+}$ and $[Ru(bpy)_2NPP]^+$ (NPP = 4-nitro-2-(2-pyridyl)phenyl), the activation energies obtained from emission intensity measurements are different from those obtained from lifetime measurements when Watts' equation is used to fit the data.[54,56] It seems that Watts' model is no longer suitable for all these situations. The contradiction is due to the temperature dependence of Φ_{em}/τ, or more likely, due to the temperature dependence of η_{isc}. However, although the intersystem crossing yield is a key parameter in the complexes photoredox properties, relatively little quantitative information is currently available, since the concurrent measurements of both lifetime and emission quantum yields are not as common as only lifetime measurements in studies of Ru(II) and Os(II) polypyridyl complexes.

II. Photochemical Processes of $Ru(bpy)_3^{2+}$

Numerous studies during the past twenty years have established the excited state redox chemistry of $Ru(bpy)_3^{2+}$ in fluid solution.[2-4,57-60] Figure 9 shows the free energy changes associated with excited state electron transfer to form $Ru(bpy)_3^{3+}$ and $Ru(bpy)_3^{+}$. The emitting MLCT state lies 2.08 eV above the ground state. While the ground state of $Ru(bpy)_3^{2+}$ is thermodynamically stable with respect to either oxidation or reduction, the excited state, being 0.84 eV and 0.77 eV higher in energy than $Ru(bpy)_3^{3+}$ and $Ru(bpy)_3^{+}$ respectively, is both a powerful oxidant and a strong reductant. Since the excited state lifetime is also long enough to participate in bimolecular processes, it can be used as either an oxidant or a reductant depending on the properties of the other reactants.

In addition to its rich photoredox chemistry, $^*Ru(bpy)_3^{2+}$ sensitizes the formation of triplet excited states of inorganic and organic molecules via the process of energy transfer.[61-63] Thus, with an external reagent, there are

Figure 9. Free energy diagram for the deactivation of the luminescent excited state of $Ru(bpy)_3^{2+}$ to the ground state via $Ru(bpy)_3^{+}$ or $Ru(bpy)_3^{3+}$.

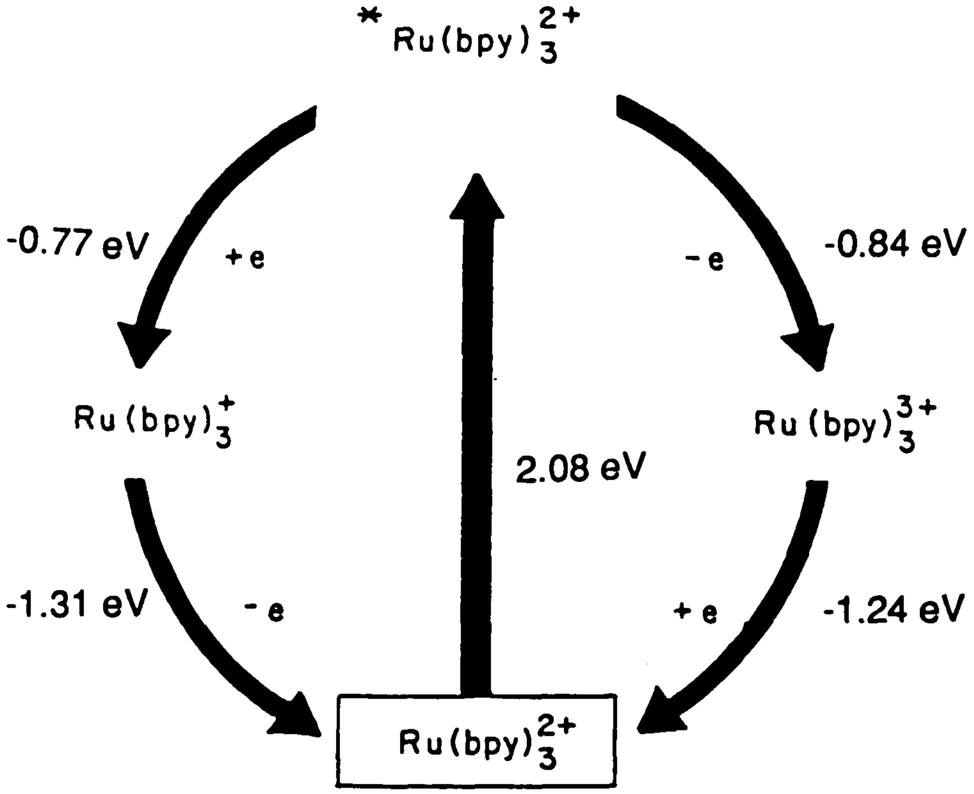

FREE ENERGY DIAGRAM

three possible means for excited state decay in bimolecular reactions

(a) Oxidative quenching in which the excited state acts as a reductant

$$*Ru(bpy)_3^{2+} + Q \text{------>} Ru(bpy)_3^{3+} + Q^- \qquad [10]$$

(b) Reductive quenching in which the excited state acts as an oxidant

$$*Ru(bpy)_3^{2+} + Q \text{------>} Ru(bpy)_3^{+} + Q^+ \qquad [11]$$

(c) Energy transfer quenching in which the excited state acts as an energy donor

$$*Ru(bpy)_3^{2+} + Q \text{------>} Ru(bpy)_3^{2+} + *Q \qquad [12]$$

The actual quenching mechanism operative for a particular quencher is determined by both thermodynamic and kinetic factors. Thermodynamically, the ability to undergo energy transfer quenching is directly related to the 0-0 spectroscopic energy levels (spectral overlap) of the donor-acceptor pair, while that for electron transfer quenching is related to the redox potentials. The kinetic factors are associated with the activation energy needed to reorganize the inner and outer shells before electron/energy transfer takes place. More than one mechanism may be operative simultaneously.

Many inorganic species quench $*Ru(bpy)_3^{2+}$ via electron or energy transfer reaction.[2-4] For example, the metal ions Fe^{3+}, Cu^{2+}, Tl^{3+}, quench the excited state oxidatively[3,64-66], whereas Eu^{2+}, $Fe(CN)_6^{4-}$ and $Mo(CN)_8^{4-}$ quench the excited state reductively.[63] On the other hand, Cr^{3+} quenches

$^{*}Ru(bpy)_3^{2+}$ by an energy transfer mechanism, as evidenced by the occurrence of an emission characteristic of the excited state Cr^{3+}.[67]

Quenching of $^{*}Ru(bpy)_3^{2+}$ by organic compounds has also been extensively studied.[2-4] Oxidative quenching by N,N'- dimethyl 4,4' -bipyridinium ion (abbreviated as MV^{2+}) has received considerable attention due to the role it plays as an electron relay between $^{*}Ru(bpy)_3^{2+}$ and a catalyst in light induced H_2 evolution from water[68-74]

$$^{*}Ru(bpy)_3^{2+} + MV^{2+} \text{----->} Ru(bpy)_3^{3+} + MV^{+} \qquad [13]$$

$$MV^{+} + H_2O \text{----->} MV^{2+} + H_2 \qquad [14]$$

However, despite of the high quenching rate constant of MV^{2+}, and suitable redox potentials (MV^{2+} / MV^{+} = - 0.43 V, and H_2O/H_2 = -0.41 V), water is not reduced to H_2 in a simple $Ru(bpy)_3^{2+}/MV^{2+}$/catalyst three component system. This is due to the rapid thermal back reaction that follows photoinduced electron transfer:

$$Ru(bpy)_3^{3+} + MV^{+} \text{----->} Ru(bpy)_3^{2+} + MV^{2+} \qquad [15]$$

The driving force for the reduction of $Ru(bpy)_3^{3+}$ and the oxidation of $Ru(bpy)_3^{+}$ are 1.24 eV and 1.31 eV, respectively, exceeding the corresponding driving force of the photo-driven electron transfer from the excited state, 0.84 eV and 0.77 eV (Figure 9). Consequently, good quenchers and good reducing agents for water reduction do not necessarily lead to good yield of photoproducts. To date, hydrogen generation from water has only been observed in the presence of a fourth component, i.e., an external electron donor, such as EDTA, that irreversibly reduces $Ru(bpy)_3^{3+}$ to $Ru(bpy)_3^{2+}$ competitively with the back reaction.[3] However, use of such sacrificial components makes cyclic water splitting, at present, economically unfeasible.

Preventing the energy-wasting, thermal back reaction, therefore, has becomes the focal point of solar energy conversion research. Consequently, research during the past decade has focussed on imposing some constraint that would allow charge separation to be competitive with an exergonic back reaction.[75] One approach is the use of heterogeneous media. The approach follows nature where many biological reactions, including photosynthesis, occur in, and to a significant extent are a consequence of the heterogeneity of the system.[76] Correspondingly, much research during the past decade has focussed on the use of heterogeneous media to organize the reaction system so that the photosensitizer, the electron donor and acceptor, and other necessary components are assembled in ways that facilitate the photo-driven electron transfer while the thermal back reaction is retarded by physical and/or energetic barriers.[75]

III. $Ru(bpy)_3^{2+}$ Redox Chemistry in Heterogeneous Media

The photophysical and photochemical properties of $Ru(bpy)_3^{2+}$ in a variety of heterogeneous media have been extensively studied.[14,15,75-110] The heterogeneous media include organic, polymeric and inorganic substrates. Typical examples of organic systems include micelles, vesicles, microemulsions, and ion exchange resins. Polymers such as synthetic cellulose, Nafion membranes, and polymethylmethacralate have been studied. Numerous inorganic materials, particularly hydroxylated silicas, layered silicates (clay minerals), zeolites, metal oxides and semiconductor materials, have attracted much recent attention as media for $Ru(bpy)_3^{2+}$ based photoredox processes.

Semiconductor supports, including TiO_2, SnO_2, WO_3 and CdS, improve charge separation by electron injection into a bulk conduction band.[106-114] These semiconductive materials have band gap energies and redox potentials suitable for direct participation in the electron transfer processes. The most popular system in this category consists of a TiO_2 colloidal suspension. When $Ru(bpy)_3^{2+}$ is introduced into the solution, visible light irradiation leads to electron transfer from the complex to the conduction band of the semiconductor particles. The electron trapped in the particle can then be "tunneled" to a catalyst doped on the particle, which in turn reduces water to molecular hydrogen.[110-113] In this case, the separation of the photoproducts is achieved by the potential barrier at the water/semiconductor interface.

In the absence of an accessible conduction band, rigidity and topology are the advantages of solid supports.[75] In these systems, where population of a bulk conduction band is energetically unlikely, the increase in the lifetime of the charge-separated state appears to be the result of the order imposed by the rigid medium.[108-109] Utilizing these characteristics to promote a specific behavior, however, requires an understanding of the nature of microstructure and microenvironment. Surface characteristics, such as the nature and density of the surface functionalities and surface charge, determine the mechanism of adsorption, and, in turn, the spectral and photophysical properties of the adsorbate. In cases where adsorbate mobility is curtailed, the adsorbent defines an adsorbate array, and adsorbent topology and porosity determine access to the photoexcited adsorbate. Regardless of the specific nature of the support, the active region is the surface and the adjacent interface with the surrounding medium.[103] Consequently, the study of a photoexcited adsorbate is as much a study of the adsorbent surface as it is a study of the photophysics and photochemistry of the adsorbate.[103] Certainly in this case, the underlying strategy is to take advantage of the properties of a solid support to impose some control, principally kinetic, on a $Ru(bpy)_3^{2+}$-based reaction system. Yet the properties that differentiate a solid support from fluid solution, i.e. those properties that one is attempting to exploit, arise from the same properties that create the experimental difficulties. With many solids, the number of atoms, typically 10^{23} /cm^3, their close spacing, and the resulting band structure, limit optical transparency.[114] Support opacity is an experimental handicap since much of our understanding of the excited states of Ru(II) diimines, particularly their photoredox properties, arises from their spectroscopic visibility.[75]

IV. Porous Vycor Glass as a Medium for Photoredox Processes

(i) Porous Vycor Glass

In the late 1970's, this laboratory began to explore the use of Corning's code 7930 porous Vycor glass (PVG) as a reaction medium. PVG is a 96% SiO_2, 3% B_2O_3 and 1% Al_2O_3 and Na_2O glass. It is prepared by acid leaching of a borosilicate glass, resulting in an open pore structure of 100±10 Å[115] cavities randomly connected in a three dimensional array throughout the entire glass. It is transparent with 50% T at 295 nm vs. air. The surface area is 183±15 $m^2 g^{-1}$, and the void volume, i.e. the volume of the cavities relative to the total sample volume, is about 30%. A summary of the characteristics of PVG is presented in Table 1.

Our interest in PVG stems from its unique combination of rigidity, transparency and porosity. Transparency offers spectroscopic access, and in turn, an amenability to optical spectroscopy and fast reaction techniques. Porosity offers chemical access; access not only in the sense of intercepting an excited adsorbate within the glass, but also in the chemical sense of utilizing the rigidity and topology of the glass surface to assemble a photochemical reaction site. In addition, it is chemically and thermally stable and possesses sufficient mechanical strength to permit experiments under varied conditions.

Diffuse reflectance FTIR (DFTIR) spectra of the calcined (550°C) glasses reveal a surface composed of free, 3744 cm^{-1}, and associated, 3655

Table 1. The properties of porous Vycor glass (code 7930)

Composition	SiO_2 96% B_2O_3 3%
Density	1.5 g/cm^3
Void space	28% total volume
Average pore size	100±10 Å
Internal surface area	183±15 m^2/g
Transparency	> 295 nm

cm^{-1}, silanol groups.[116-118] The zeta potential of PVG in water, -26 mV, indicates an anionic surface relative to the bulk solvent,[119] and the adsorption of acid-base indicators reveals a surface pH of 4-5.[120] In both surface functionality and potential, PVG resembles silica gel,[116,121,122] but one difference should be noted. Because of its method of preparation, PVG, unlike silica gel, possesses surface B_2O_3 Lewis acid sites.[116] The number of these sites depends on the extent of acid leaching, but some estimates suggest that as much as one-third of the surface could be B_2O_3.[123]

(ii) Results of Previous Studies

(1) Adsorption and Distribution of the Complex

Like other hydroxylated silicas, PVG acts as a cation exchanger. Earlier studies in this laboratory[110,124,125] have established that cationic complexes, such as $Ru(bpy)_3^{2+}$, displace the slightly acidic silanol protons and adsorb onto the glass without coadsorption of the counter-anions. Neutral complexes physisorb onto the glass, but anionic complexes are electrostatically repelled from the surface.

PVG offers two surfaces for adsorption; the outermost surfaces of the glass and the surface of the interconnected 100±10 Å diameter cavities. Despite the availability of silanol groups throughout the glass and the relative large pore diameter, conventional solution impregnation techniques do not yield a uniform distribution of $Ru(bpy)_3^{2+}$ amongst these surfaces. It was found that $Ru(bpy)_3^{2+}$ is distributed preferentially on the outer surfaces, but not throughout the interior of the glass due to the narrower tortuous pathways which connect the pores. However, optical density measurements establish a uniform distribution of the complex in the impregnated volume defined by the area of a particular side and the penetration depth. Emission polarization measurements establish the immobility of the complex on the surface.[110]

(2) Photophysical Measurements

The UV-visible absorption spectrum $Ru(bpy)_3^{2+}$ adsorbed onto PVG, designated $Ru(bpy)_3^{2+}$(ads), is close to that of the complex in aqueous solution in band maxima and relative extinction coefficients. The resonance Raman (RR) spectrum shows that adsorption does not change the positions of the seven bipyridine vibration modes resonant with the 452-nm MLCT excitation, but does reduce the intensity of the prominent band at 1492 cm^{-1}. RR frequency is a ground state property, whereas intensity is related to the distortion of the excited state structure relative to that of the ground state. The excited state properties of $Ru(bpy)_3^{2+}$(ads) are further clarified by emission spectroscopy. Although the emission spectrum of the adsorbed complex is close to that in water solution in band maximum and band shape, the emission decay patterns are different in the two media. In aqueous solution, the decay is a single exponential, while on PVG with high intensity excitation, a non-exponental decay is found which shows that a fast component precedes a slower component. The measured emission lifetime τ

and quantum yield Φ_{em} for $Ru(bpy)_3^{2+}(ads)$ at room temperature are all higher than those in aqueous solution. Moreover, the temperature dependence of Φ_{em} indicated that Φ_{em} of the adsorbed complex is more sensitive to temperature than in aqueous solution.

(3) Photochemical Reactions

(a) Quenching

Energetically, the excited state chemistry accessible on the glass is equivalent to that in fluid solution. However, emission polarization and macroscopic distribution measurements establish that $Ru(bpy)_3^{2+}(ads)$ is immobilized on the glass surface. The absence of adsorbate mobility distinguishes this from homogeneous fluid solution.

Quenching of the excited complex adsorbed onto PVG by the gases N_2O, SO_2, and O_2 has been examined.[125] The quenching pattern involves static or dynamic quenching, and the process that dominates depends on whether the quencher adsorbs strongly or weakly on the PVG surface. The weakly adsorbed N_2O quenches the emission by an almost purely dynamic process, whereas the more strongly adsorbed SO_2 and O_2 show mostly static quenching.

Emission quenching of $Ru(bpy)_3^{2+}$ on PVG by coadsorbed Cr^{3+}, Cu^{2+}, Fe^{2+} and MV^{2+} was examined[110] and the rates of quenching are considerably slower than those in aqueous solutions. The reduction was attributed to the curtailed mobility of the reagents on the PVG surface.

(b) Photoredox Chemistry

While quenching experiments focus on the formation of the donor-quencher pair, photoredox experiments focus on charge separation. Photoinduced disproportionation of $Ru(bpy)_3^{2+}$ on PVG has been studied and compared with that in aqueous solution.[124] As in aqueous solution, the reaction proceeds via a mechanism that involves a biphotonic ionization of $Ru(bpy)_3^{2+}$. The photodetached electron then reduces another $Ru(bpy)_3^{2+}$, i.e.,

$$Ru(bpy)_3^{2+} \xrightarrow{2\,h\nu} Ru(bpy)_3^{3+} + e^- \qquad [16]$$

$$e^- + Ru(bpy)_3^{2+} \longrightarrow [Ru(bpy)_2(bpy^-)]^+ \qquad [17]$$

$$2Ru(bpy)_3^{2+} \xrightarrow{2\,h\nu} Ru(bpy)_3^{3+} + [Ru(bpy)_2(bpy^-)]^+ \qquad [18]$$

Although the reaction mechanisms in these two media are similar, the stability of the photoproducts is surprisingly different. The reduced complex, $[Ru(bpy)_2(bpy^-)]^+$, generated by radiolysis or UV photolysis in aqueous solution has lifetimes from 2 ms to 3s.[127,128] In contrast, $[Ru(bpy)_2(bpy^-)]^+$ generated on PVG can persist for days in the absence of air. The result is even more significant if one considers that the driving force of the back reaction between $[Ru(bpy)_2(bpy^-)]^+$ and $Ru(bpy)_3^{3+}$, 2.5 eV, is the largest that will be encountered in an $Ru(bpy)_3^{2+}$-photoinduced electron-transfer reaction.

UV-visible and EPR spectra prove the formation of the photoproducts.[124] Emission polarization and macroscopic mobility measurements indicate the photolysis converts a fixed array of immobilized reactants into a fixed array of immobilized products.[110] Flash photolysis studies reveal that the transient intermediate is a photodetached electron.[124] Furthermore, the dependence of quantum yield of the product, $[Ru(bpy)_2(bpy^-)]^+$, upon the concentration of the adsorbates, or the mean separation between the adsorbants on glass, indicates that the maximum yield occurs when the mean separation is ca. 50 Å and approaches 0 when the mean separation is ≤ 13 Å.[124] The former distance is in excellent agreement with the distance of electron migration on PVG,[129,130] while the latter distance corresponds to the contact distance between two adsorbent molecules.[124] These results suggest that, on PVG, the photodriven electron transfer occurs between a fixed array of adsorbed reactants. The photodetached electron from the excited $Ru(bpy)_3^{2+}$ molecule can, when mediated by the PVG surface, migrate over a distance of 50 Å to reduce another $Ru(bpy)_3^{2+}$. On the other hand, the thermally activated back electron transfer can only take place when the distance between the reacting molecules is < 13 Å. The unusual stability of the photoproducts in PVG seems to arise from two critical conditions: a) the $Ru(bpy)_3^{2+}$ complex must be immobilized on the surface and b) the distance between the complex molecules must be beyond that of the thermal electron transfer (13 Å), but within that of the photodriven electron transfer (50±10 Å).

Since the band gap, 6.9 eV in SiO_2, as well as the absence of lifetime or intensity quenching when the complex is adsorbed into the support preclude direct electron injection into a bulk conduction band, a surface conduction model has been proposed where electron conduction is thought to involve the population of intermediate surface acceptor sites. These sites are thought to be shallow energy wells from which the electron can be thermally activated but present an energy barrier to prevent immediate recombination. The temperature dependence of the quantum yield of $[Ru(bpy)_2(bpy^-)]^+$(ads) formation suggest that the average depth of the surface acceptor site(s) is $\leq$ 6.87 + 0.11 kcal/mol.[126]

(iii) Objectives of This Study

(1) Temperature Dependence Measurements

Although the absorption and resonance Raman spectra established that the ground state of $Ru(bpy)_3^{2+}$(ads) is equivalent to that in aqueous solution, previous measurements clearly reveal changes in the excited state properties of $Ru(bpy)_3^{2+}$(ads) as evidenced by the decrease in the intensity in the resonance Raman spectrum, as well as emission decay measurements.[110] For example, the measured τ and Φ_{em} for $Ru(bpy)_3^{2+}$(ads) at room temperature are all larger than those in water solution, and the calculated ratio of Φ_{em}/τ

for $Ru(bpy)_3^{2+}$(ads) is 1.5±0.2x10^5 s^{-1} at room temperature,[110] while in aqueous solution, it is 0.7±0.1x10^5 s^{-1}.[8] Since $\Phi_{em}/\tau = k_r\eta_{isc}$, it means that the product of $k_r\eta_{isc}$ differs between two media.

Obviously, the excited state properties of $Ru(bpy)_3^{2+}$(ads) deserve more investigation. Much of the understanding of the excited states dynamics derives from the temperature dependence of emission quantum yield and lifetime. In H_2O and D_2O solution, between 5 to 90 °C, the temperature dependent lifetime and quantum yield data were fit very well with Watts' equation, and the fitting generated the values of all kinetic parameters.[8] Therefore, similar experiments were carried out with $Ru(bpy)_3^{2+}$(ads). The emission quantum yields and luminescent lifetimes of $Ru(bpy)_3^{2+}$(ads) were determined between 5 to 90 °C with different surface coverage. The absorption and emission spectra of $Ru(bpy)_3^{2+}$(ads) were also examined as a function of temperature. Although diffusional separation of photoproducts is more limited on the glass surface, photoinduced ligand loss can occur since the coordinatively unsaturated metal can react with either the silanol groups or chemisorbed water. Consequently, the quantum yield of ligand labilization for $Ru(bpy)_3^{2+}$(ads) was determined at high temperature to provide additional information about the excited state. For comparison, equivalent measurements were also done with degassed aqueous solutions of the complex over the same temperature range.

Based on these measurements, computer modeling of the measured temperature dependence of τ and Φ_{em} were carried out to provide a theoretical explanation about the excited state dynamics of $Ru(bpy)_3^{2+}$ on PVG.

(2) Photoinduced Electron Transfer on PVG

Previous experiments firmly established that photoinduced disproportionation on this glass occurs within a fixed array of immobilized reactants by means of mobile photodetached electrons.[124] Although these electrons can migrate ca. 50 Å on the surface, it seems they are not actually free before they reduce another adsorbed molecule. The fact that the appearance of the product, $[Ru(bpy)_2(bpy^-)]^+$, occurs 3 to 4 μs after excitation implies that a significant number of electrons must reside on some surface acceptor sites for a finite period of time. The nature of these surface acceptor sites is not known, but they are thought to be shallow energy wells from which the electron can be thermally activated but, nevertheless, present an energy barrier to prevent immediate recombination.[124]

Experiments described here were undertaken in an attempt to identify these surface acceptor sites. One possibility is the surface Lewis acid sites. PVG is 96% SiO_2, 3%B_2O_3 and 1% Al_2O_3. Because of the method of manufacture of the glass, however, some estimates indicate that as much as 33% of the surface may be B_2O_3.[123] Their number and Lewis acid character suggest that they could act as electron acceptors, but in forming a radical species, would remain sufficiently reactive to liberate an electron on thermal activation.

Loss of the Lewis acid character, however, would affect their electron acceptor properties. Consequently, their role in the electron transport process was examined by selectively reacting these sites with NH_3. NH_3 is found to be adsorbed on the glass by physisorption and chemisorption.[116] The physisorbed NH_3 is formed via H-bonding, and can be removed from the surface under vacuum, while the chemisorbed NH_3 is formed via the coordination of its lone electron pair to surface Lewis acid, i.e., B_2O_3, and can not be removed under vacuum until 200 °C.[116] To examine the role of the B_2O_3 sites, a series of glass samples with different loadings of $Ru(bpy)_3^{2+}$ was exposed to NH_3 and then evacuated according to the procedures described by Cant and Little.[116] Photolysis was carried out with NH_3-treated samples, and compared with the untreated samples. The quantum yields of disproportionation were measured as a function of surface loading for NH_3-treated samples in order to examine the effect of binding surface B_2O_3 sites with NH_3 on the electron migration distance on the surface.

EXPERIMENTAL

I. Materials

$[Ru(bpy)_3]Cl_2$ was prepared according to the method of Palmer and Piper,[131] and twice recrystallized from distilled water as the chloride salt. Aqueous solutions of the complex were prepared with distilled water. Absorption, emission and resonance Raman spectra of the complex in aqueous solution agreed with published spectra,[2-5,34] and the FTIR spectrum of the crystalline complex also agreed with published spectra.[132-134] NH_3 gas was obtained from Linde company and used without further purification since it had a purity of $\geq 99\%$.

Code 7930 porous Vycor glass (PVG) was obtained from Corning Inc. in the form of 25mm x 25mm x 2mm polished plates. Pieces of PVG were continuously extracted first with acetone for 12 hours, and then with distilled water for 24 hours, with a change to fresh distilled water after 12 hours. The extracted pieces were then dried under reduced pressure ($P \sim 0.1$ torr) in a vacuum oven at 30 °C. Drying at 30 °C under reduced pressure is to remove the water incorporated during extraction, which is crucial to prevent cracking during subsequent calcination. Removal of the entrapped water is visually apparent; as water evaporation occurs, the glass first turns a translucent white and eventually returns to its transparent form upon loss of the incorporated water. Consequently, the glass samples were kept in the vacuum oven until they became transparent. This always required at least 24 hours and in some cases longer times. Upon removal of the incorporated water, the glass samples were calcined at 650 °C in a muffle furnace for at least 72 hours and stored at that temperature until needed.

Crushed PVG was obtained by grinding cleaned samples of PVG with a mortar and pestle. The glass particles, ranging from 250 to 1000 microns in diameter, were sized with standard sieves.

II. Sample Preparation

(i) Impregnation

Samples of PVG were impregnated with $Ru(bpy)_3^{2+}$ by solution adsorption techniques. The impregnating solutions were aqueous solutions of $Ru(bpy)_3Cl_2.6H_2O$, $1x10^{-5}$ M to $1x10^{-4}$ M. Typically, one to three clean PVG plates were weighed and mounted upright in an Eastman Kodak Chromagram Developing Jar, and 50 mL of the impregnating solution was added. The amount of complex adsorbed was determined spectroscopically by periodically recording the UV-visible spectrum of the impregnating solution. Samples were exposed to the impregnating solutions for times ranging from several hours to two days depending on the desired loading of the glass. The samples were then removed from the solution and rinsed with water to prevent a layering of the adsorbate on the glass surface. The solvent incorporated during impregnation was then removed by pumping under vacuum ($\leq 1\text{x}10^{-5}$ torr) at room temperature for at least 12 hours. Under these conditions, weighing the samples before and after impregnation and drying showed that ≥ 99.99% of the water incorporated during impregnation was removed.[124]

The amount of $Ru(bpy)_3^{2+}$ adsorbed onto the PVG sample was calculated from the change in absorbance of the impregnating solution at 452-nm. The number of moles of the compound absorbed, n_{ads}, was obtained from the relationship

$$n_{ads} = [(A_i - A_f)/A_i] \times n_i \qquad [19]$$

where A is the absorbance at 452-nm. The subscripts i and f denote the absorbance before and after impregnation, and n_i is the number of moles of adsorbate in the solution prior to impregnation. Dividing n_{ads} by the weight of the calcined glass yields the number of moles adsorbed per gram of PVG. Typically, samples used in these experiments weighed 1.5-2.0 g, and loading levels, which ranged from $1\text{x } 10^{-7}$ to $1\text{x } 10^{-6}$ moles of $Ru(bpy)_3^{2+}$/g of PVG, were found to be suitable for the physical measurements (see below).

For photoinduced disproportionation measurements, a wider range of loadings from $1\text{x}10^{-8}$-$2\text{x}10^{-5}$ moles of $Ru(bpy)_3^{2+}$/g of PVG were required. Although loadings of $\leq 1\text{x}10^{-6}$ moles of $Ru(bpy)_3^{2+}$/g of PVG correspond to a surface coverage of ≤1%, increasing the amount of complex adsorbed was difficult and extremely slow; often requiring exposure times on the order of weeks. A more convenient means of obtaining loadings $\geq 10^{-5}$ moles of $Ru(bpy)_3^{2+}$/g of PVG was to take advantage of the rapid movement of the impregnating solution through the dry glass,[110,124] i.e., impregnate, dry and reimpregnate the same sample. After the first impregnation, the sample was dried under vacuum at room temperature to remove the incorporated solvent, and then immersed again in the same or a fresh impregnating solution. The cycle was repeated until the desired loading of the glass was reached. However, the amount adsorbed declines with each exposure so that the highest loading in these experiments, 2.5×10^{-5} moles of $Ru(bpy)_3^{2+}$/g of PVG, required five exposures to the impregnating solution, and still took more than 10 days to complete. More concentrated initial solutions ($\sim 10^{-3}$ M) were also used for impregnation, but in this case, their absorbances at 452-nm were so high that the absorbance at 500-nm was used to calculate the moles of $Ru(bpy)_3^{2+}$ adsorbed onto glass.

To impregnate the powdered glass samples, a minimal amount of a $Ru(bpy)_3^{2+}$ solution, typically 1×10^{-3} M, was added to a pre-weighed amount of powdered PVG ($< 250\ \mu$). The solution and powdered glass were kept in a coverd flask until the impregnating solution became colorless. At that point, the solvent was removed under vacuum. The loading level was about 10^{-6} moles of $Ru(bpy)_3^{2+}$/g of powder PVG, assuming that all of the solute was adsorbed by the glass.

(ii) Mounting of Impregnated Samples in Cells

Impregnated glass particles were placed in a thin quartz tube equipped with a vacuum stopcock (Figure 10) for low temperature emission and for EPR measurements. Measurements between 273 K and 368 K were carried out with the dry, evacuated, impregnated plates. For absorption and emission lifetime measurements, the plates were cut to a 25mm x 9mm x 2mm size and rigidly mounted in an upright position with a Teflon holder in a 40mm x 10mm x 10mm quartz cell (Figure 11). For emission intensity measurements, which were very sensitive to the position of the sample in the emission spectrometer, it was necessary to use thin 25mm x 9mm x 1mm impregnated plates, and mount the impregnated samples in a 40mm x 10mm x 2mm quartz cell. The quartz cell was evacuated to $P \leq 10^{-5}$ torr (see below), and then mounted in a thermostated cell holder machined to the dimensions of the quartz cell (Figure 12). The tight fit of the sample in the cell, and the cell in the cell holder reduced the repositioning error to ≤ 2% (see below).

(iii) Degassing

Since O_2 strongly adsorbs onto the glass and quenches the excited complex,[125] and since the amount adsorbed declines with increasing temperature, its presence would introduce a systematic error in the observed temperature dependence. Therefore, the cells containing either the impregnated plates or glass particles were maintained under a dynamic vacuum ($\leq 1 \times 10^{-5}$ torr) at room temperature for at least 12 hours prior to measurement. Aqueous solutions of the complex, which were used as a

Figure 10. PVG particles are mounted in a thin quartz tube equipped with a vacuum stopcock.

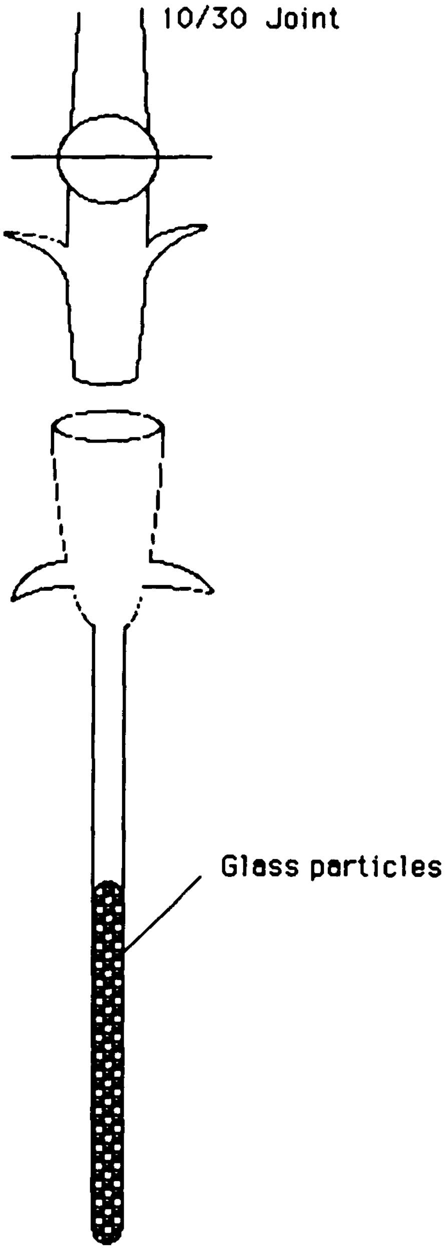
10/30 Joint
Glass particles

Figure 11. A PVG plate is rigidly mounted in a 1-cm square cell with a Teflon holder.

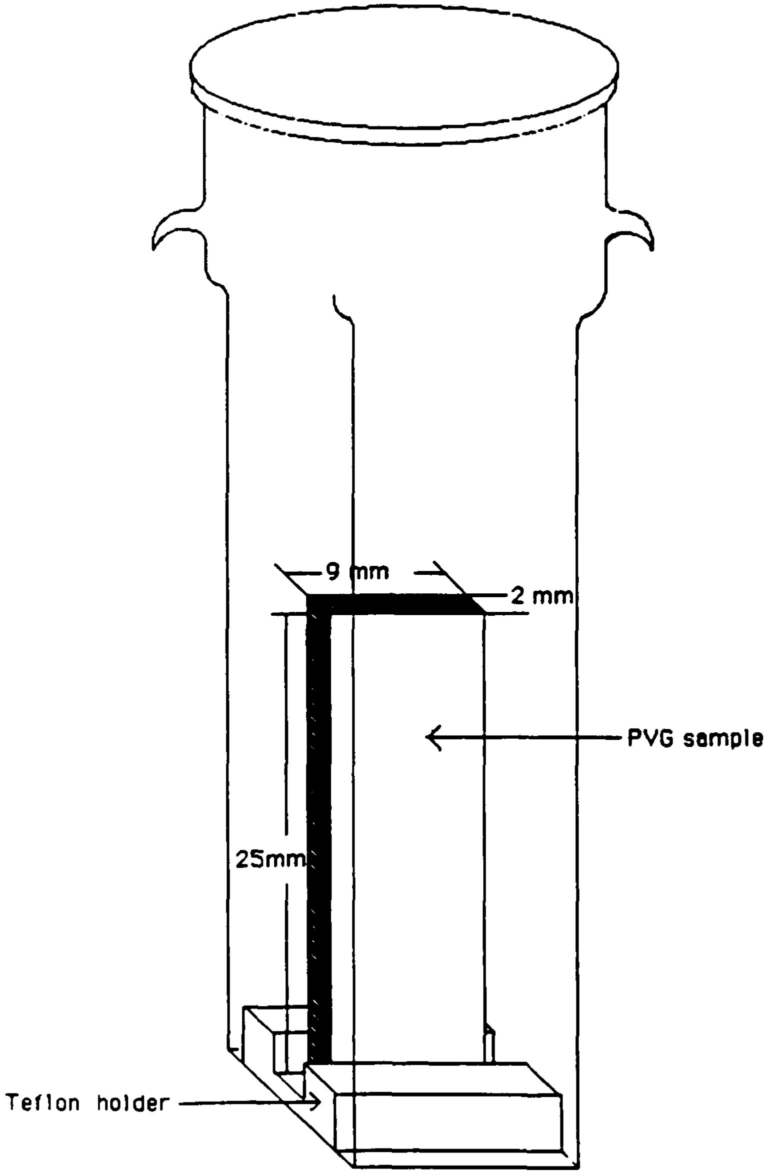
9 mm
2 mm
PVG sample
25mm
Teflon holder

Figure 12. A thermostatted cell holder designed for measuring emission intensity from the front surface of the samples.

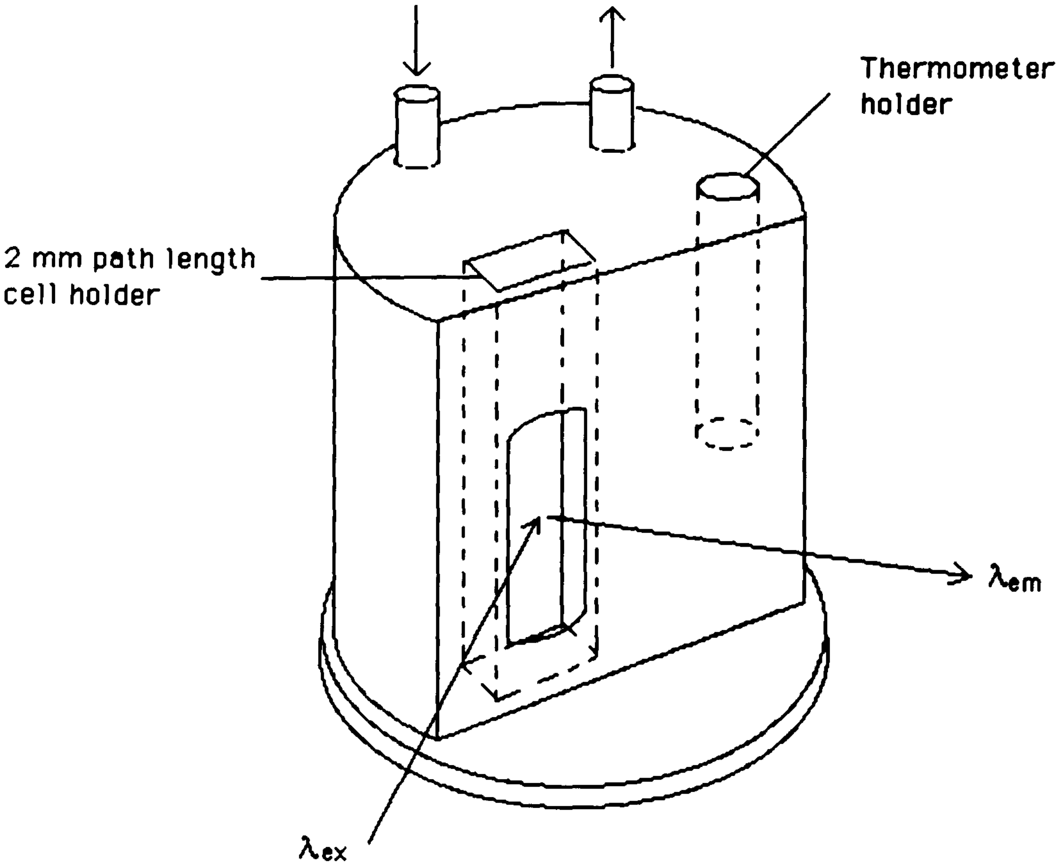
Thermometer holder
2 mm path length cell holder
λ_{em}
λ_{ex}

reference for the glass samples, were degassed by at least three freeze-pump-thaw cycles prior to measurements.

(iv) NH_3 Adsorption.

To selectively react NH_3 with B_2O_3 Lewis acid sites on the surface of PVG, the procedures described by Cant and Little were used.[116] Impregnated or blank samples, in either powdered or plate form, were mounted in the cells (Figures 10 and 11) and evacuated to $\leq 1 \times 10^{-5}$ torr. NH_3 gas (Linde) was expended into a 250 ml bulb to a pressure of about 1 atm. The bulb was closed off, and the line was evacuated. The bulb was then opened and NH_3 was allowed to expand into the line and over the samples. After a 30 minute exposure to the sample, the bulb was shut off and the cell and line were evacuated to a pressure of 10^{-5} torr for at least four hours to remove gas phase NH_3 and physisorbed NH_3 on the glass surface.

III. Physical Measurements

(i) Electronic Absorption Spectra

UV-visible spectra were recorded on an Aviv Model 14DS spectrophotometer. Spectra of the impregnated samples were recorded relative to a clean piece of PVG, which was used as a reference to compensate for absorption and scattering of light by the glass itself. The absorption spectra at different temperatures were obtained by placing the sample cell in the Haake Model FK-2 constant temperature bath for half an hour and then quickly transferring the cell to the sample compartment and recording the spectra immediately.

(ii) Steady State Emission

(1) Emission Spectra

Emission spectra were recorded on a Perkin-Elmer Hitachi MPF-2A emission spectrophotometer equipped with a red-sensitive Hamamatsa R818 photomultiplier, and a thermostatted cell holder. All samples were excited with 450-nm light, and emission intensity was monitored at 90° to the excitation axis. To record the emission spectra at different temperatures, the 1-cm square thermostatted cell holder was connected to the Haake constant temperature bath described above. Degassed aqueous solutions of the complex were contained in 1-cm quartz cells, while the impregnated PVG samples were rigidly mounted in 1-cm quartz cells with Teflon holder and emission was monitored from the edge of the samples (Figure 13).

The emission spectra of the impregnated samples were also measured at 77K. Impregnated glass particles were placed in the quartz tube (Figure 10) and degassed, and then immersed in a standard low temperature emission Dewar filled with liquid nitrogen. A separate cell holder was used to hold the Dewar in the sample compartment.

(2) Quantitating Emission Intensity

Figure 13. An illustration of the conventional sample positions in emission spectrometer (a) Aqueous solution, and (b) Impregnated glass plate.

(a)

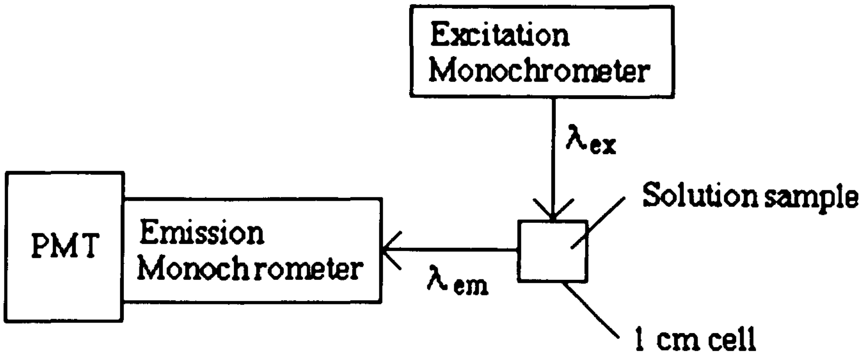
Excitation Monochrometer
λex
Solution sample
PMT
Emission Monochrometer
λem
1 cm cell

(b)

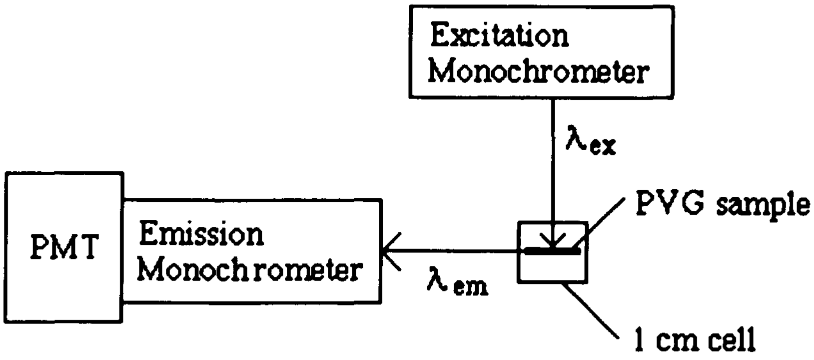
Excitation Monochrometer
λex
PVG sample
PMT
Emission Monochrometer
λem
1 cm cell

To obtain the temperature dependence of emission quantum yields from 273 to 373 K (see Results section), emission intensities of degassed aqueous solutions and impregnated glass samples were initially measured with the emission spectrometer equipped with a 1-cm square thermostatted cell holder connected to the Haake constant temperature bath. Tests with the cell filled with distilled water showed that the temperature in the cell differed by ca.5 °C from the bath temperature.

However, the observed emission intensity, which was measured at the emission maximum, turned out to be very sensitive to the position of the sample. As a result, reproducibility was largely dependent on how well one could reproduce the position of the sample in the spectrometer. In short, the arrangement shown in Figure 13 with a conventional 1-cm square cell mounted in the sample holder proved to be inadequate to quantitate the emission intensity for impregnated glass samples. Although the Teflon holder tightly held the glass plate, its slight movement within the cell prevented an exact repositioning of the sample. Consequently, the emission intensity measured from the edge of the glass plate would change when the sample was taken out and put back to the sample compartment, and when the sample was remounted into the cell. The error introduced by an inability to exactly reproduce the sample position could be as large as 30%.

To quantitate the emission intensity of the glass samples, front surface techniques were required. A special thermostatted cell holder (Figure 12) was machined to the dimension of a 2-mm quartz cell. A 2-mm path length cell was chosen because a thin glass sample with 1-mm thickness could tightly fit in the cell. By using a 2-mm pathlength cell, both the aqueous reference solution and the glass samples could be measured in the same cell and under essentially identical conditions. With both solution and glass samples, the emission was monitored from the front surface of the sample which was mounted at 35° to the excitation light. A filter which transmitted wavelengths ≥ 480 nm was placed between the sample and the emission monochromator to eliminate the scattered 450-nm excitation light. The tight fit of the cell in the cell holder and the tight fit of the glass sample plate in the cell significantly improved the reproducibility of the measurement. Tests with the same sample and with different samples containing the same loadings showed that with this arrangement, the repositioning error was reduced to ≤ 2% (Table 2).

(iii) Resonance Raman Spectra

Resonance Raman spectra of $Ru(bpy)_3^{2+}$ were recorded on a spectrometer composed of a Spex Model 14018 double monochrometers equipped with RCA C31034A PMT. The excitation source was a Spectra Physics Model 164-88 CW Ar^+ laser. All samples were excited with 457.9-nm laser light and spectra were scanned over the 1000 cm^{-1} to 1700 cm^{-1} region with a resolution of ≤ 1 cm^{-1}.

(iv) Emission Decay Lifetimes

Table 2. Emission Intensities of Ru(bpy)$_3$$^{2+}$(ads) measured by front-surface method (Figure 12) for two different samples with the same loadings. At each temperature, each sample was measured at least three times.

T(°C)	I_{em}(sample 1) (C= 1.45x10^{-6} mole/g PVG)			I_{em} (sample 2) (C= 1.45x10^{-6} mole/g PVG)		
5	80	80.5	80.5	79.5	80.5	79.5
15	63	63.5	63.5	64	64	63.5
25	51	50.5	50.5	51	51	51
35	43	42.5	43.5	41.5	41.5	41.5
45	32.5	33	33	33	32.5	33.5
55	27	27	27	27	27	27
65	23.5	22.5	22	21.5	21.5	21.5
75	18	18.5	18.5	18	18	18
85	16	16	16	15	15	15

The luminescent lifetimes of $Ru(bpy)_3^{2+}$ in degassed aqueous solution and adsorbed onto PVG as a function of temperature between 273K and 368K were determined with the apparatus shown in Figure 14. All samples were mounted in a cell holder thermostatted with the constant temperature bath described above, and excited with the 355-nm harmonic (7 ns fwhm, 0.01 mJ/pulse) from a Quanta Ray Model DCR-2A Nd:YAG laser. The emitted light was monitored at the emission maximum (610-nm) through a Bausch and Lomb Model 33-86-76 0.25-m monochrometer and detected with an RCA C31034A photomultiplier (PM). The PM output was displayed on a Tektronix Model 7834 scope by dropping the PM current across the 50-Ω input impedance of a Model 7A29 vertical amplifier. The sweep of the scope was triggered by the laser pulse and photographed with a Tektronix Model C-5C camera. For aqueous solutions, the emission decay was monitored at 90° to the excitation axis; while for glass samples, the emission decay was monitored either through the edge of the sample (right-angle method) or from the front surface of the sample (front-surface method) (Figure 15). The measured lifetimes were independent of the excitation-analysis geometry.

Picosecond decay measurements were carried out in collaboration with Professor Nick Serpone at Concordia University, Montreal, Quebec, Canada. Impregnated samples at room temperature were excited with the 355-nm harmonic (ca. 30 ps fwhm, 1-2 mJ/pulse) from a passively mode-locked Nd:YAG laser. Identical experiments were also carried out with unimpregnated calcined samples of PVG to establish a baseline for both

Figure 14. The apparatus for emission lifetime measurement.

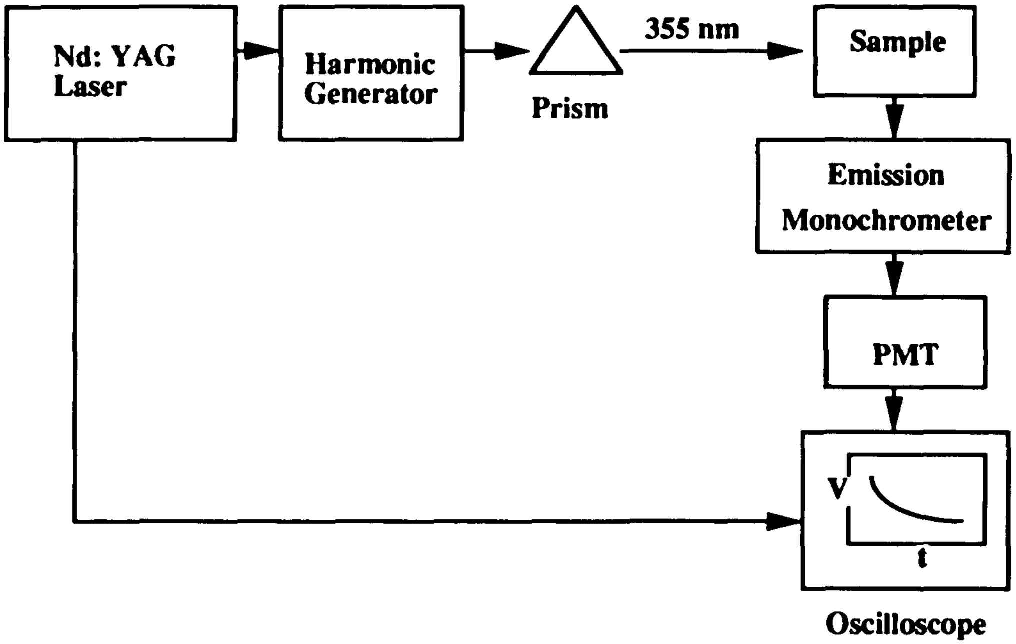
Nd: YAG Laser
Harmonic Generator
Prism
355 nm
Sample
Emission Monochrometer
PMT
V
t
Oscilloscope

Figure 15. An illustration of two methods for measuring emission lifetimes of impregnated PVG samples (a) Right-angle method and (b) Front-surface method.

(a)

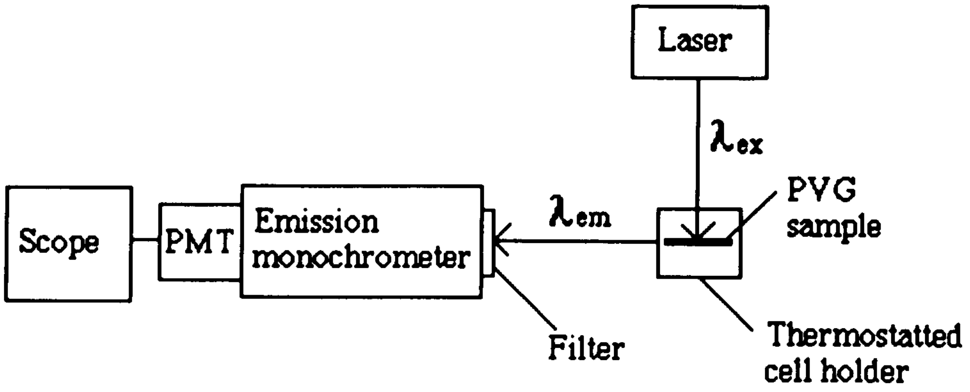
Laser
λ_{ex}
PVG
sample
Scope
PMT
Emission
monochrometer
λ_{em}
Filter
Thermostatted
cell holder

(b)

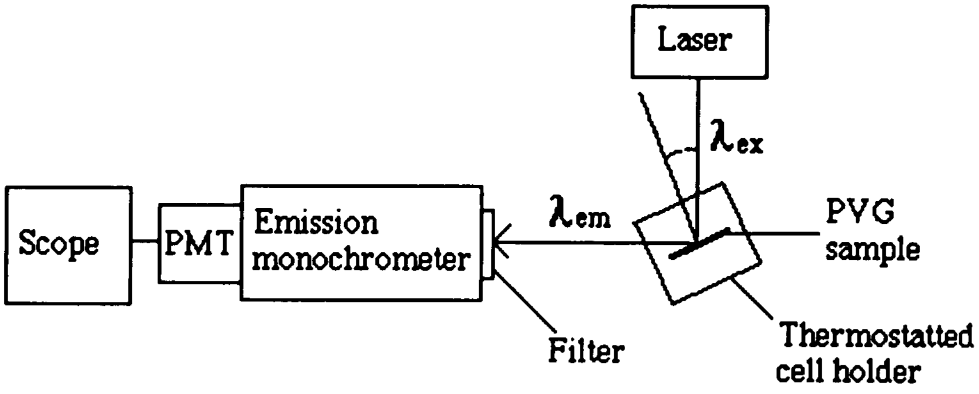
Laser
λ_{ex}
PVG
sample
Scope
PMT
Emission
monochrometer
λ_{em}
Filter
Thermostatted
cell holder

picosecond and nanosecond Ru(bpy)$_3^{2+}$(ads) decay measurements.

(v) Temperature Dependence of Refractive Index of PVG

The refractive index of consolidated glass is independent of temperature in the 5 to 95 °C range, but it was not clear whether this was also true for the porous glass used in these experiments. Consequently, the temperature dependence of its refractive index, n_x, was determined with a Michelson interferometer.[135] The interferometer (Figure 16) was composed of (a) a He-Ne laser light source (647-nm), (b) a 50 % beam splitter, (c) a fixed mirror, (d) an adjustable mirror, and (e) a projection board. A thermostatted cell holder containing the PVG sample was placed between the beam splitter and the adjustable mirror. The incident light was split into two beams by the beamsplitter: one went to the fixed mirror and was reflected back; while the other passed through the glass sample, onto the adjustable mirror and back through the sample. The distance of the second mirror was adjusted so that, when the two beams combined at the beam splitter, a fringe pattern was observed on the projection board.

Tests with the empty quartz cell showed no change in the fringe pattern in the 5 to 95 °C range. A calcined PVG sample was then placed in the cell and evacuated to $\leq 10^{-5}$ torr. If any change of the refractive index of the glass occurred due to the temperature change, it would cause a change in the optical length of the second beam. The change in optical pathlength would then cause a movement of the parallel light-dark bars in fringe pattern. The

Figure 16. Michelson interferometer for measuring temperature dependence of refractive index of PVG.

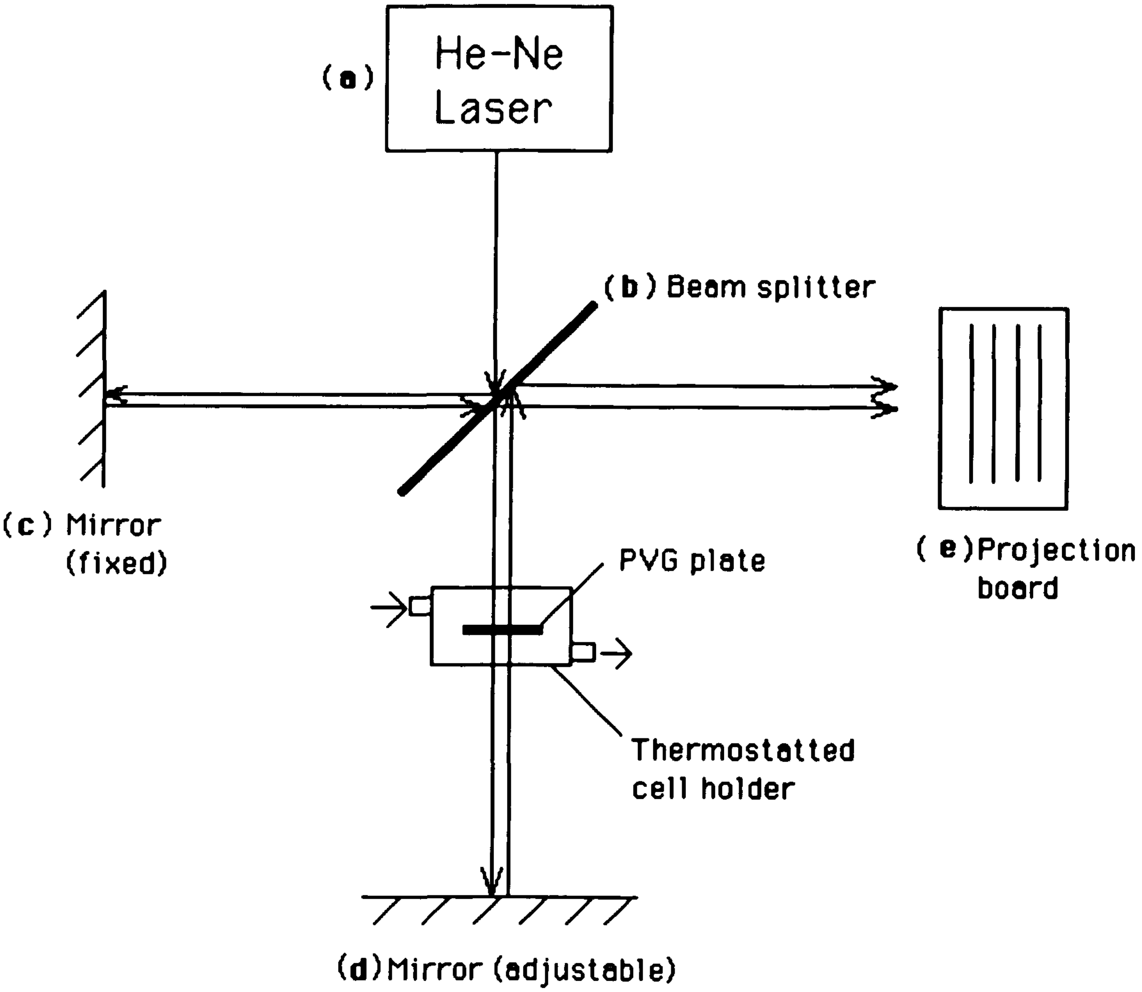

$$2d\,\Delta n_g = k \cdot \frac{\lambda}{2} \qquad k = 1, 2, 3, \ldots\ldots$$

relation between the change in the fringe pattern and the change in refractive index of the glass, Δn_g, is given by[135]

$$2d\Delta n_g = k\lambda /2 \qquad [20]$$

where d is the thickness of the glass (1.99±0.1 mm), λ is the wavelength of the light source (647-nm), and k is an integer representing that the number of light-dark lines in the fringe pattern that are displaced. However, the lack of any change in the fringe pattern observed between 5 to 95 °C indicated that the refractive index of the porous glass changed by $\leq 0.01\%$ over the entire temperature range. As a result, n_g was taken to be independent of temperature.

IV. Photochemical Measurements

The photochemical behavior of $Ru(bpy)_3^{2+}$ in degassed 0.1 M HCl aqueous solution and adsorbed onto PVG were examined. Solution and impregnated glass samples were irradiated in a Rayonet photochemical reactor (Southern New England Ultraviolet). The temperature of the samples was maintained as high as possible, which was 83 °C in these experiments, by a thermostatted cell holder connected to the Haake Model FK2 constant temperature bath. The samples were irradiated with 350-nm light from four germicidal lamps symmetrically placed within the round reactor. The excitation light intensity was determined by ferrioxalate actinometry.[136] UV-visible spectra were recorded at different times of photolysis with the spectrophotometer described above, and the amount of $Ru(bpy)_3^{2+}$ reacted was calculated from the change in absorbance at 452-nm according to the procedure of Wong and Allen.[130] The quantum yields of the photochemical reactions were calculated from the following equations[136]

$$\Phi_R = n_R / I_{abs} \qquad [21]$$
$$= n_R / I_0 (1 - 10^{-A}) t$$

where n_R is the number of moles of $Ru(bpy)_3^{2+}$ reacted by photolysis. The absorbed intensity, I_{abs}, is related to the incident intensity, I_0, determined by ferrioxalate actinometry, by $I_{abs} = I_0(1-10^{-A})$ where A is the average absorbance of reactant before and after photolysis at the excitation wavelength, and t is the photolysis time in seconds.

V. The Effect of NH_3 on the Photoinduced Disproportionation of $Ru(bpy)_3^{2+}(ads)$

(i) Diffuse Reflectance FTIR Experiments

Diffuse reflectance FTIR spectra were recorded on a Nicolet 5/20 DX FTIR equipped with a Harrick Scientific diffuse reflectance accessory. Crushed, blank or impregnated PVG samples with a particle diameter of ≤ 250 μ, or powdered silica gel, were diluted with KBr (1:30), and mounted in the vacuum chamber of the diffuse reflectance accessory. The chamber was connected to an external vacuum line by two tubes. One was used for evacuation, while the other was used for transferring gases. The sample was evacuated to P ~10^{-3} torr first, then NH_3 gas was introduced into the chamber through the other tube. The gas was allowed to equilibrate with the sample for 30 minutes and then the sample chamber was evacuated to P ~10^{-3} torr. FTIR spectra were recorded before and after the introduction of NH_3, and as functions of evacuation time and temperature.

(ii) Continuous Photolysis

(1) UV-visible Study

Two identical PVG samples were obtained by cutting off a 25mm x 25mm x 2mm size impregnated sample into 25mm x 9mm x 2mm pieces. Each piece was then mounted with a Teflon holder in a 1-cm square cell as shown in Figure 11. One of the pieces was evacuated to 10^{-5} torr and used as a reference. The other was exposed to NH_3, allowed to equilibrate as described above, and then evacuated for several hours to remove gas phase NH_3 and physisorbed NH_3. Each sample was irradiated with 457.9-nm light from a Spectra-Physics Model 164-08 Ar^+ laser with an incident power of 0.1 Watts. To check the concentration dependence, these experiments were also repeated for samples with different initial loadings of $Ru(bpy)_3^{2+}$(ads). UV-visible spectra were recorded before, during and after photolysis. To ensure the alignment of the spectrometer light beam with the region of glass sample photolyzed, a mask with a 3-mm diameter hole was taped onto the spectrometer cell holder. A cell containing the sample was then placed in the cell holder and the entire apparatus (cell plus cell holder) was removed and aligned in front of the laser so that the laser exposed the region of glass defined by the mask (Figure 17). To compensate for the presence of the mask, an equivalent mask was also taped on the reference cell holder. This was necessary to balance the intensities in the sample and reference beam in order to obtain a reasonable baseline.

(2) EPR Study

EPR spectra were recorded on a IBM-Bruker 200E-SRC spectrometer equipped with a 9.78 GHz microwave source. The impregnated powder PVG samples, with loading of 3×10^{-5} moles of $Ru(bpy)_3^{2+}$/g of PVG, were placed in the tube (Figure 10) and evacuated to 1×10^{-5} torr. To prepare the sample containing the chemisorbed NH_3, the degassed sample was exposed to NH_3 for 30 minutes, and then evacuated overnight. The evacuated samples in the tubes, either with or without NH_3, were photolyzed in the cavity of the EPR with a 350 W high-pressure Hg arc lamp (Illumination Industries) ($\geq$ 250 nm). As shown in Figure 18, the incident light was passed through a water filled 12-cm quartz cell to remove IR radiation, and the spectra were recorded as a function of photolysis time.

(iii) Quantum Yields as a Function of Loading

Impregnated glass plates with loadings ranging from 1×10^{-8} to 2×10^{-5} moles of $Ru(bpy)_3^{2+}$/g of PVG were prepared according to the method

Figure 17. An illustration of the apparatus used for continuous photolysis of impregnated PVG plates with Ar^+ laser.

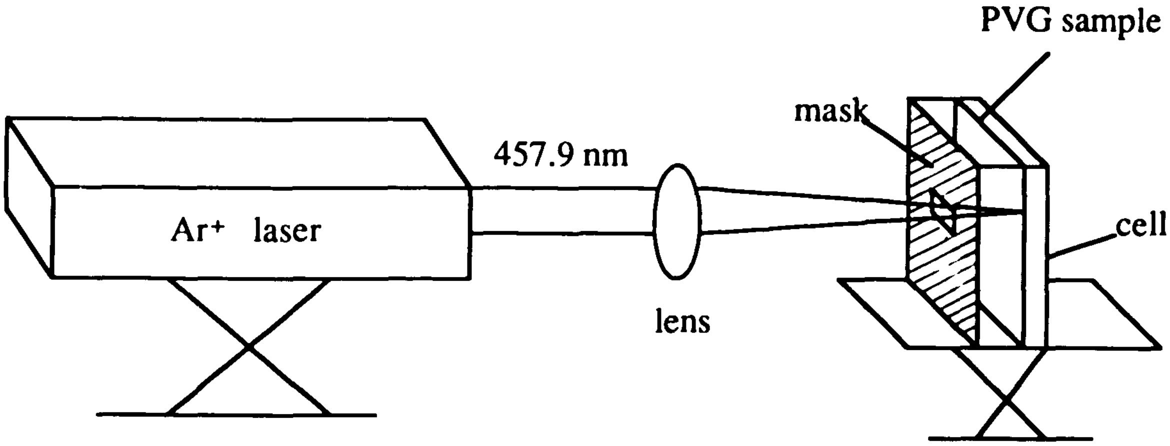
PVG sample
mask
457.9 nm
Ar+ laser
cell
lens

Figure 18. The apparatus for simultaneous continuous photolysis and EPR measurements.

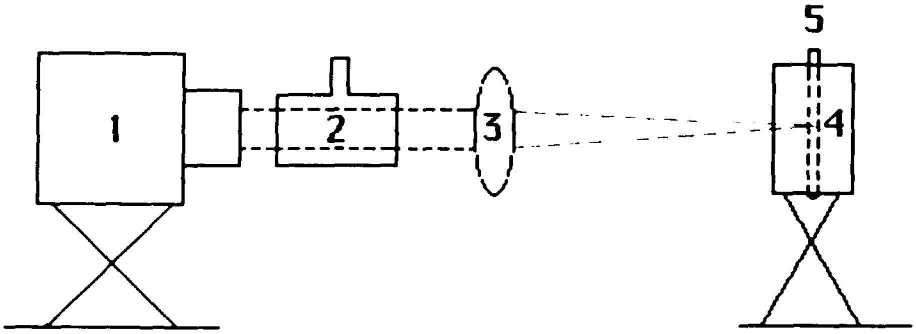

1. 350W Hg lamp
2. 12cm quartz cell filled with H_2O
3. Lens
4. EPR cavity
5. Sample tube

described above. For comparison, the quantum yields of the photoinduced disproportionation of $Ru(bpy)_3^{2+}$(ads) were determined as a function of loading for both degassed samples without exposure to NH_3, and samples exposed to NH_3 for 30 minutes and evacuated for 4 hours under $P \leq 1 \times 10^{-5}$ torr. Under each set of conditions, at least 20 different samples with differnt loadings were photolyzed and spectroscopically analyzed.

The samples were mounted in the cell shown in Figure 17, and were irradiated with 0.1 Watts of 457.9-nm light from Ar^+ laser described above. The quantum yields were obtained by measuring the initial rates of the $[Ru(bpy)_2(bpy^-)]^+$ formation by monitoring the increase in absorbance at 510-nm.[124] Initially, absorbance changes at 452-nm and 510-nm were recorded every 30 seconds, but as the rate of reaction decreased as the photolysis proceeded, the analysis interval was increased to minutes. Plots of the absorbance at 510-nm against the photolysis time were constructed, and the initial rates of product formation were calculated from the slope of the curve extropolated to t = 0.

RESULTS

I. Porous Vycor Glass

Porous Vycor glass (PVG) is a 96% SiO_2, 3% B_2O_3 and 1% Na_2O and Al_2O_3 glass. When the borosilicate melt is cooled below its phase transition temperature, the borate phase separates. Acid leaching of this phase yields a transparent (50% T at 295 nm vs. air) glass with a random three dimensional array of interconnected pores throughout the glass.[75] After calcination, typically at 650 °C, scanning electron microscopy (SEM) and transmission electron microscopy (TEM) reveal an amorphous material composed of randomly interconnected SiO_2 nodules with intervening crevices that contain openings into the interior pore structure (Figure 19).[138] TEM shows that the intervening spaces range from 40 to 100 Å, while BET measurements yield a surface area of 183 ± 15 m^2/g, and analysis of the desorption isotherms yields an average pore diameter of 100 ± 10 Å.[115]

As with any support, the active region of this glass is the surface upon which the molecules adsorb. Diffuse reflectance FTIR spectra of calcined PVG (650 °C) exhibit strong bands at ca. 3700 cm^{-1} and ≤ 1900 cm^{-1} (Figure 20). The latter are due to skeletal matrix vibrations, whereas the former are assigned to the SiO-H vibrations of the surface silanol groups. The strong band at 3744 cm^{-1} is assigned to free or isolated individual SiOH group, while the lower frequency shoulder at 3650 cm^{-1} is assigned to associated, or

Figure 19. The scanning electron micrograph of PVG.

POL PVG PLATE - PVG6

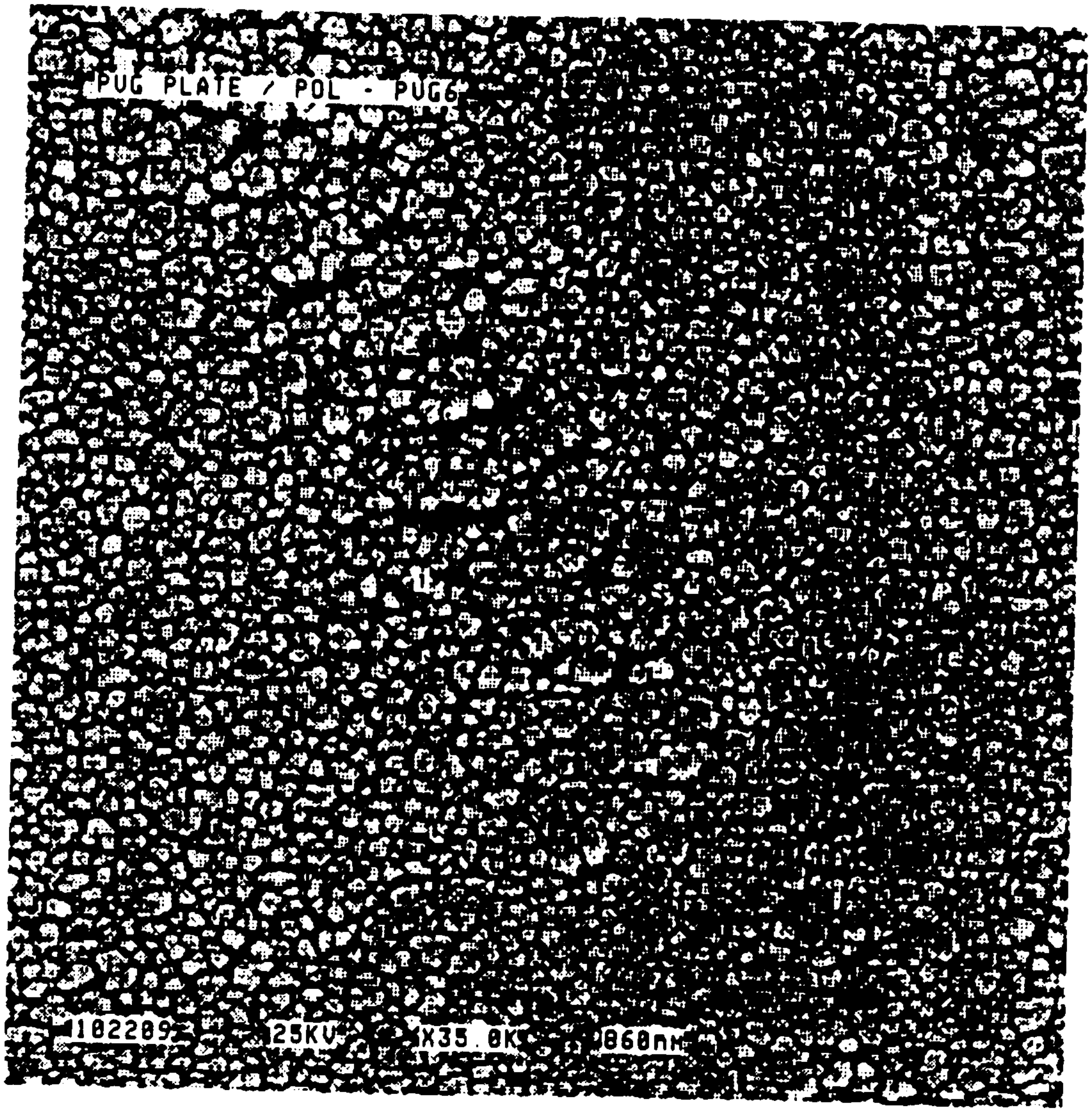

Figure 20. The diffuse reflectance FTIR spectrum of calcined PVG.

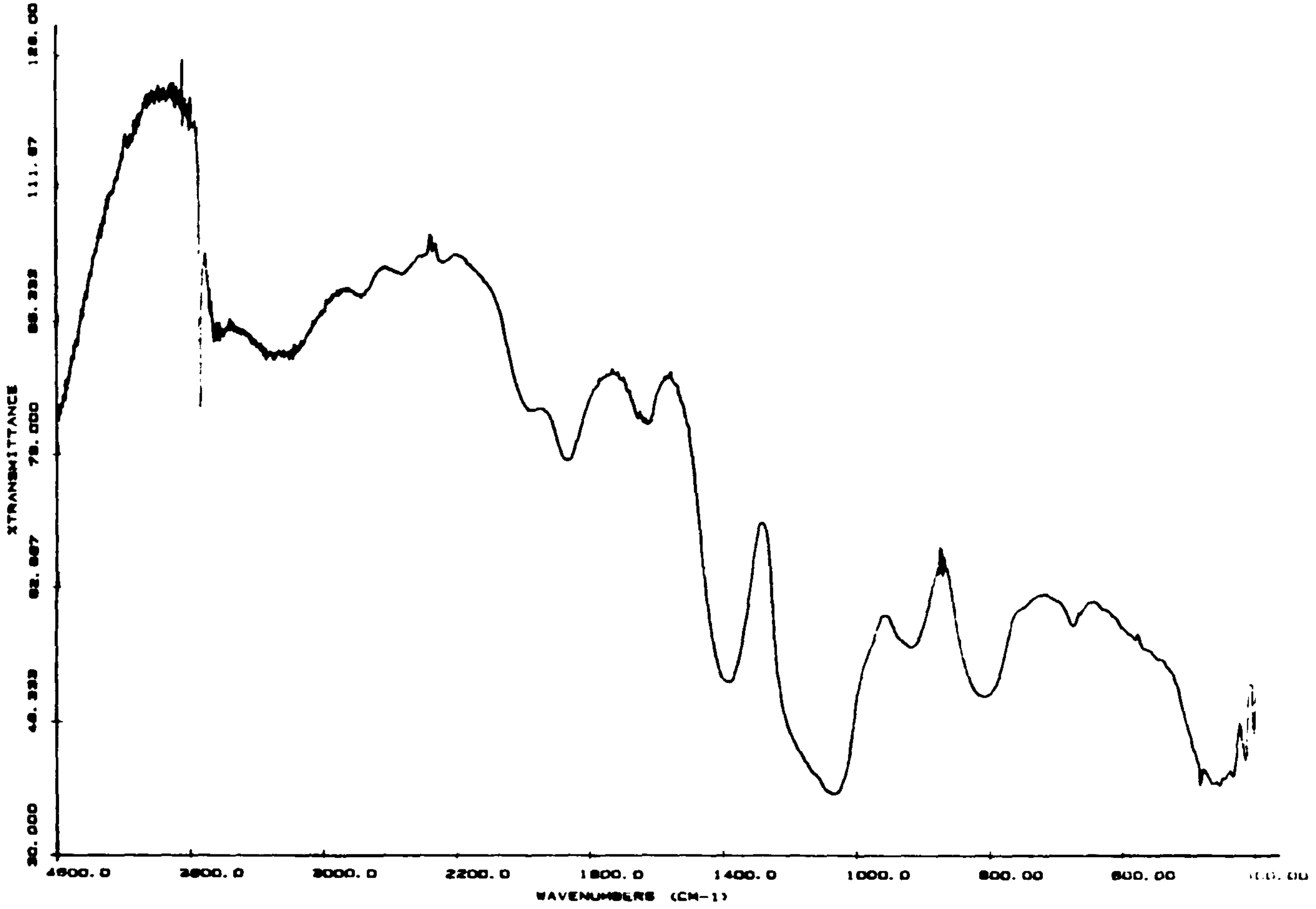
XTRANSMITTANCE
30.000
46.333
62.667
79.000
95.333
111.67
128.00
4600.0
3800.0
3000.0
2200.0
1800.0
1400.0
1000.0
800.00
600.00
400.00
WAVENUMBERS (CM-1)

hydrogen bonded silanol groups. Although all glass samples used in these experiments are calcined at 650 °C for at least 24 hours, in many cases, a weak broad band centered at ca. 3500 cm^{-1} reveals the presence of chemisorbed water. The intensity of this band, however, was never more than 10% of that of the silanol groups. Although water hydrogen-bonded to the surface is present, the dominant surface functionalities are the free and associated silanol groups. The number of silanol groups present, designated by the silanol number, depends on the thermal history of the sample, but previous studies of a variety of hydroxylated silicas yield silanol numbers of 4-7/100 $Å^2$.[116]

II. Impregnation

The silanol groups behave as weak Bronsted acids, i.e.

$$SiOH \text{ ---> } SiO^- + H^+ \qquad [22]$$

and on silica gel, exhibit a pK_a of ca. 9.[121] The pK_a of those on PVG has not been directly measured, but adsorption of various colorimetric acid-base indicators suggests a surface pH of ca.4-5.[120] When pulverized and dispersed in distilled water, PVG develops a zeta potential of -26 mV.[119] Consequently, relative to bulk water, PVG possesses an anionic surface with slightly acidic surface functionalities. As a result, the glass acts as a cation exchanger, and when placed in an aqueous solution of $[Ru(bpy)_3]Cl_2$, $Ru(bpy)_3^{2+}$ adsorbs onto the glass (Figure 21) without concurrent adsorption of the Cl^- counter anion.[124] The slightly acidic silanol groups are present throughout the pore structure of the glass. In fact, the highest density is thought to be within the pores.[75] Nevertheless, $Ru(bpy)_3^{2+}$ does not uniformly impregnate the entire sample volume. Despite their availability and the open pore structure of the glass, under typical impregnating conditions, where the concentration of the impregnating solution is 10^{-5} to 10^{-3} M, and the exposure time is ≤ 48 hours, the complex penetrates 0.2±0.1 mm into the glass from each side. The interior of the glass, ca. 80% of the total volume, remains vacant. Increasing the exposure time increases the penetration depth, but uniform impregnations of the entire sample require exposure times on the order of months. Regardless of the initial distribution of $Ru(bpy)_3^{2+}$, once adsorbed onto the glass, no redistribution of the complex is detected even if the impregnated sample is placed in pure water for several months.

Although the nonuniform distribution of $Ru(bpy)_3^{2+}$ precludes an accurate calculation of surface coverage, estimates of surface coverage are useful, at least in a relative sense. Under the usual conditions, the loadings in these experiments, $\leq 1.2 \times 10^{-6}$ moles of compound/g of PVG, correspond to surface coverages of ≤ 1% in the impregnated volumes defined by the penetration depth and the area of a particular side. It should be emphasized that although the cross sectional distribution is not uniform, electronic spectra recorded at various points along the surface are equivalent within experimental error indicating a uniform distribution of the complex within

Figure 21. An illustration of cation exchange of $Ru(bpy)_3^{2+}$ with PVG surface silanol proton.

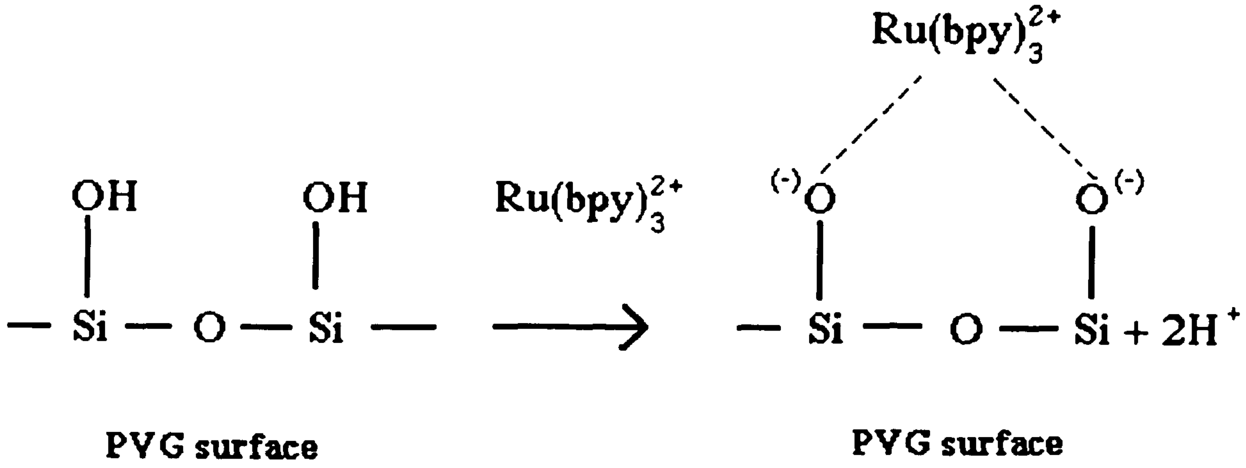
Ru(bpy)$_3^{2+}$
OH
OH
Ru(bpy)$_3^{2+}$
$^{(-)}$O
O$^{(-)}$
— Si — O — Si —
— Si — O — Si + 2H$^+$
PVG surface
PVG surface

the impregnated volume.

III. Photophysical Results

(i) UV-visible Spectra

The UV-visible spectrum of $Ru(bpy)_3^{2+}$(ads) is similar to that of $Ru(bpy)_3^{2+}$ in aqueous solution in the number of bands, maxima and relative extinction coefficients (Figure 22). In aqueous solution, the extinction coefficient of the 452-nm peak is 1.46×10^4 $M^{-1}cm^{-1}$, while that for the adsorbed complex, calculated assuming an optical pathlength equivalent to the penetration depth and a concentration of moles/unit volume of impregnated glass, is 1.49×10^4 $M^{-1}cm^{-1}$ (Table 3). The agreement is excellent considering the differences in light scattering and the uncertainty in the measured penetration depth. However, some distortion does occur. A broadening of the 452-nm MLCT transition is observed upon adsorption (Figure 23). The halfwidth of this band is 3763 ± 100 cm^{-1} in aqueous solution, while it is 4960 ± 100 cm^{-1} on PVG. Another spectral difference occurs in the UV, where adsorption causes a slight reduction in the intensity of the bipyridine π-π^* transition. The calculated ratio of absorbance at π-π^* transition relative to that of the 450-nm MLCT transition is 5.8 ± 0.1 for the adsorbed complex, while that calculated from aqueous solution spectrum is 6.3 ± 0.1 in the 5 to 90 °C range (Table 3). Neither absorption spectrum exhibits a pronounced temperature dependence and for both media, spectra

Figure 22. Absorption and emission spectra of $Ru(bpy)_3^{2+}$ at room temperature (a) in aqueous solution and (b) adsorbed onto PVG.

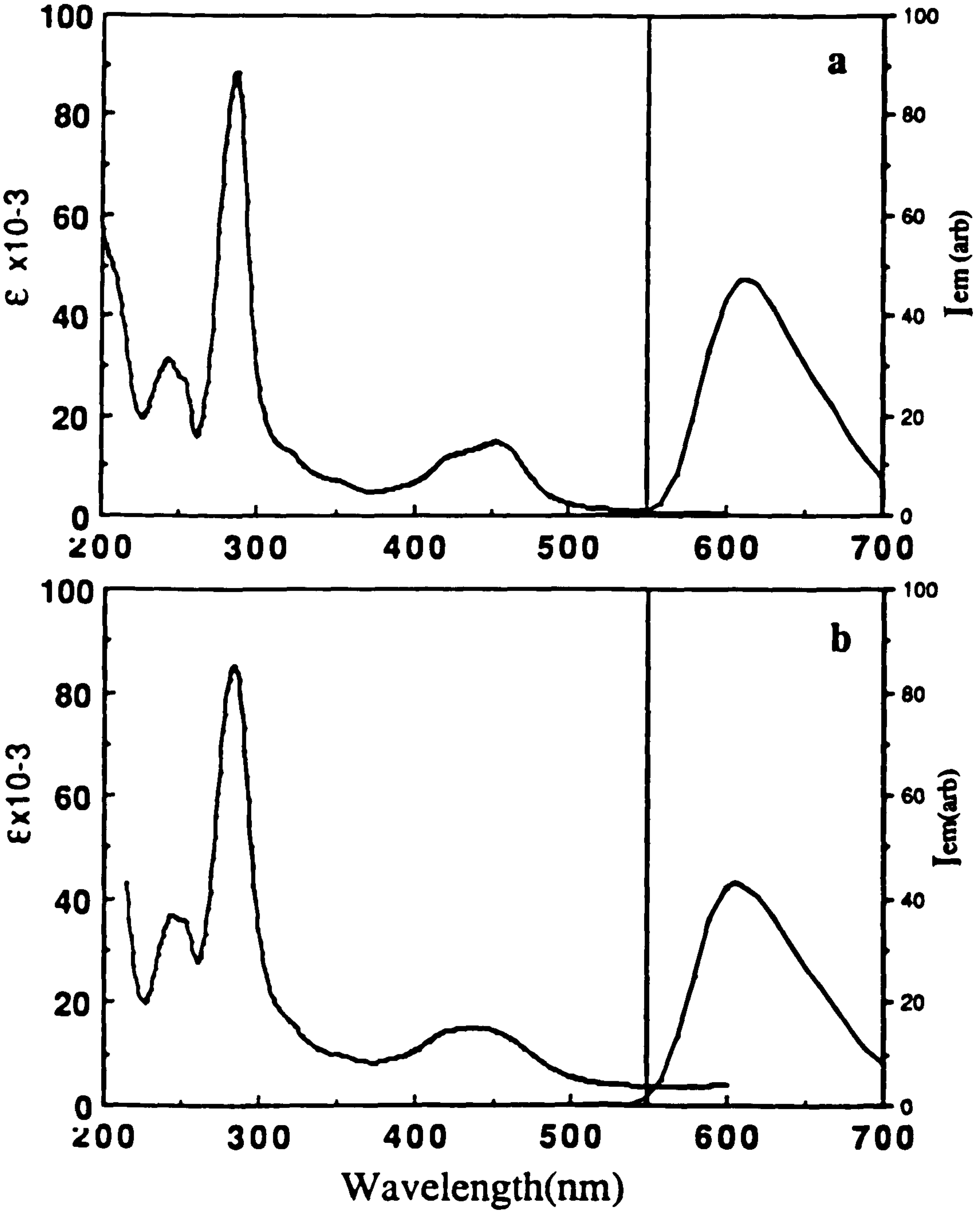
a
b
ε x10-3
εx10-3
Iem (arb)
Iem(arb)
0
20
40
60
80
100
200
300
400
500
600
700
Wavelength(nm)

Figure 23. A comparison of the bandwidth of the 452-nm MLCT transition for $Ru(bpy)_3^{2+}$ (a) in aqueous solution, and (b) adsorbed onto PVG.

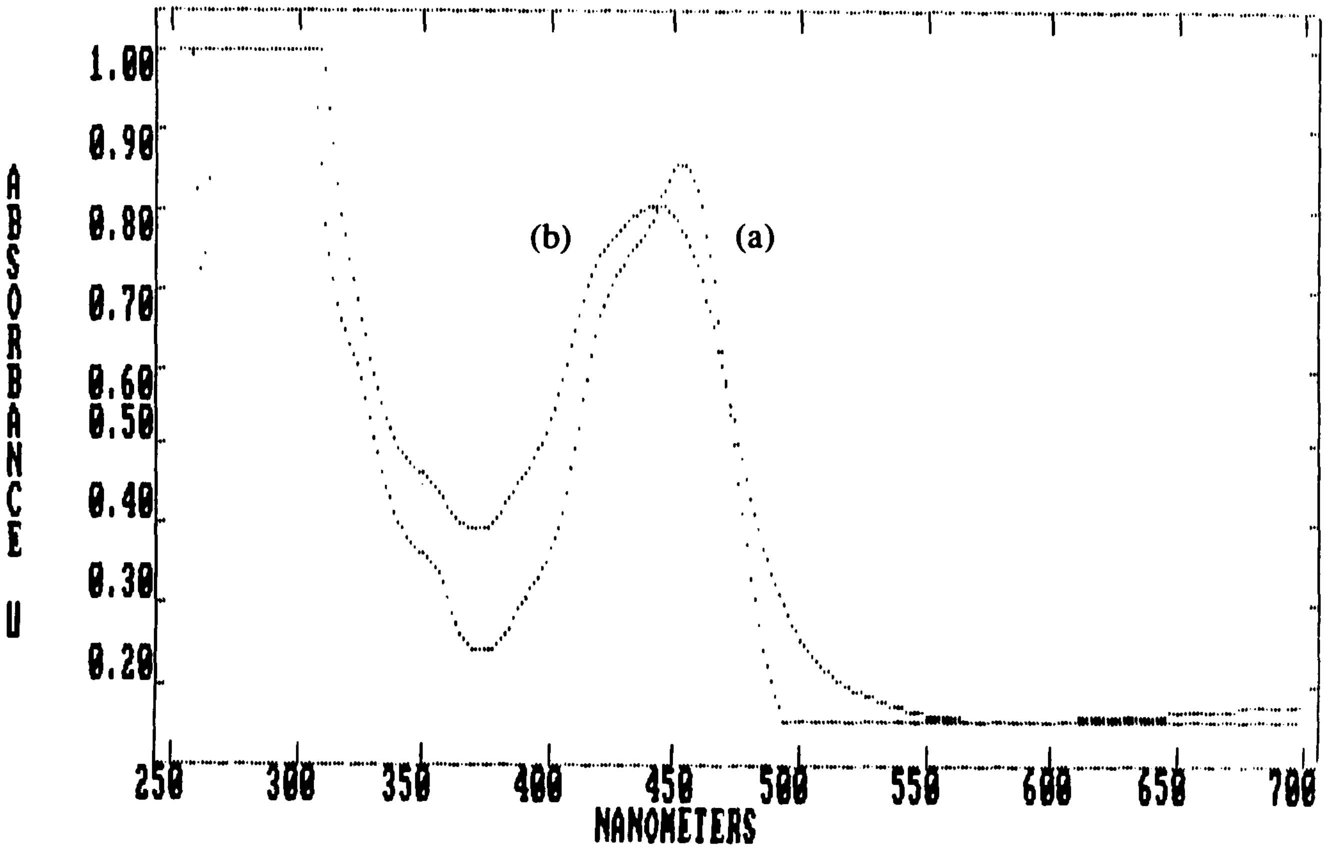
ABSORBANCE U
1.00
0.90
0.80
0.70
0.60
0.50
0.40
0.30
0.20
(b)
(a)
250
300
350
400
450
500
550
600
650
700
NANOMETERS

Table 3. Band maxima, relative extinction coefficients of $Ru(bpy)_3^{2+}$ in aqueous solution and adsorbed onto PVG.

Medium	λ_{max}(nm)		ε_{MLCT}($M^{-1}cm^{-1}$)	$\varepsilon_{\pi-\pi*}/\varepsilon_{MLCT}$
	$\pi-\pi*$	MLCT		
H_2O	286	452	$1.46x10^4$	6.3±0.1
PVG	284	444	$1.49x10^4$	5.8±0.1

recorded at 5 °C agree in band maxima, halfwidth, and relative extinction coefficient with those recorded at 90 °C (Figure 24).

(ii) Emission Spectra

Emission spectra of the complex in aqueous solution and adsorbed onto the glass are also similar. At room temperature, both exhibit a structureless emission (Figure 22). The emission maximum for the adsorbed complex occurs at ca. 605 nm, while that in aqueous solution occurs at ca. 615 nm. Increasing the temperature from 5 to 90 °C shifts the maximum ca. 7 nm to red for adsorbed complex (Figure 25) and ca.3 nm to red for aqueous solution (Figure 26), and, in both media, the emission intensities decline by ca. 80%.

Emission spectra and excitation spectra for $Ru(bpy)_3^{2+}$(ads) at 77K and 25 °C are shown in Figure 27. The excitation spectrum at 77 K is almost the same as that at room temperature. However, the emission maximum at 77K is at 588 nm, while that at room temperature is at 605 nm. The 478 cm^{-1} blue shift observed for $Ru(bpy)_3^{2+}$(ads) as temperature decreases from room temperature to 77 K is consistent with that observed for $Ru(bpy)_3^{2+}$ in alcoholic solution, where the emission peak is blue shifted ca. 1059 cm^{-1} corresponding to the same temperature change.[5]

(iii) Resonance Raman Spectra

Figure 24. Absorption spectra of $Ru(bpy)_3^{2+}$ at 5 and 90 °C (overlapped) (a) in aqueous solution and (b) adsorbed onto PVG.

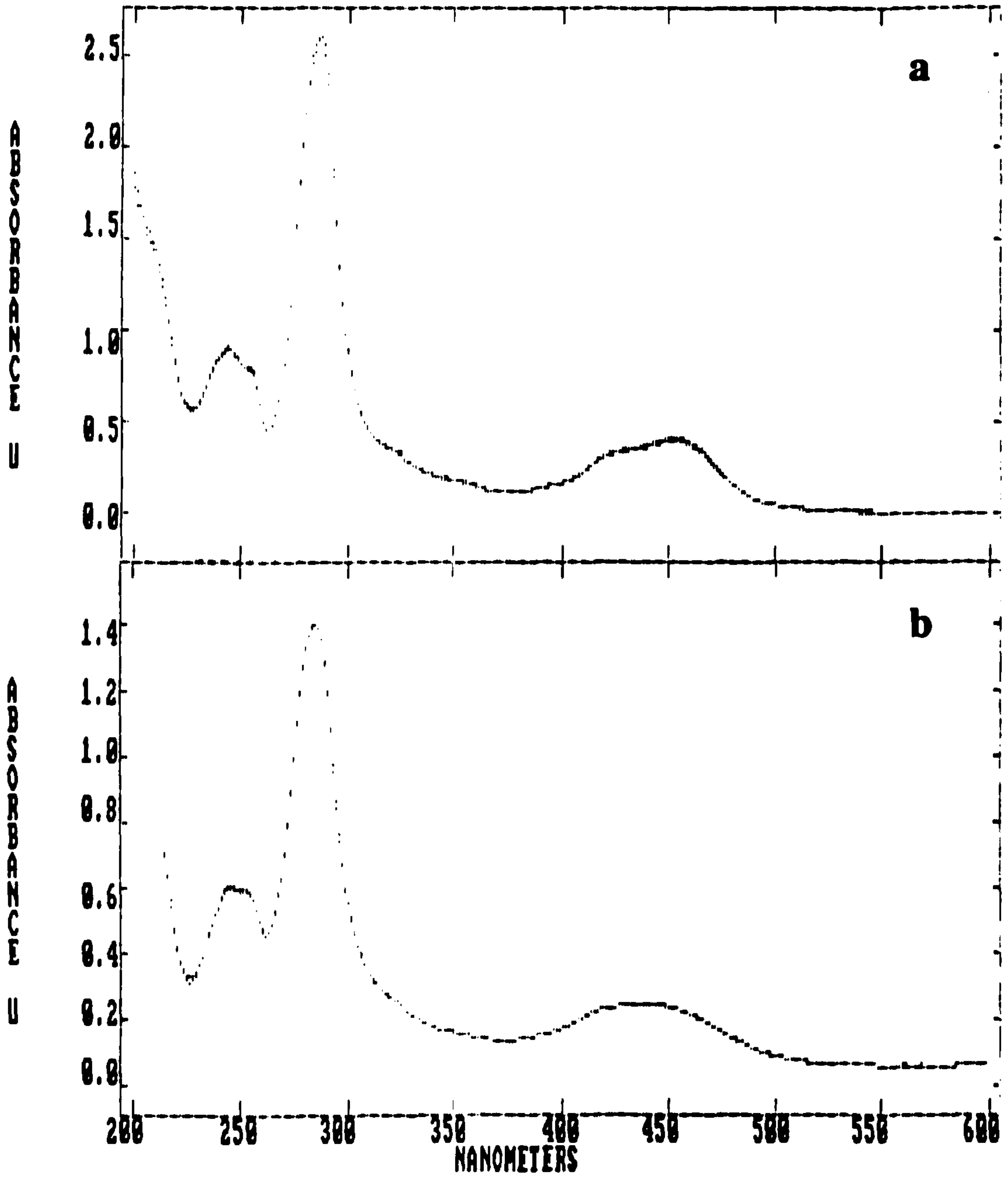
a
b
ABSORBANCE U
2.5
2.0
1.5
1.0
0.5
0.0
ABSORBANCE U
1.4
1.2
1.0
0.8
0.6
0.4
0.2
0.0
200
250
300
350
400
450
500
550
600
NANOMETERS

Figure 25. Emission spectra of $Ru(bpy)_3^{2+}$(ads) recorded at different temperatures.

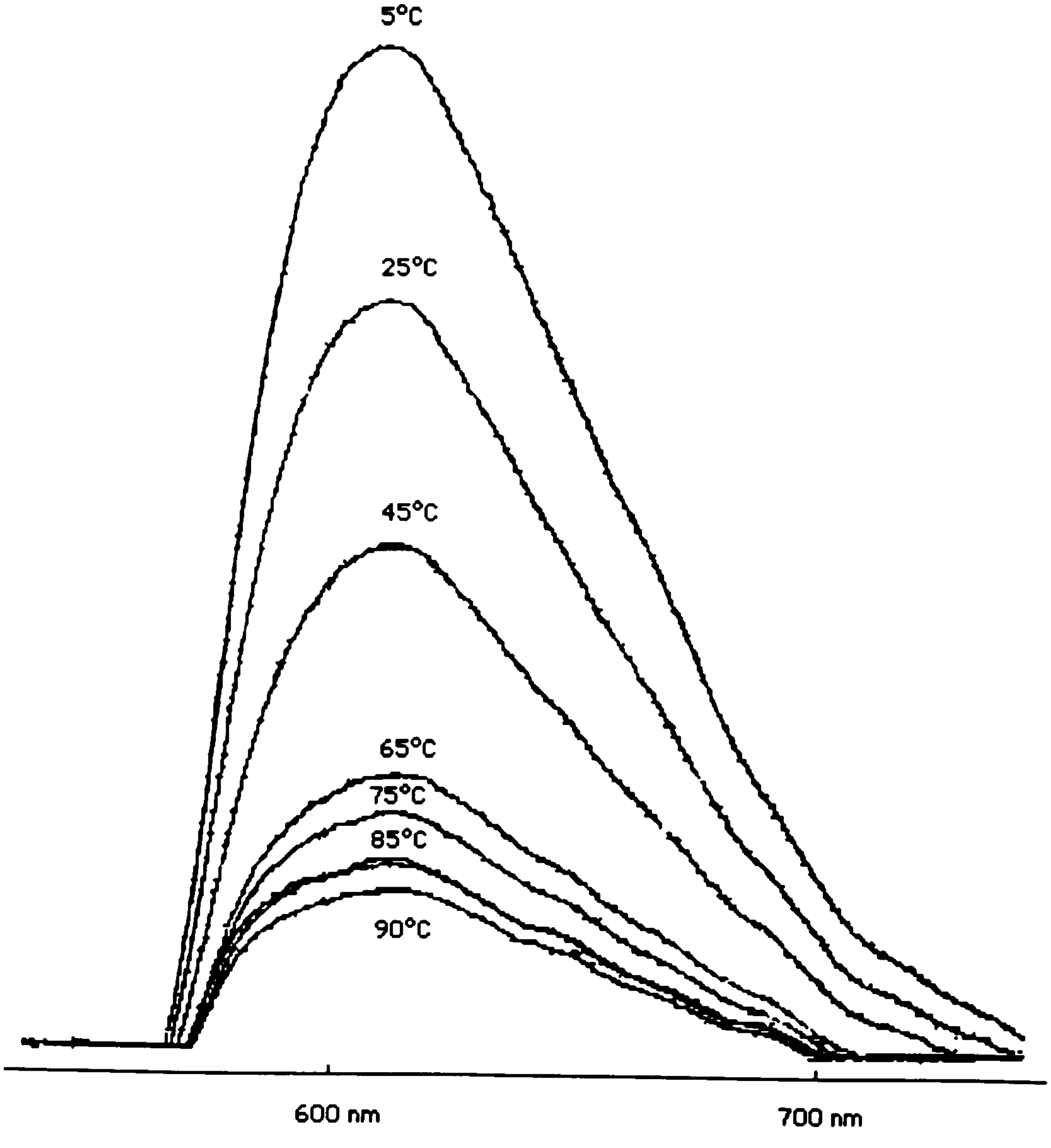
5°C
25°C
45°C
65°C
75°C
85°C
90°C
600 nm
700 nm

Figure 26. Emission spectra of $Ru(bpy)_3^{2+}$ in aqueous solution recorded at different temperatures.

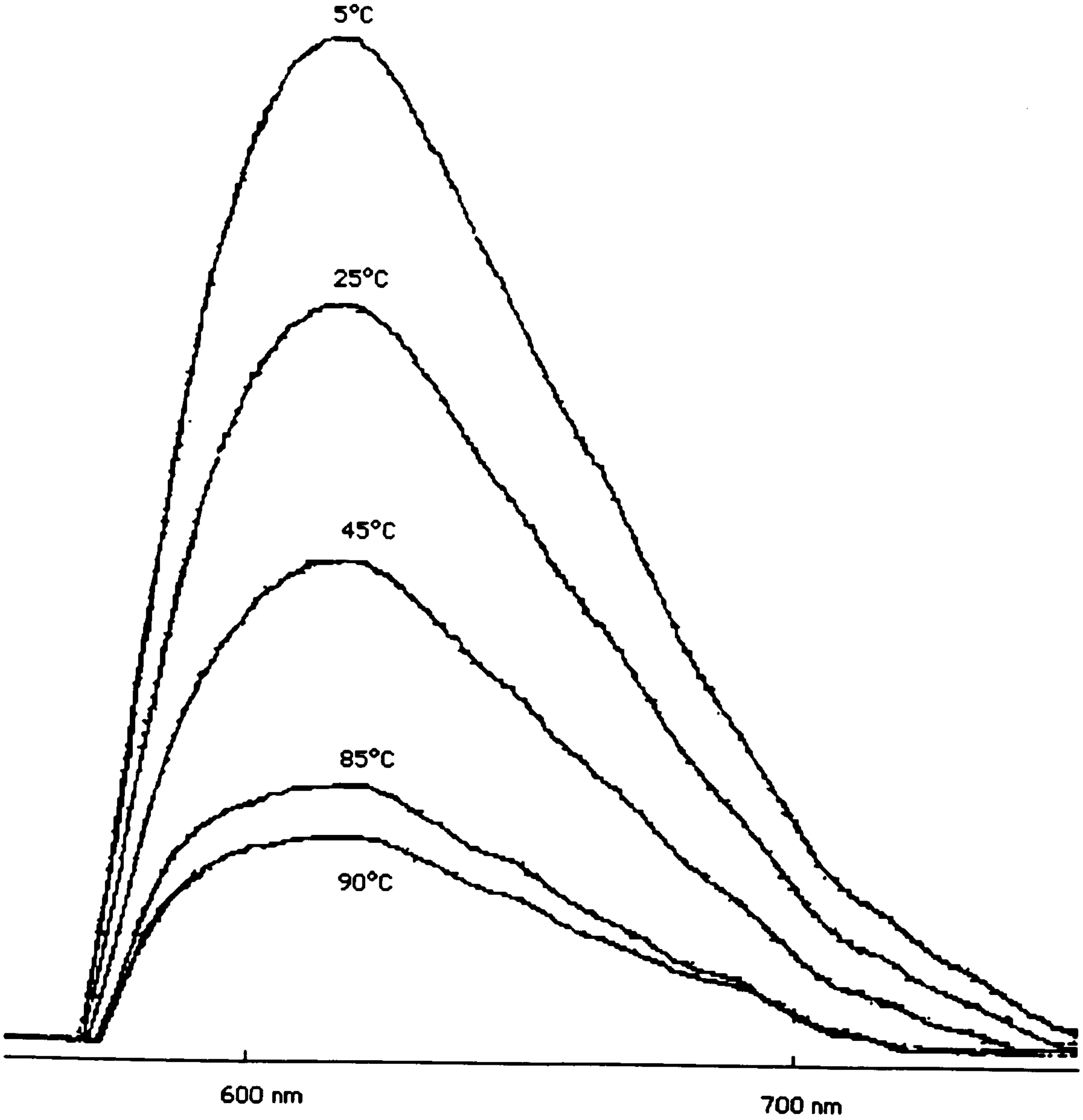
5°C
25°C
45°C
85°C
90°C
600 nm
700 nm

Figure 27. A comparison of (a) emission spectra and (b) excitation spectra of $Ru(bpy)_3^{2+}$(ads) at 77 K and room temperature.

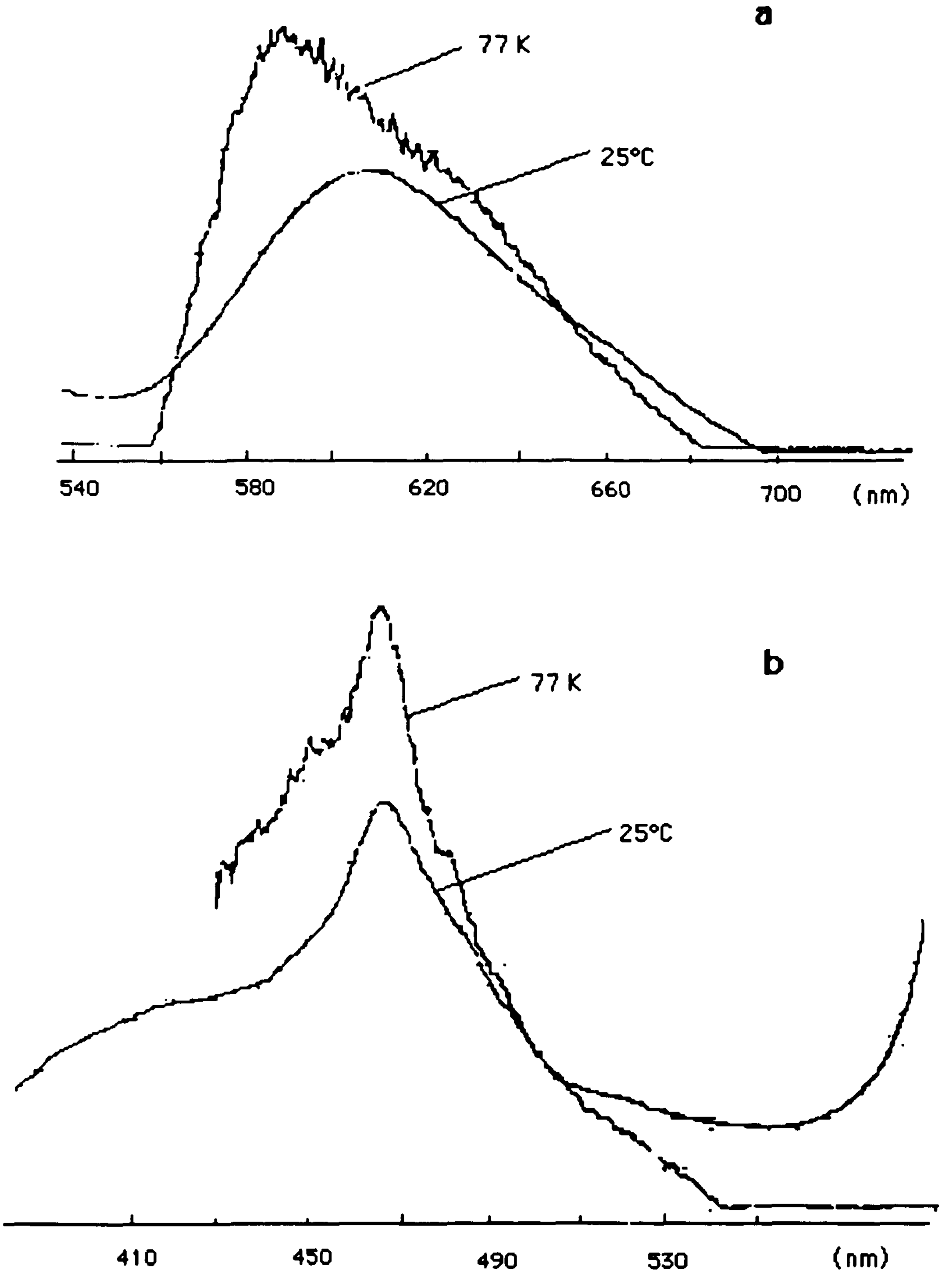
a
77 K
25°C
540
580
620
660
700
(nm)
b
77 K
25°C
410
450
490
530
(nm)

The resonance Raman spectrum of the adsorbed complex, in the region between 1000 cm^{-1} and 1700 cm^{-1}, shows seven bipyridine bands resonant with the 452-nm MLCT transition (Figure 28b). The band maxima differ by < 1 cm^{-1} from the corresponding aqueous solution bands (Figure 28a), and, in both media, the frequencies are independent of temperature in the 5 to 90 °C range. However, adsorption reduces the relative intensity of the prominent 1492-cm^{-1} vibration. It was not possible to measure absolute intensities due to the lack of a standard applicable to both the glass and aqueous solution, but Figure 28 illustrates the relative change. While the relative intensities of the other six bands are within experimental error in both media, that of the 1492 cm^{-1} band is significantly reduced. When the intensity of this band is compared with, for example, that of the 1609 cm^{-1}, a ratio of 4.4 is obtained for the complex in aqueous solution. However, the ratio reduces to 2.5 for that adsorbed on PVG.

(iv) Emission Lifetimes

At each temperature, the emission decay for $Ru(bpy)_3^{2+}$ in degassed aqueous solution is described by a single exponential, and semilogarithmic plots of emission intensity versus time are linear through 2-3 lifetimes (Figure 29a). Lifetimes, τ, taken as the time required for the intensity to drop to 1/e of the initial values, are listed in Table 4 and are in excellent agreement with the values reported by Van Houten and Watts (Figure 30).

Unlike that found in aqueous solution, the emission decay for

Figure 28. Resonance Raman spectra of $Ru(bpy)_3^{2+}$ (a) in aqueous solution and (b) adsorbed onto PVG. λ_{ex} = 457.9 nm.

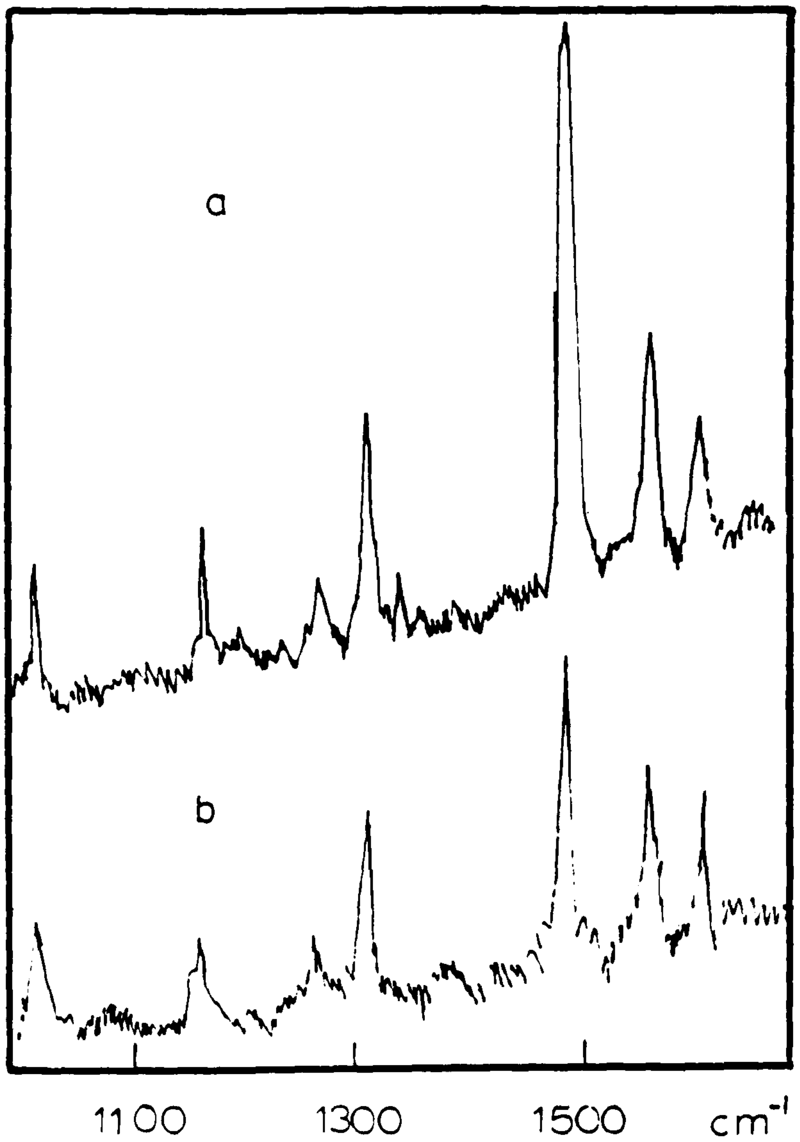
a
b
1100
1300
1500
cm⁻¹

Figure 29. Emission decay profiles of $Ru(bpy)_3^{2+}$ (a) in aqueous solution and (b) adsorbed onto PVG. The straight lines are ln emission intensity, I_{em}, vs. time.

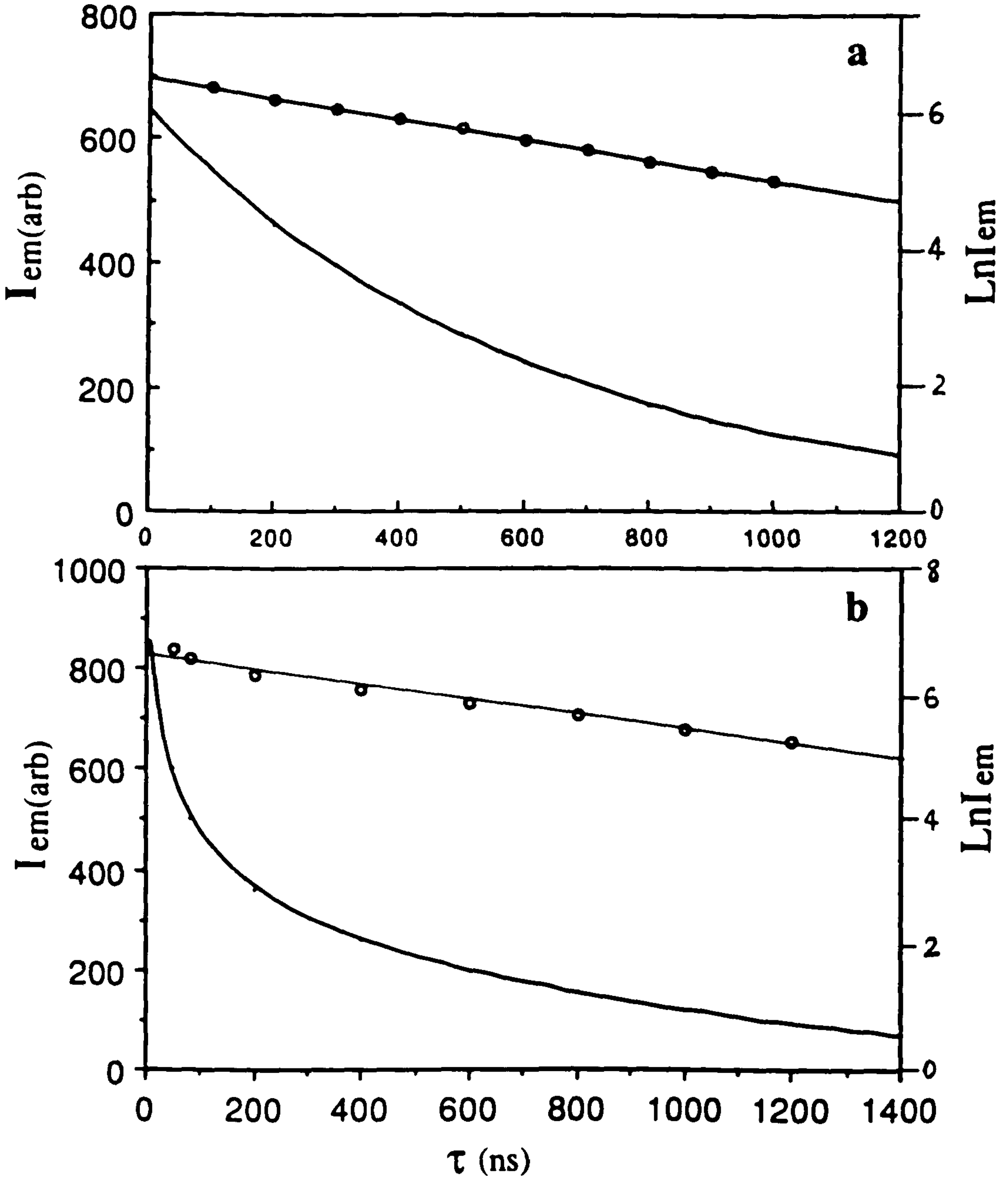
a
800
600
400
200
0
I em(arb)
6
4
2
0
LnI em
0
200
400
600
800
1000
1200
b
1000
800
600
400
200
0
I em(arb)
8
6
4
2
0
LnI em
0
200
400
600
800
1000
1200
1400
τ (ns)

Table 4. Measured and calculated τ, Φ_{em} of $Ru(bpy)_3^{2+}$ in aqueous solution

T(°C)	τ_m (ns)	τ_c (ns)	Φ_{em}^{m}	Φ_{em}^{c}
5	720±25	721	.052±.003	.051
15	690±21	677	.048±.003	.048
25	600±20	616	.042	.043
35	527±15	529	.035±.002	.037
45	420±18	422	.029±.002	.030
55	350±25	328	.023±.002	.023
65	244±10	241	.017±.001	.017
75	157±10	168	.012±.001	.012
85	123±8	118	.0091±.001	.0083

Figure 30. Temperature dependence of τ and Φem of $Ru(bpy)_3^{2+}$ in aqueous solution. Open points are data reported by Watts (Ref.8); closed points are data measured in our experiments.

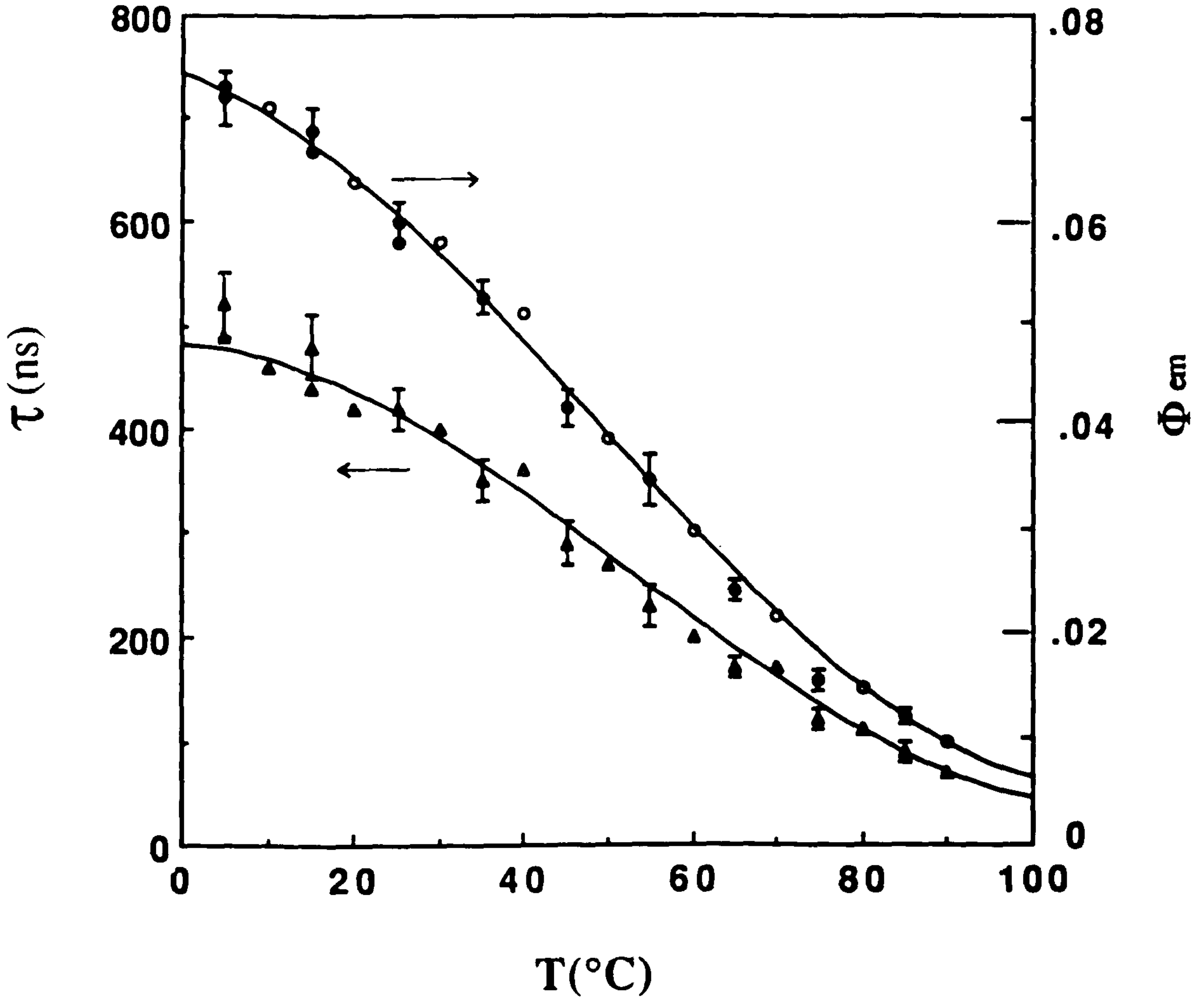

800
600
400
200
0
.08
.06
.04
.02
0
0
20
40
60
80
100
τ (ns)
Φ em
T(°C)

$Ru(bpy)_3^{2+}$(ads) is non-exponential (Figure 29b), and semilogarithmic plots of emission intensity versus time exhibit upward deviations at short times, $t \leq 70$ nsec. At all temperatures, the decay curves show a fast decay component preceding a slower exponential decay. Satisfactory fits of these plots require a biexponential equation

$$I(t) = A_s \exp(-t/\tau_s) + A_l \exp(-t/\tau_l) \qquad [23]$$

where A_s and A_l are weighting factors for the short and long decay components, and τ_s and τ_l are the corresponding lifetimes. Non-linear least squares fitting was accomplished with the Simplex algorithm, where the model function, equation 23, was tested against the observed data. Initial guesses of the values of each parameter were entered into the computer, which then repetitively increases each value by 10% to minimize χ^2. χ^2 is given by[139]

$$\chi^2 = \sum_N Ri^2 \qquad [24]$$

where N is the number of data points, and R_i is the residual. The residual is the difference between the observed data, y_i, and the value of the model function evaluated at x_i, i.e.$F(x_i)$

$$R_i = y_i - F(x_i) \qquad [25]$$

Achieving a minimum rapidly, and, in some cases, achieving the correct minimum, is very dependent on the initial guess. For these two component decays, initial guesses were obtained by the component stripping method.[139] Emission decays were recorded over a sufficient length of time to isolate the long decay component. Plots of ln I(t) vs. t would be linear at longer time (Figure 31), and the initial estimates of A_l and τ_l were obtained from the intercept and slope, respectively. After obtaining values of A_l and τ_l, the contribution of the long component was subtracted from total emission intensity I(t) to obtain the time dependence of the emission of short lived component, I'(t)

$$I'(t) = A_s e^{-t/\tau_s} = I(t) - A_l\, e^{-t/\tau_l} \qquad [26]$$

A ln I'(t) vs. t plot was then drawn (Figure 31) to obtain the initial guesses for A_s and τ_s.

The computer generated values for these four parameters at temperatures between 5 and 85 °C are listed in Table 5. It was immediately apparent from these analyses that the lifetime of the short component, τ_s, is independent of temperature (≤70 ns), while that of the long component, τ_l, declines with increasing temperature. The different temperature dependence suggests quite different origins, and picosecond experiments with impregnated and unimpregnated samples confirm that the short component arises from the glass itself. The nature of this short-lived emission is not known. It appears to involve multiphoton excitation since PVG absorbs very little, if at all, at the 355-nm excitation wavelength, and the preceding fast component is observed only with pulsed laser excitation. Since the fast

Figure 31. A demonstration of component stripping method used in evaluation of the sum of two exponentials for $Ru(bpy)_3^{2+}$(ads) emission decay. I_{em} is the total emission intensity and I_{em}' is the emission intensity of the short-lived component.

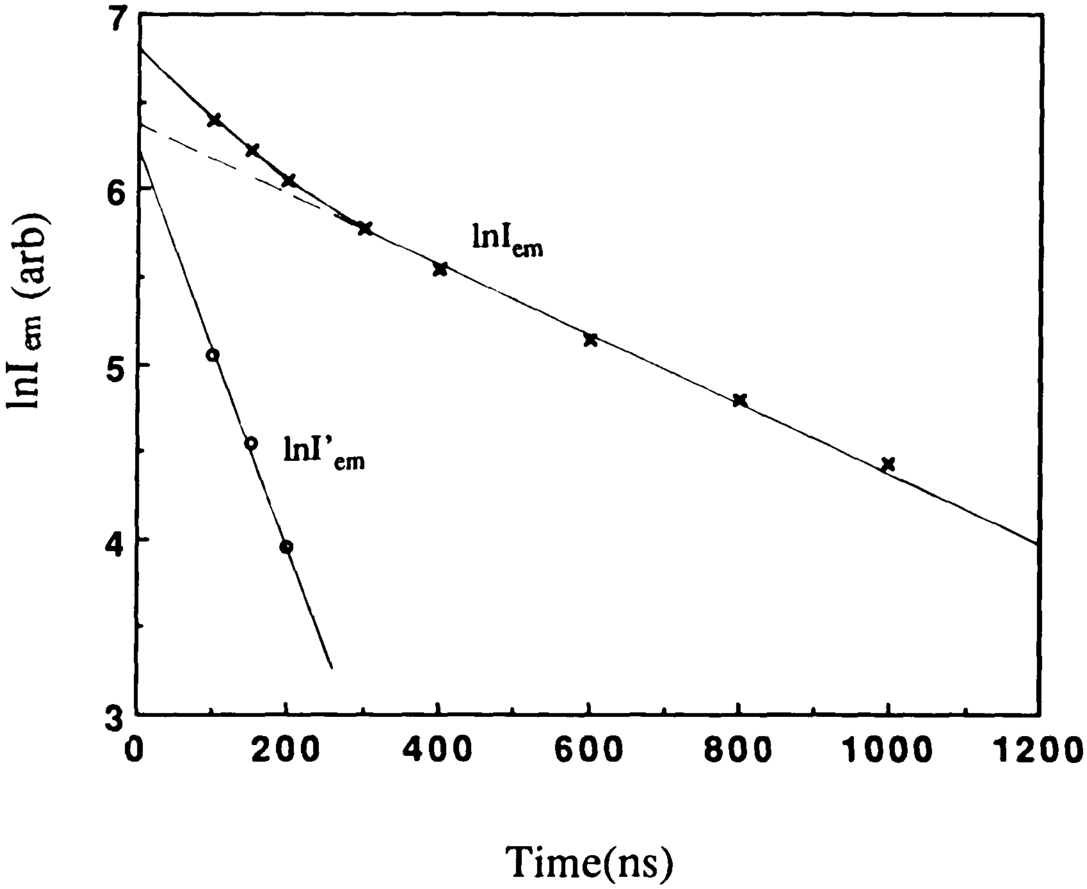
7
6
5
4
3
0
200
400
600
800
1000
1200
lnI em (arb)
Time(ns)
$\ln I_{em}$
$\ln I'_{em}$

Table 5

Temperature dependence of the parameters derived from a biexponential fit of the Ru(bpy)$_3^{2+}$(ads) emission decays.

T(°C)	A_l[a]	A_s[b]	τ_s(ns)	τ_l (ns)
0	.68	.32	87±7	1148±16
5	.61	.39	79±11	1049±8
15	.54	.46	57±12	892±10
25	.40	.60	47±3	746±4
35	.52	.48	66±6	694±6
45	.43	.57	73±15	598±14
55	.41	.59	70±5	509±6
65	.38	.62	78±8	469±9
75	.37	.63	80±6	418±17
85	.27	.73	67±11	348±9

a. Relative value = A_l / A_l+A_s.
b. Relative value = A_s / A_l+A_s.

component arises from the glass itself, the emission lifetimes of $*Ru(bpy)_3^{2+}$(ads) at the different temperatures are those obtained from the long component, i.e., τ_l. Table 6 lists the emission lifetimes of $*Ru(bpy)_3^{2+}$(ads) between 5 and 85 °C and at 77 K. Within experimental error, the measured lifetimes are independent of initial loadings, which in these experiments ranged from 5.1×10^{-7} to 1.8×10^{-6} moles of $Ru(bpy)_3^{2+}$/g of PVG.

(v) Emission Quantum Yields

(1) Aqueous Solution

Emission quantum yields of $Ru(bpy)_3^{2+}$ in aqueous solution were measured relative to aqueous solution standards. The emission quantum yield, Φ_{em}, at a specific temperature is calculated from the equation[41]

$$\Phi_{em} = I_{em} / I_{abs} = I_{em} / I_0 (1-10^{-A}) \qquad [27]$$

where I_{em} is the emission intensity and I_{abs} is the absorbed intensity. The latter is equal to the product of the incident excitation intensity, I_0, and the fraction of light absorbed, $(1-10^{-A})$, where A is the absorbance of $Ru(bpy)_3^{2+}$ at the excitation wavelength. The ratio of quantum yields at two different temperatures is given by

$$\Phi_{em}(T_2)/ \Phi_{em}(T_1) = I_{em}(T_2)/I_{em}(T_1) [(1-10^{-A})_{T1}/(1-10^{-A})_{T2}] \qquad [28]$$

Table 6. Measured and calculated τ, and Φ_{em} of $Ru(bpy)_3^{2+}$(ads) vs. T(°C).

T(°C)	τ_m (ns)	τ_c(ns)	Φ_{em} (m)	Φ_{em} (c)
5	1049 [a]	1044	.082 [a]	.077
	1061 [b]		.073 [b]	
	1034 [c]		.075 [c]	
	1052 [d]		.081 [d]	
	1049±15 [e]		.078±.004 [e]	
15	887 [a]	891	.066 [a]	.064
	883 [b]		.059 [b]	
	907 [c]		.060 [c]	
	——		.067 [d]	
	892±15 [e]		.063±.004 [e]	
25	747 [a]	776	.052 [a]	.052
	748 [b]		.047 [b]	
	750 [c]		.049 [c]	
	770 [d]		.053 [d]	
	754±16 [e]		.050±.002 [e]	
35	650 [a]	674	.043 [a]	.041
	688 [b]		.037 [b]	
	699 [c]		.041 [c]	
	682 [d]		.041 [d]	
	680±30 [e]		.041±.002 [e]	
45	590 [a]	585	.034 [a]	.032
	592 [b]		.030 [b]	
	597 [c]		.031 [c]	
	585 [d]		.032 [d]	
	591±6 [e]		.032±.001 [e]	
55	520 [a]	519	.028 [a]	.025
	511 [b]		.024 [b]	
	519 [c]		.025 [c]	
	521 [d]		.025 [d]	
	518±7 [e]		.026±.002 [e]	
65	466 [a]	461	.022 [a]	.021
	459 [b]		.020 [b]	
	462 [c]		.021 [c]	
	484 [d]		.020 [d]	
	468±16 [e]		.021±.001 [e]	
75	408 [a]	408	.018 [a]	.018
	404 [b]		.017 [b]	
	443 [c]		.018 [c]	
	392 [d]		.017 [d]	
	412±20 [e]		.018±.001 [e]	
85	340 [a]	366	.015 [a]	.016
	347 [b]		.014 [b]	
	360 [c]		.015 [c]	
	338 [d]		.014 [d]	
	346±14 [e]		.015±.001 [e]	
77k	5.8±.3μs			

a-- C= $5.08\text{X}10^{-7}$ mole/g, b--C= $9.50\text{x}10^{-7}$ mole/g, c--C= $1.45\text{x}10^{-6}$ mole/g, d--C=$1.75\text{x}10^{-6}$ mole/g, e-- ave. values.

In equation 28, the factors $(1-10^{-A})$ at two temperatures cancel since the absorbance of $Ru(bpy)_3^{2+}$, A, is independent of temperature. Correspondingly, equation 28 reduces to

$$\Phi_{em}(T_2)/\ \Phi_{em}(T_1) = I_{em}(T_2)/I_{em}(T_1) \qquad [29]$$

Taking a degassed aqueous solution of $Ru(bpy)_3^{2+}$ at 25°C as a reference, since Φ_{em} has been determined to be 0.042±0.002,[8] the emission quantum yield of $Ru(bpy)_3^{2+}$ of aqueous solution at different temperatures is calculated from the relation

$$\Phi_{em}(T2) = \Phi_{em}(25^\circ C) \times\ I_{em}(T_2)\ /\ I_{em}\ (25^\circ C) \qquad [30]$$

$$= 0.042 \times\ I_{em}(T_2)\ /\ I_{em}\ (25^\circ C)$$

At each temperature, and for each concentration, the emission intensities of $Ru(bpy)_3^{2+}$ in aqueous solution were measured at least three times. The calculated quantum yields between 5 and 85 °C are listed in Table 4 and the graphical expression of the data (Figure 30) shows the excellent agreement with the values reported by Van Houten and Watts.[8]

(2) Adsorbed Complex

Emission quantum yields of $Ru(bpy)_3^{2+}(ads)$ at different temperatures were also measured relative to aqueous solution standards. However, in these experiments, emission quantum yields were calculated from the following equation[140]

$$\Phi_{em}{}^{x} = \Phi_{em}{}^{R}\ (I_{em}{}^{x} / I_{em}{}^{R})\ [(1\text{-}10^{-A})^{R}/(1\text{-}10^{-A})^{X}]\ (n_x / n_R)^2 \qquad [31]$$

$$= 0.042\ (I_{em}{}^{x} / I_{em}{}^{R})\ (n_x / n_R)^2$$

where X and R refer to the adsorbed complex and the degassed, reference aqueous solution of the complex at 25°C ($\Phi_{em}{}^{R} = 0.042$). n_x and n_R are the refractive indices of H_2O, 1, and PVG, 1.33, and are used to correct for the change in medium. One criterion of this method is that the concentration of the reference solution be adjusted to have the same optical density as the glass sample at the excitation wavelength so that the two fractions of light adsorbed, $(1\text{-}10^{-A})$, cancel. Another criterion is that the geometry and position of the reference solution be as close as possible to that of the glass sample so that the detector would "see" the same emitting area from both the aqueous reference solution and the glass sample. This is achieved by using the front surface cell holder shown in Figure 12. Using the front surface method, emission quantum yields of $Ru(bpy)_3{}^{2+}$(ads) were measured at least three times at each temperature and for each loading, and the procedures were repeated with at least four samples with different loadings. The individual values are listed in Table 6, and, consistent with the lifetime measurements, the values of Φ_{em} for the adsorbed complex are independent of initial loading. Unfortunately, due to light scattering from the crushed glass samples, it was not possible to accurately measure Φ_{em} at 77 K.

(vi) Temperature Dependence of Φ_{em}/τ Ratio

The plots of measured τ and Φ_{em} of $Ru(bpy)_3^{2+}$(ads) vs. temperature are shown in Figure 32. Comparing Figure 32 with Figure 30 shows that the temperature dependence of τ and Φ_{em} of $Ru(bpy)_3^{2+}$(ads) differs from that in degassed aqueous solution. The values measured at the different temperatures yield a Φ_{em}/τ ratio that declines with increasing temperature for $Ru(bpy)_3^{2+}$(ads) (Figure 33b), while it is independent of temperature in aqueous solution (Figure 33a). Since $\Phi_{em}/\tau = \eta_{isc}k_r$[4] the temperature dependence is a surprising departure from fluid solution behavior, where η_{isc} is temperature independent and assumed to be unity, and by its very nature, k_r is expected to be temperature independent.[8]

An immediate concern was whether the observed dependencies were biased by the temperature dependence of self quenching, or impurity quenching. Temperature dependent impurity quenching is discounted since the results were reproducible on seven different samples of the glass, and independent of whether the glass was calcined at 650 °C in an oxidizing (air) or reducing (H_2) atmosphere. Self quenching occurs in PVG, but at room temperature it requires loadings of $\geq 10^{-4}$ mole/g, i.e., at least monolayer coverage, whereas the maximum loading in these experiments, $\leq 10^{-6}$ mole/g, corresponds to surface coverages of $\leq 1\%$. Under these conditions, self quenching requires either a long-range interaction, or an increase in adsorbate mobility with increasing temperature. The probability of a long

Figure 32. Temperature dependence of τ and Φ_{em} of $Ru(bpy)_3^{2+}$(ads). Points are measured data; solid lines are computer fitted curves (see Discussion section).

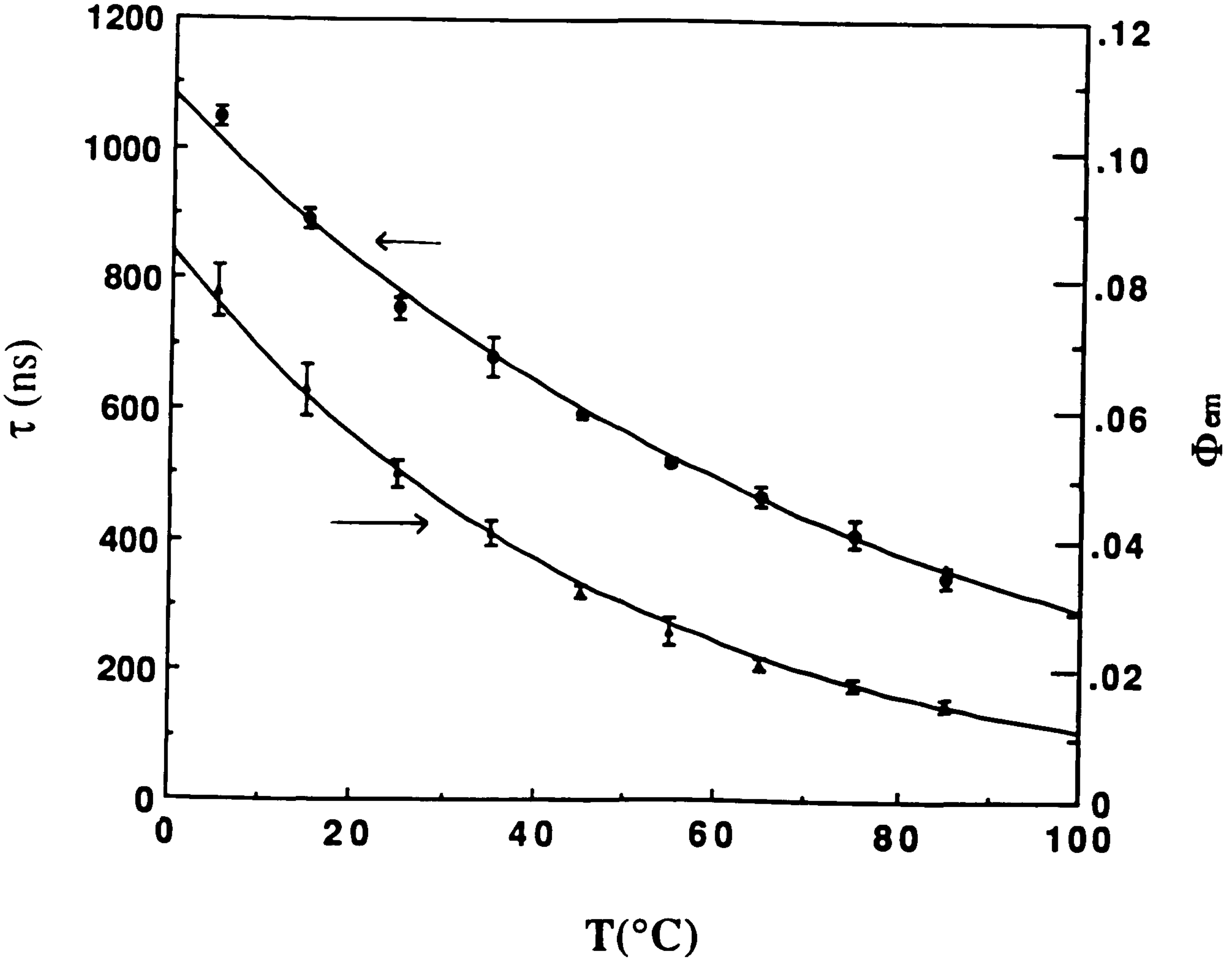
1200
1000
800
600
400
200
0
τ (ns)
.12
.10
.08
.06
.04
.02
0
Φem
0
20
40
60
80
100
T(°C)

Figure 33. Temperature dependence of Φ_{em}/τ ratio for $Ru(bpy)_3^{2+}$ (a) in aqueous solution (o calculated from data reported by Watts, Ref.8; • calculated from this experiment) and (b) adsorbed onto PVG.

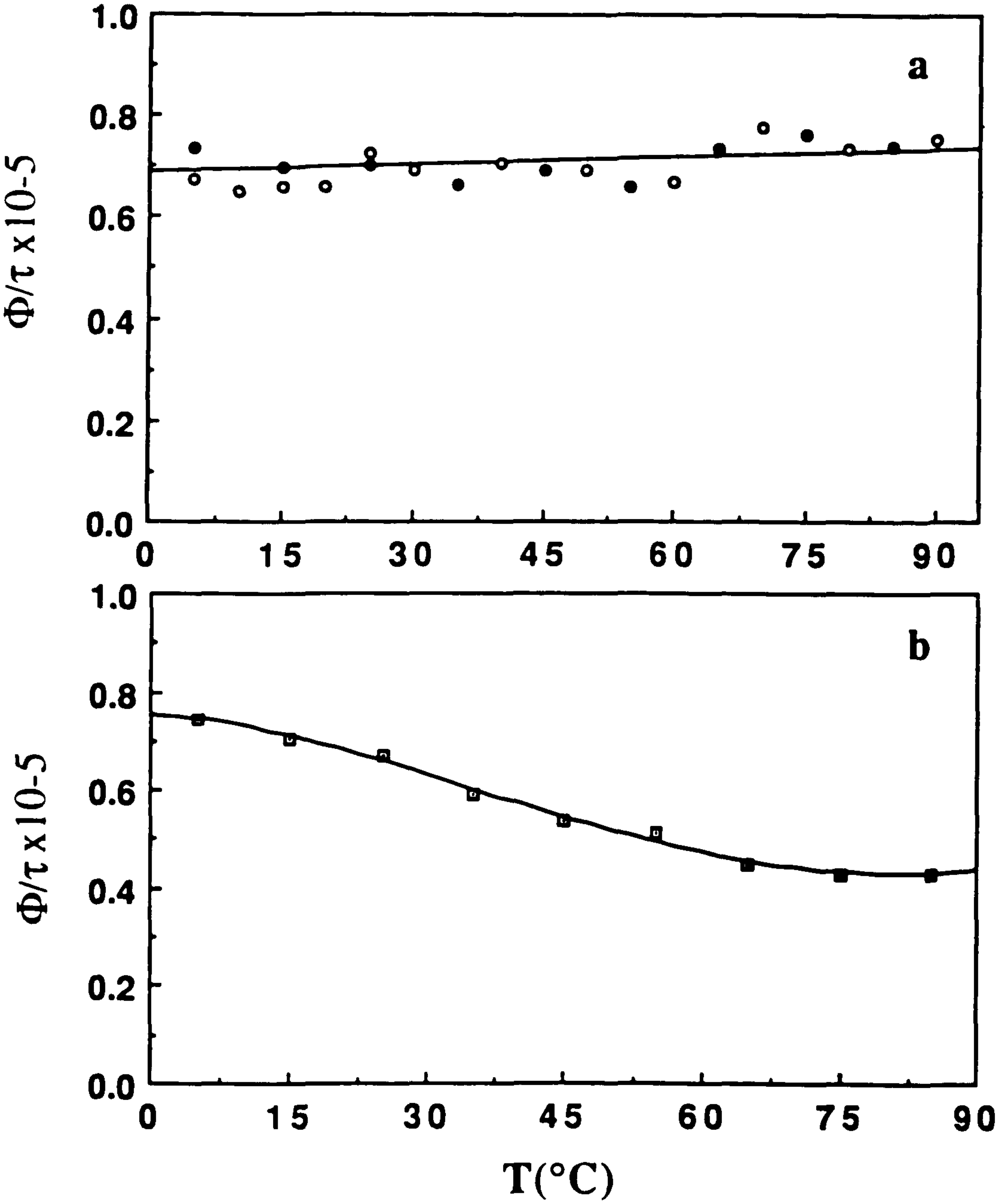
a
b
Φ/τ x10-5
Φ/τ x10-5
1.0
0.8
0.6
0.4
0.2
0.0
0
15
30
45
60
75
90
T(°C)

range interaction increases with increasing surface coverage. Yet, the results obtained in these experiments are independent of initial loading. Furthermore, spectral data indicate a uniform distribution of $Ru(bpy)_3^{2+}$(ads), so that loadings of $\leq 10^{-6}$ mole/g correspond to average spacings of ≥55 Å between the adsorbate ions.[124] Since this is more than double currently known long-range interaction distances,[141] a long range interaction seems unlikely and is discounted. Instead, self quenching requires some degree of adsorbate mobility to achieve a more reasonable interaction distance, or consistent with previous results, a contact interaction. Yet, the emission polarization ratio for $Ru(bpy)_3^{2+}$(ads), 0.16 ± 0.02 with 465-nm excitation, is within experimental error of that measured in 77K hydrocarbon glasses, and independent of temperature from 5°C to 90°C.[110] Since rotational motion would be expected to accompany translational mobility, the excited complex is immobile during its excited state lifetime, and the temperature dependence reflects the intrinsic differences in the excited state dynamics of $Ru(bpy)_3^{2+}$(ads) as compared with those of $Ru(bpy)_3^{2+}$ in aqueous solution.

III. Photochemistry

A 350-nm photolysis of 5.5×10^{-5} M $Ru(bpy)_3^{2+}$ in degassed 0.1 M HCl at 83 °C causes a decline in absorbance at 450 nm, and a corresponding increase at 370 nm (Figure 34a). The spectral changes are similar to those reported by Van Houten and Watts,[8] although with 350-nm excitation, a

Figure 34. Spectral changes during 350-nm photolysis of $Ru(bpy)_3^{2+}$ at 83 °C in (a) 0.1 M HCl aqueous solution and (b) adsorbed onto PVG. Numbers refer to photolysis times in hours.

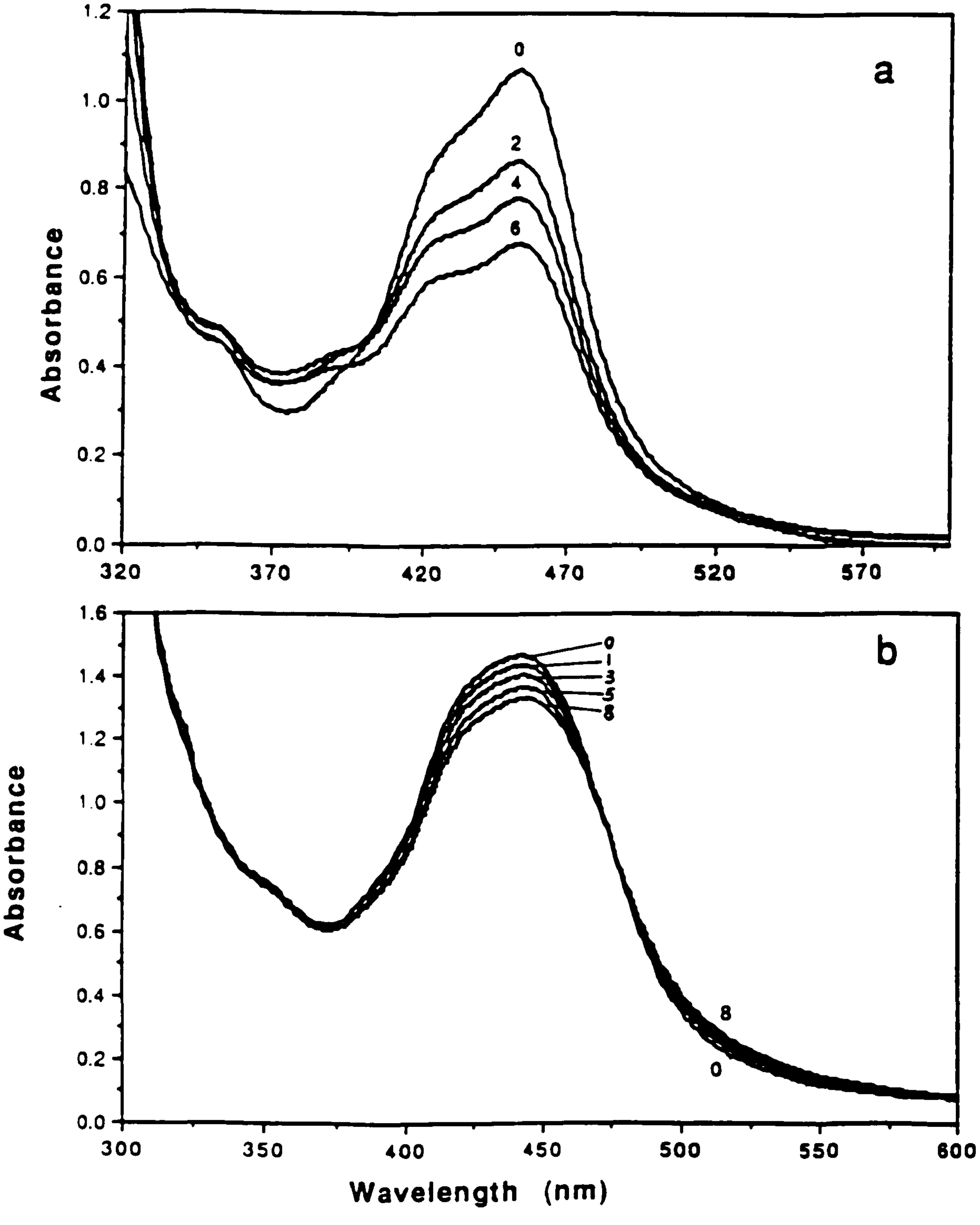
a
0
2
4
6
Absorbance
1.2
1.0
0.8
0.6
0.4
0.2
0.0
320
370
420
470
520
570
b
0
1
3
5
8
8
0
Absorbance
1.6
1.4
1.2
1.0
0.8
0.6
0.4
0.2
0.0
300
350
400
450
500
550
600
Wavelength (nm)

shoulder at 500 nm did not appear during the initial stages of photolysis. Nevertheless, the subsequent changes indicate bipyridine photolabilization, and, at 83 °C, the quantum efficiency of the process, calculated via equation 21, is $3.8\pm0.7\text{x } 10^{-3}$ with 350-nm excitation.

The HCl concentration can not be duplicated in the glass matrix since, at 83 °C, the concentration of H^+ needed to trap the dissociated ligand is also sufficient to dissolve the glass matrix. However, the silanol groups on the glass surface are capable of coordinating metal ions and complexes, and trapping a variety of photogenerated intermediates. Cation exchanging $Ru(bpy)_3^{2+}$ onto the glass places two $Si\text{-}O^-$ functionalities near the complex, and based on an average of 4-7 silanol groups/100 $Å^2$,[116] the planar surface area covered by the complex, 171 $Å^2$, places 7-10 silanol groups in the immediate vicinity of the complex. A reduction in quantum efficiency may occur, but not necessarily a change in reaction pathway. However, the spectral changes that occur during a 350-nm photolysis of a degassed sample containing $1.2\text{x}10^{-6}$ mole of $Ru(bpy)_3^{2+}$(ads) at 83 °C (Figure 34b) are inconsistent with ligand labilization. A decline in absorbance at 452 nm accompanied by an increase in the 510-520-nm region in the ratio of 2.2 ± 0.1 is similar to spectral changes observed during the photoinduced disproportionation of $Ru(bpy)_3^{2+}$(ads).[124] The quantum efficiency of $Ru(bpy)_3^{2+}$(ads) disappearance, $4.1\pm0.1\text{x}10^{-4}$, is also within the range of values found for the disproportion reaction.[124]

IV. The Effect of NH_3 on Photoinduced Disproportionation of $Ru(bpy)_3^{2+}(ads)$

(i) Diffuse Reflectance FTIR Spectra

Previous studies have suggested that the photoinduced electron transfer chemistry of $Ru(bpy)_3^{2+}$ on the PVG surface involved photoinduced ionization of the complex and the population of intermediate surface acceptor sites by the photodetached electrons.[124] One possibility is that the B_2O_3 surface Lewis acid sites are the surface acceptor sites. The B_2O_3 Lewis acid sites are a consequence of the method of manufacture of the glass. PVG, 96% SiO_2, 3% B_2O_3 and 1% Al_2O_3, is acid leached to remove the boron phase. Nevertheless, some boron remains, and some estimates indicate that as much as 33% of the surface maybe B_2O_3.[123] Their number and Lewis acid character suggest that they could act as electron acceptors, but in forming a radical species would remain sufficiently reactive to liberate an electron on thermal activation.[124]

The role of these surface B_2O_3 Lewis acid sites in the electron transport process was examined by selectively reacting these sites with NH_3. NH_3 can be adsorbed on PVG surface via two mechanisms.[117] One mechanism involves physisorption, where the NH_3 molecule is bonded to surface hydroxyl group through H-bonding. The other involves chemisorption, where the NH_3 molecule reacts with the surface Lewis acid sites through the nitrogen lone-pair electrons to form a donor-acceptor complex. IR spectra of PVG exposed to NH_3 showed that, in the N-H stretching region, bands occurring at 3320 and 3400 cm^{-1} were easily removed by evacuation, and were assigned to physisorbed NH_3. Additional bands occurring at 3280 and 3365 cm^{-1} were not removed by evacuation even at temperatures as high as 150 °C, and were assigned to chemisorbed NH_3.[117]

To confirm these results and to obtain the conditions for selectively adsorbing NH_3 onto the B_2O_3 sites, tests were carried out on blank and impregnated PVG samples to determine the optimal exposure and evacuation times. FTIR spectra of calcined PVG between 3900 and 3100 cm^{-1} (Figure 35a) show a sharp band at 3744 cm^{-1}, which is assigned to free surface silanol groups, and a broad band at 3660 cm^{-1}, which is assigned to adjacent hydrogen bonded hydroxyl groups, i.e., associated silanol groups. After a 30 minute exposure to 760 torr of NH_3, the silanol bands disappear, and a series of bands in the 3400-3200 cm^{-1} region appear (Figure 35b). Longer exposure times of up to 2 hours cause no further spectral change. The intense band at 3333 cm^{-1} is assigned to NH_3 in the surrounding gas phase (Figure 35b).[116] Evacuating the chamber ($P = 6 \times 10^{-3}$ torr) at room temperature causes the 3333 cm^{-1} band to disappear within 10 minutes and a continuous decline of the 3400 and 3320 cm^{-1} bands occurs over a period of 3 to 4 hours (Figure 36). Concurrent with the latter change is a regrowth of 3744 and 3660 cm^{-1} silanol bands (Figure 36). However, the bands at 3365 and 3280 cm^{-1} are unchanged at room temperature even after overnight evacuation (Figure 36), but disappear if the sample is heated to 200 °C. Consequently, the bands at

Figure 35. FTIR spectra of calcined PVG (a) before exposure to NH_3 and (b) after exposure to 760 torr of NH_3 for 30 minutes.

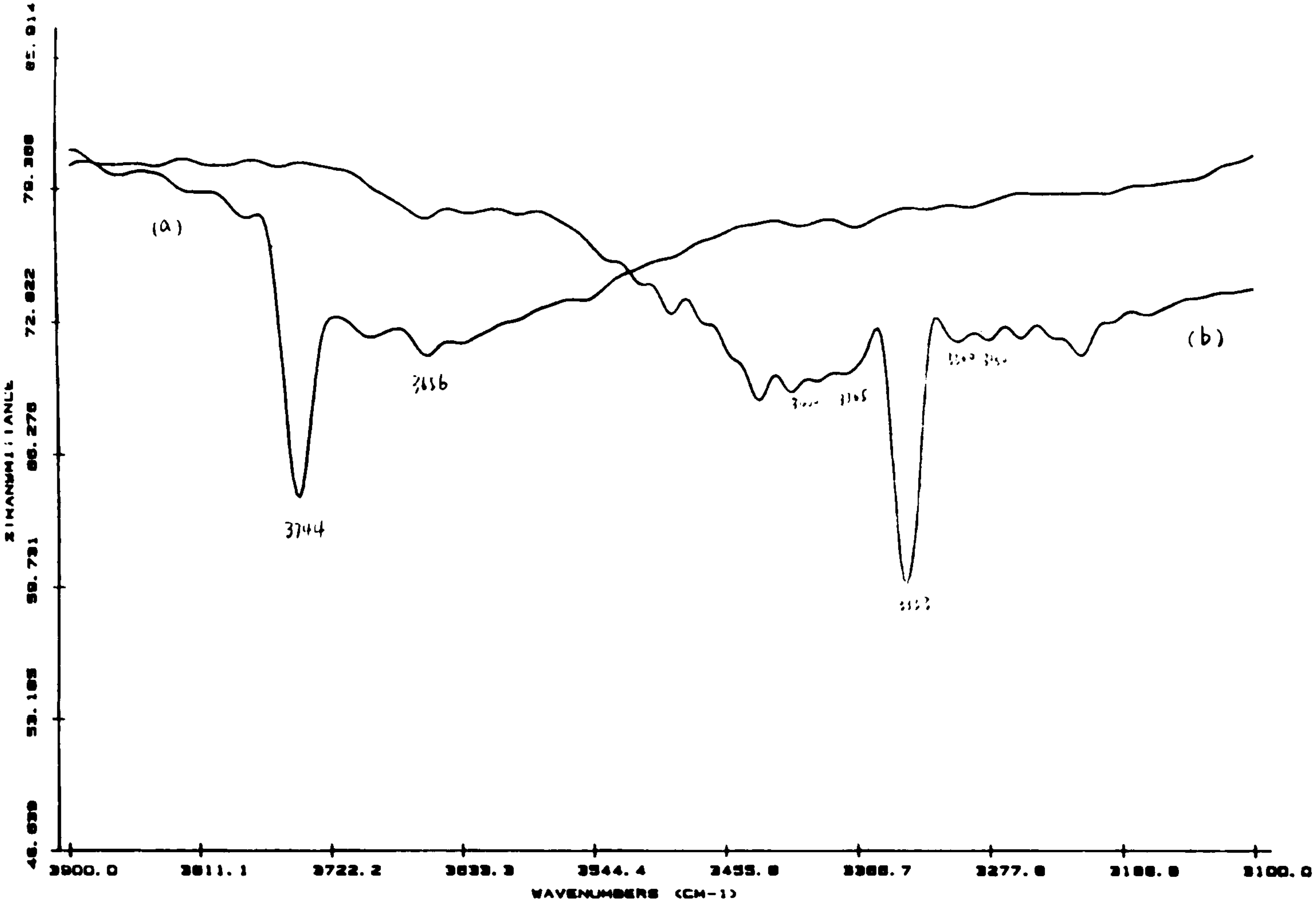
85.914
79.368
72.822
66.278
59.731
53.185
46.639
%TRANSMITTANCE
3900.0
3811.1
3722.2
3633.3
3544.4
3455.6
3366.7
3277.8
3188.9
3100.0
WAVENUMBERS (CM-1)
(a)
(b)
3744
3656
3305

Figure 36. FTIR spectra recorded during evacuation of a calcined PVG sample which had been exposed to NH_3 for 30 minutes.

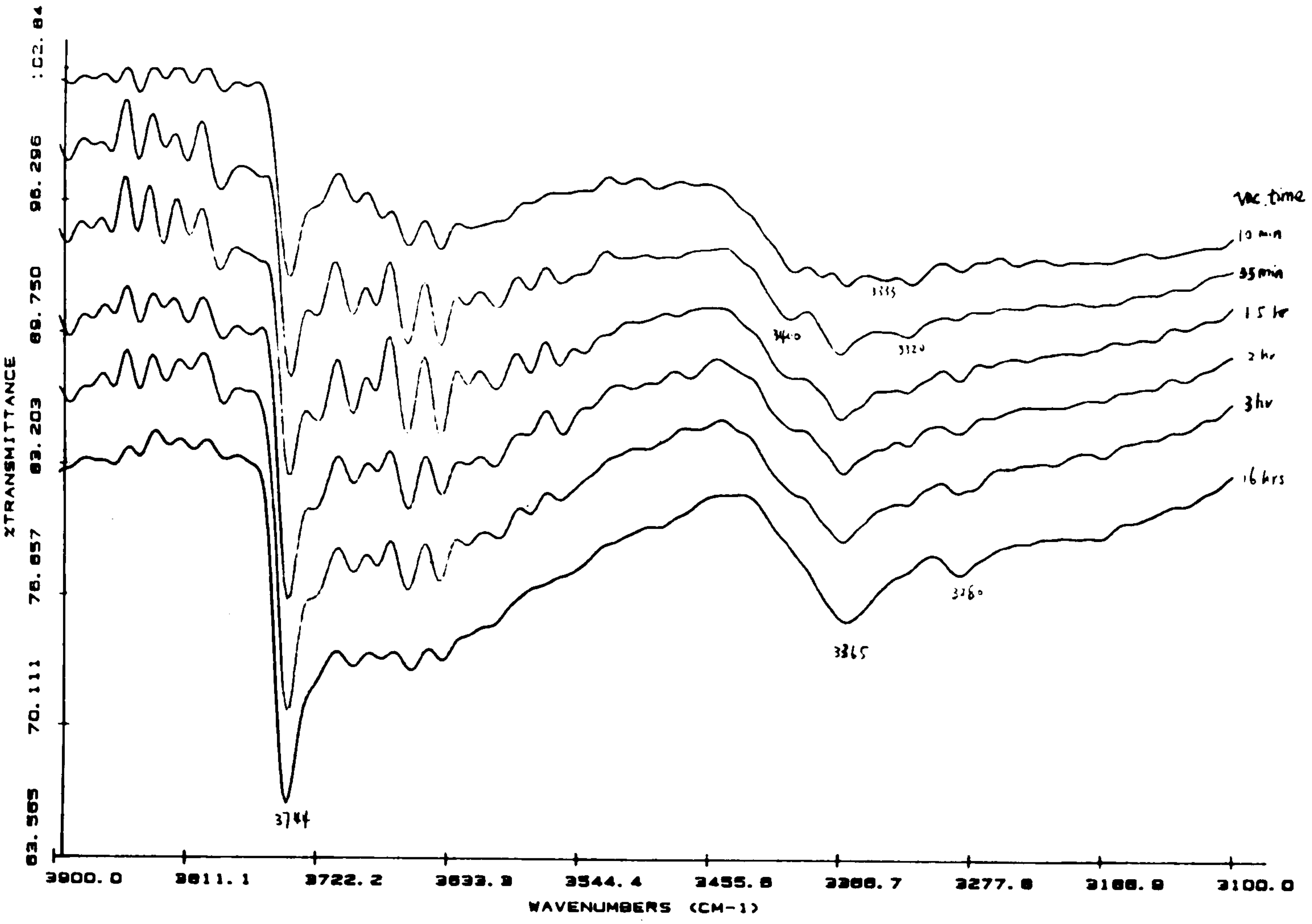
%TRANSMITTANCE
63.565
70.111
76.657
83.203
89.750
96.296
102.84
3900.0
3811.1
3722.2
3633.3
3544.4
3455.6
3366.7
3277.8
3188.9
3100.0
WAVENUMBERS (CM-1)
3744
3400
3335
3320
3365
3260
Vac. time
10 min
35 min
1.5 hr
2 hr
3 hr
16 hrs

3400 and 3320 cm^{-1} are assigned to physisorbed NH_3, while the bands at 3365 and 3280 cm^{-1} are assigned to chemisorbed NH_3. Desorption of the physisorbed NH_3 without a concurrent loss of the chemisorbed NH_3 indicated that it would be possible to selectively tie up the B_2O_3 Lewis acid sites. To further establish the point, similar experiments were carried out with silica gel.

The composition of silica gel is same as PVG, except that the former does not contain B_2O_3 Lewis acid sites. Therefore, only physisorption would be expected to occur. The FTIR spectrum of silica gel (Figure 37a) is similar to that of blank PVG (Figure 35a). The band at 3740 cm^{-1} is assigned to free surface OH, and as found with PVG, rapidly disappears after a 30 minute exposure to 760 torr of NH_3, with the concurrent appearance of N-H bands in the 3400-3200 cm^{-1} region (Figure 37b). However, in contrast with the PVG sample, after pumping out the NH_3 in surrounding gas phase, only bands at 3400 and 3320 cm^{-1} are found (Figure 38). Continuous pumping of the sample at room temperature ($P \leq 1 \times 10^{-2}$ torr) leads to a loss of the 3400 and 3320 cm^{-1} bands and concurrent reappearance of the 3740 cm^{-1} silanol band (Figure 38). The decline in intensity of the 3400 and 3320 cm^{-1} bands at room temperature indicates physisorbed NH_3, and consistent with the absence of B_2O_3 Lewis acid sites in silica gel, there is no spectroscopic evidence of chemisorbed NH_3.

Similar results are obtained with powdered PVG samples impregnated

Figure 37. FTIR spectra of silica gel (a) before exposure to NH_3 and (b) after exposure to 760 torr of NH_3 for 30 minutes.

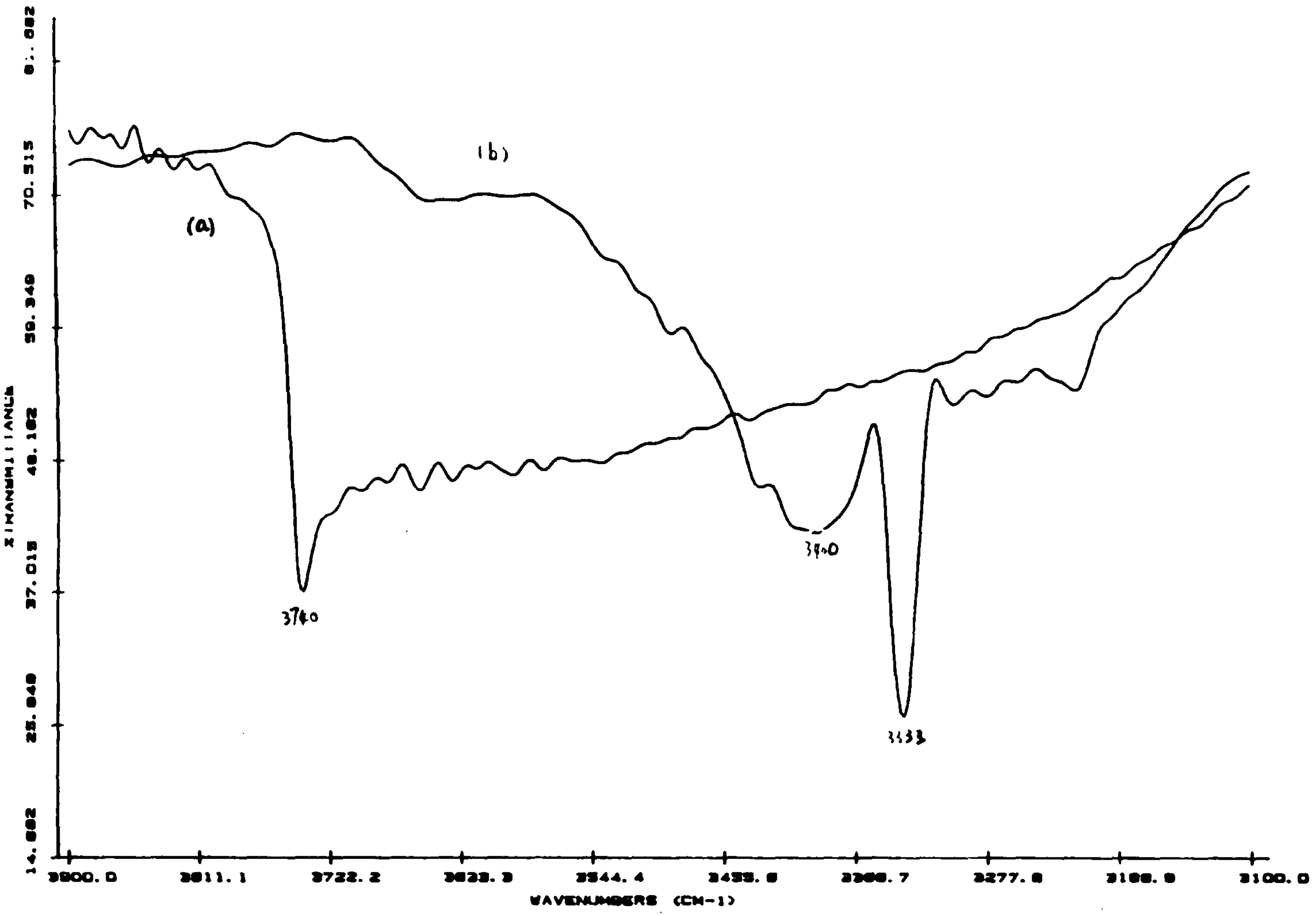
81.682
70.515
59.349
48.182
37.015
25.849
14.682
%TRANSMITTANCE
3900.0
3811.1
3722.2
3633.3
3544.4
3455.6
3366.7
3277.8
3188.9
3100.0
WAVENUMBERS (CM-1)
(a)
(b)
3740
3400
3333

Figure 38. FTIR spectra recorded during evacuation of a silica gel sample which had been exposed to NH_3 for 30 minutes.

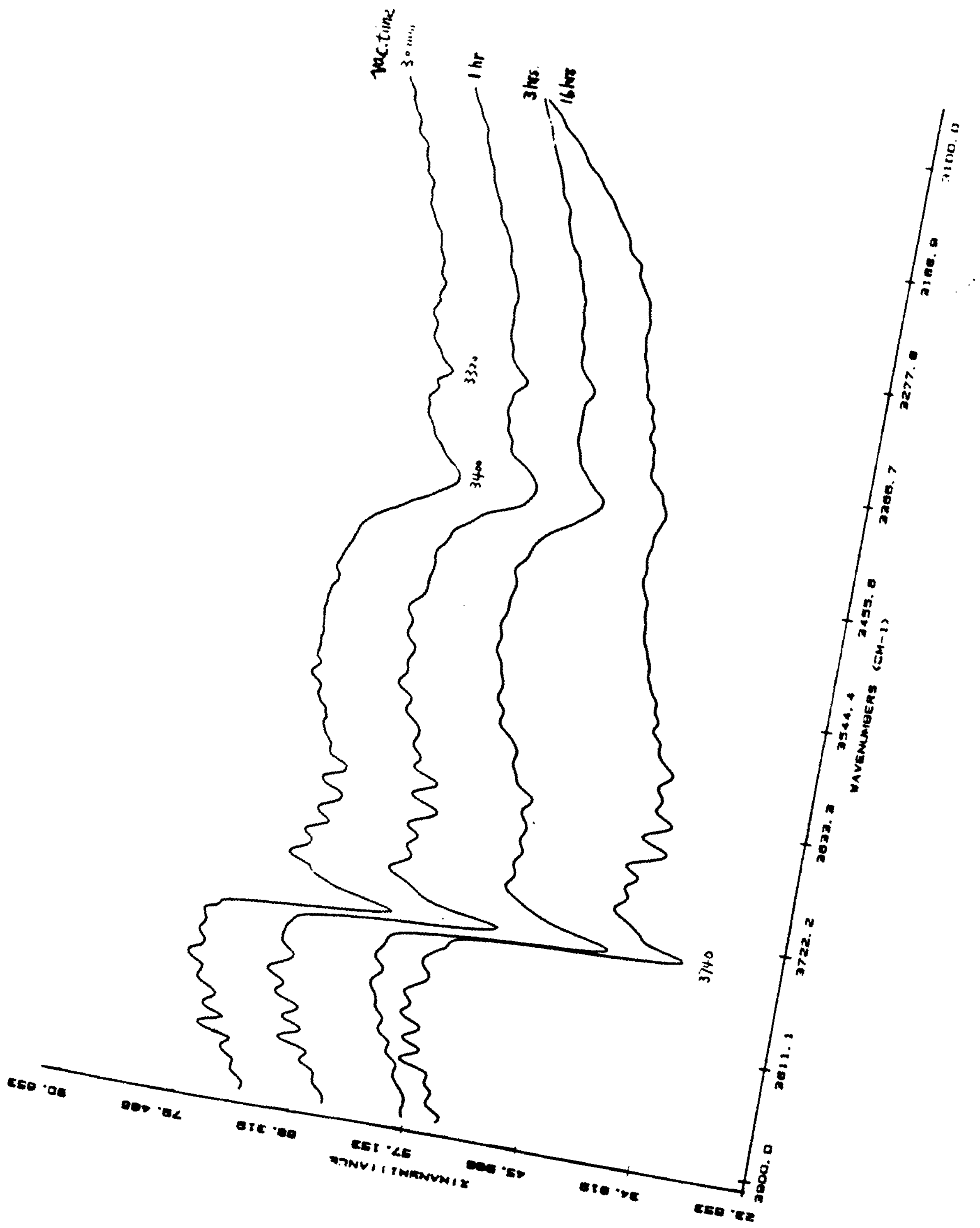
vac. time
30 min
1 hr
3 hrs
16 hrs
3320
3400
3740
3900.0
3811.1
3722.2
3633.3
3544.4
3455.6
3366.7
3277.8
3188.9
3100.0
WAVENUMBERS (CM-1)
23.653
34.818
45.986
57.153
68.319
79.486
90.653
%TRANSMITTANCE

with $Ru(bpy)_3^{2+}$(ads). FTIR spectra were recorded before and after exposure to NH_3 for samples with loadings of 1.2×10^{-7} to 3.8×10^{-6} moles of $Ru(bpy)_3^{2+}$/g of PVG. Figure 39 is the FTIR spectrum between 3900 and 3100 cm^{-1} recorded before the sample was exposed to NH_3. Compared with that of blank PVG, the decrease of intensity of the free silanol band at 3744 cm^{-1} is due to the adsorption of the compound via cation exchange with silanol proton. Figure 40 is the spectra recorded during the evacuation of the sample ($P \leq 1 \times 10^{-2}$ torr) after a 30 minute exposure to NH_3. Consistent with the other results, as the time of evacuation increases, bands assigned to physisorbed NH_3 decrease, while those assigned to chemisorbed NH_3 remain constant.

(ii) Continuous Photolysis

(1) UV-visible Spectra

Continuous photolysis of the impregnated PVG sample in vacuum with 457.9-nm Ar^+ laser causes disproportionation

$$2Ru(bpy)_3^{2+}(ads) \text{--->} Ru(bpy)_3^{3+}(ads) + [Ru(bpy)_2(bpy^-)]^+(ads) \qquad [32]$$

The reduction product, $[Ru(bpy)_2(bpy^-)]^+$(ads), is stable and exists for several days in vacuum. During the photolysis, the region being photolyzed turns darker. As shown in Figure 41, the color change corresponds to a decrease in absorbance at 450-nm, indicative of the loss of $Ru(bpy)_3^{2+}$, and a

Figure 39. FTIR spectra of degassed Ru(bpy)$_3^{2+}$(ads) sample between 3100 and 3900 cm^{-1}.

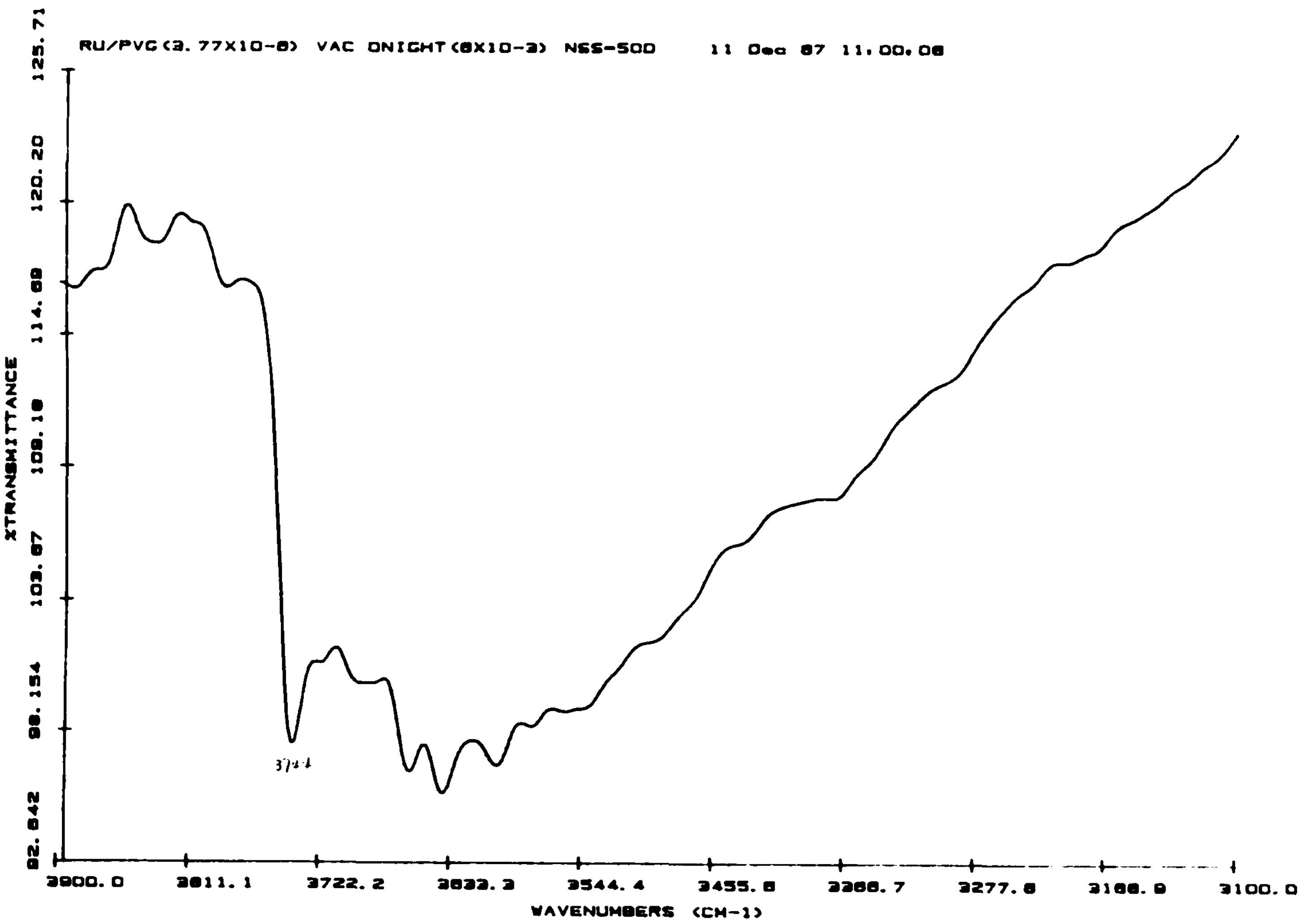
RU/PVC(3.77X10-6) VAC ONIGHT(6X10-3) NSS-500 11 Dec 87 11:00:06
%TRANSMITTANCE
125.71
120.20
114.69
109.18
103.67
98.154
92.642
3744
3900.0
3811.1
3722.2
3633.3
3544.4
3455.6
3366.7
3277.8
3188.9
3100.0
WAVENUMBERS (CM-1)

Figure 40. FTIR spectra recorded during evacuation of a $Ru(bpy)_3^{2+}$(ads) sample which had been exposed to NH_3 for 30 minutes.

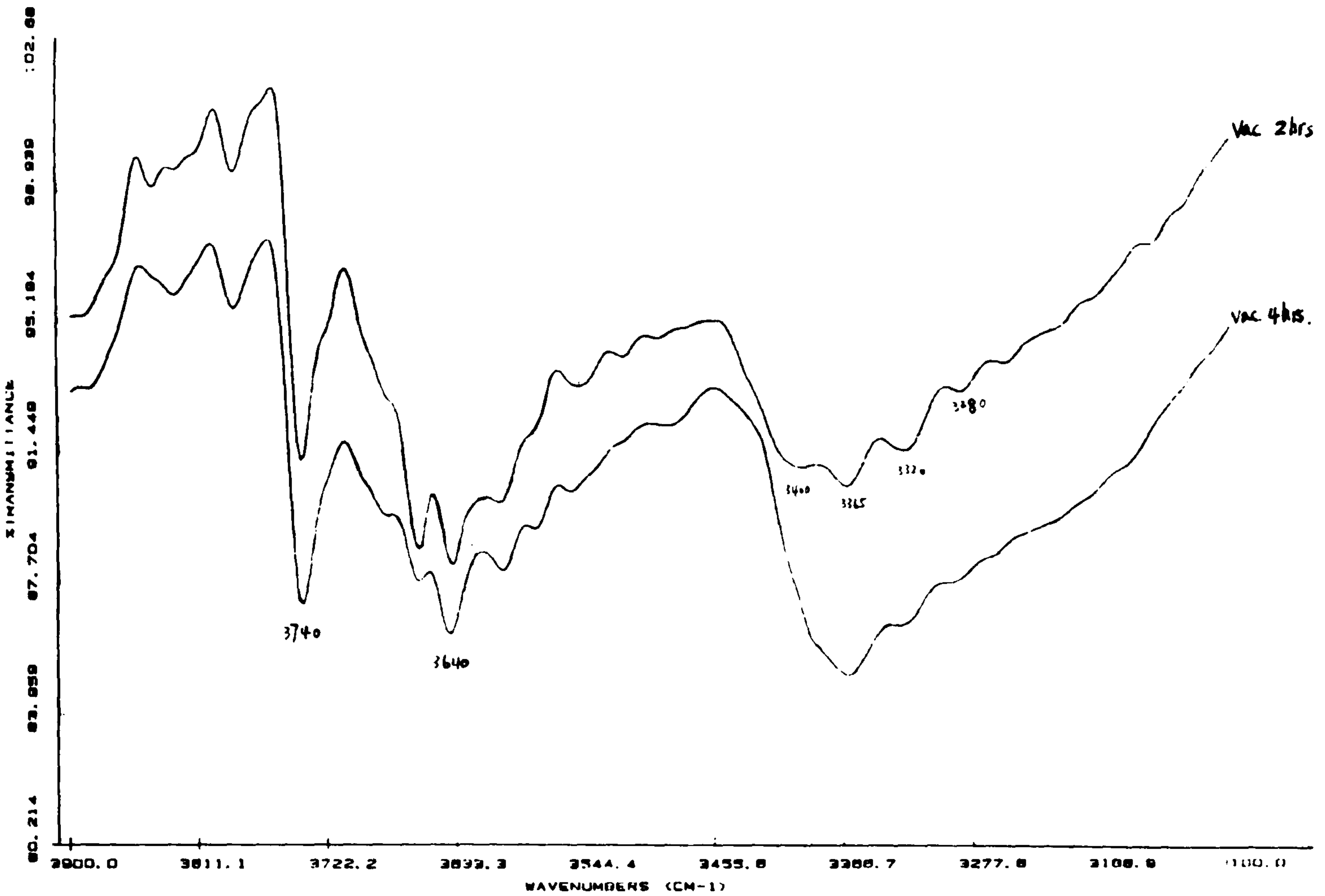
102.68
98.939
95.184
91.448
87.704
83.959
80.214
%TRANSMITTANCE
3900.0
3811.1
3722.2
3633.3
3544.4
3455.6
3366.7
3277.8
3188.9
3100.0
WAVENUMBERS (CM-1)
Vac 2hrs
Vac 4hrs.
3740
3640
3400
3365
3320
3280

concurrent increase in absorbance at 510-nm, indicative of the formation of $[Ru(bpy)_2(bpy^-)]^+$(ads). All of these results are consistent with previous work.[124] However, the interesting thing is when the photolysis was carried out on the degassed impregnated samples containing chemisorbed NH_3. The same reaction was observed, but the rate of the reaction is much faster, since the region being photolyzed turned darker much more quickly than the unexposed samples. Figure 42 shows the spectral changes before and after the photolysis of a degassed sample containing chemisorbed NH_3. Compared with Figure 41, although the initial loadings and the photolysis conditions are the same, the changes of the absorbance at 510-nm and 452-nm are larger for NH_3 treated samples than for the untreated sample. However, although the reaction rates differ, both spectra show that the ratio of the absorbance changes, $\Delta A_{450\text{-nm}}/ \Delta A_{510\text{-nm}}$, is about 2, and it is independent of the initial loadings. Calculation of the reaction stoichiometry from these absorbance changes by using the corresponding molar extinction coefficients ($\varepsilon = 1.2x10^4\ M^{-1}cm^{-1}$ at 510-nm for $[Ru(bpy)_2(bpy^-)]^+$(ads) and $\varepsilon = 1.49x10^4\ M^{-1}cm^{-1}$ at 450-nm for $Ru(bpy)_3^{2+}$(ads)) shows that for every one mole of $[Ru(bpy)_2(bpy^-)]^+$(ads) produced, 2.1±0.6 moles of $Ru(bpy)_3^{2+}$(ads) are consumed in the NH_3 untreated samples, while the ratio is 2.2±0.8 in the NH_3 treated samples. In both cases, the ratios are consistent with a photoinduced disproportionation.

(2) EPR spectra

Figure 41. UV-visible spectra recorded before (a) and after (b) photolysis of a degassed Ru(bpy)$_3^{2+}$(ads) sample. λ_{ex} = 457.9 nm, P = 0.1 W.

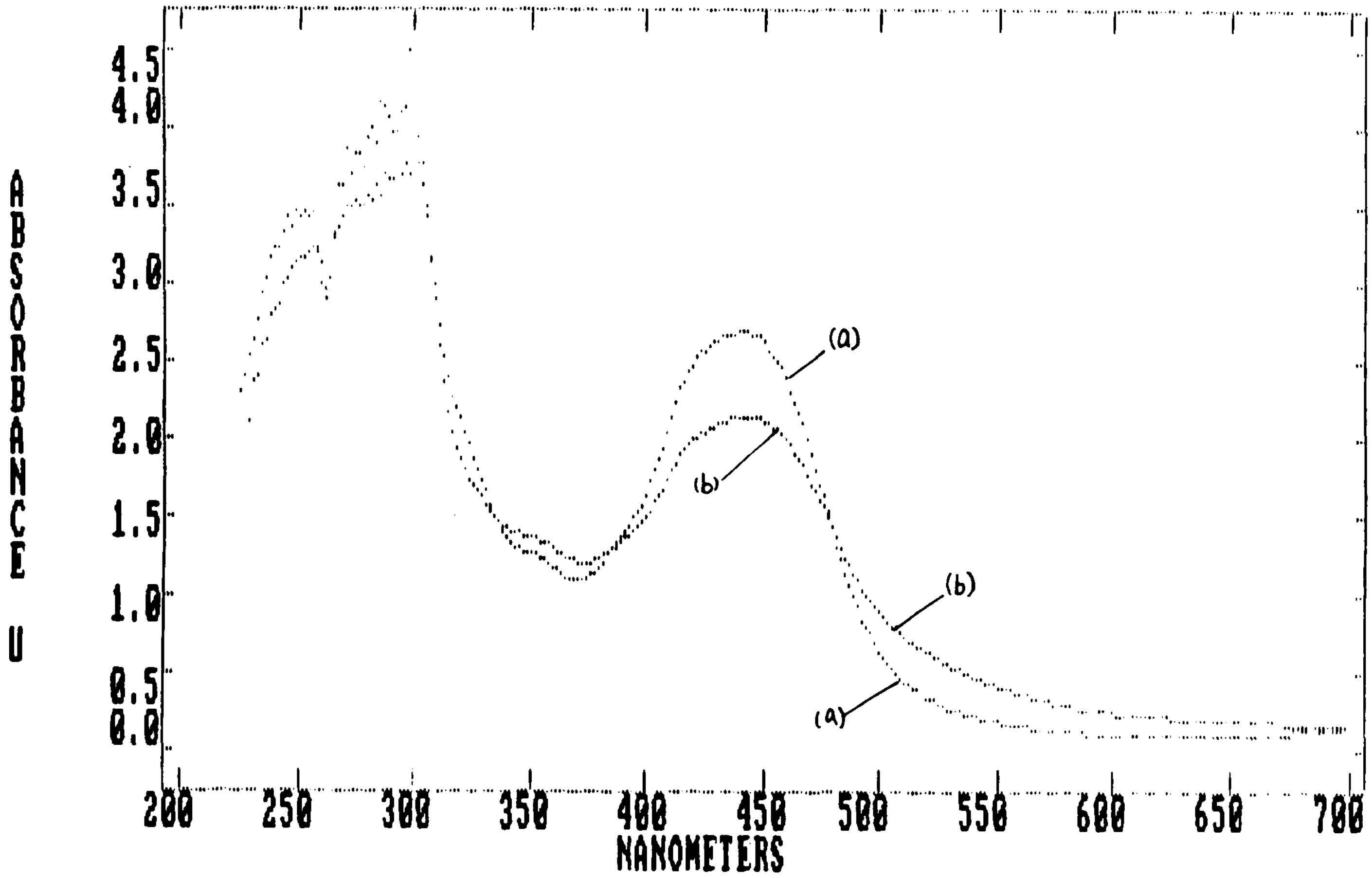
ABSORBANCE U
4.5
4.0
3.5
3.0
2.5
2.0
1.5
1.0
0.5
0.0
200
250
300
350
400
450
500
550
600
650
700
NANOMETERS
(a)
(b)
(b)
(a)

Figure 42. UV-visible spectra recorded before (a) and after (b) photolysis of a degassed Ru(bpy)$_3^{2+}$(ads) sample with chemisorbed NH$_3$. λ_{ex} = 457.9 nm, P = 0.1 W.

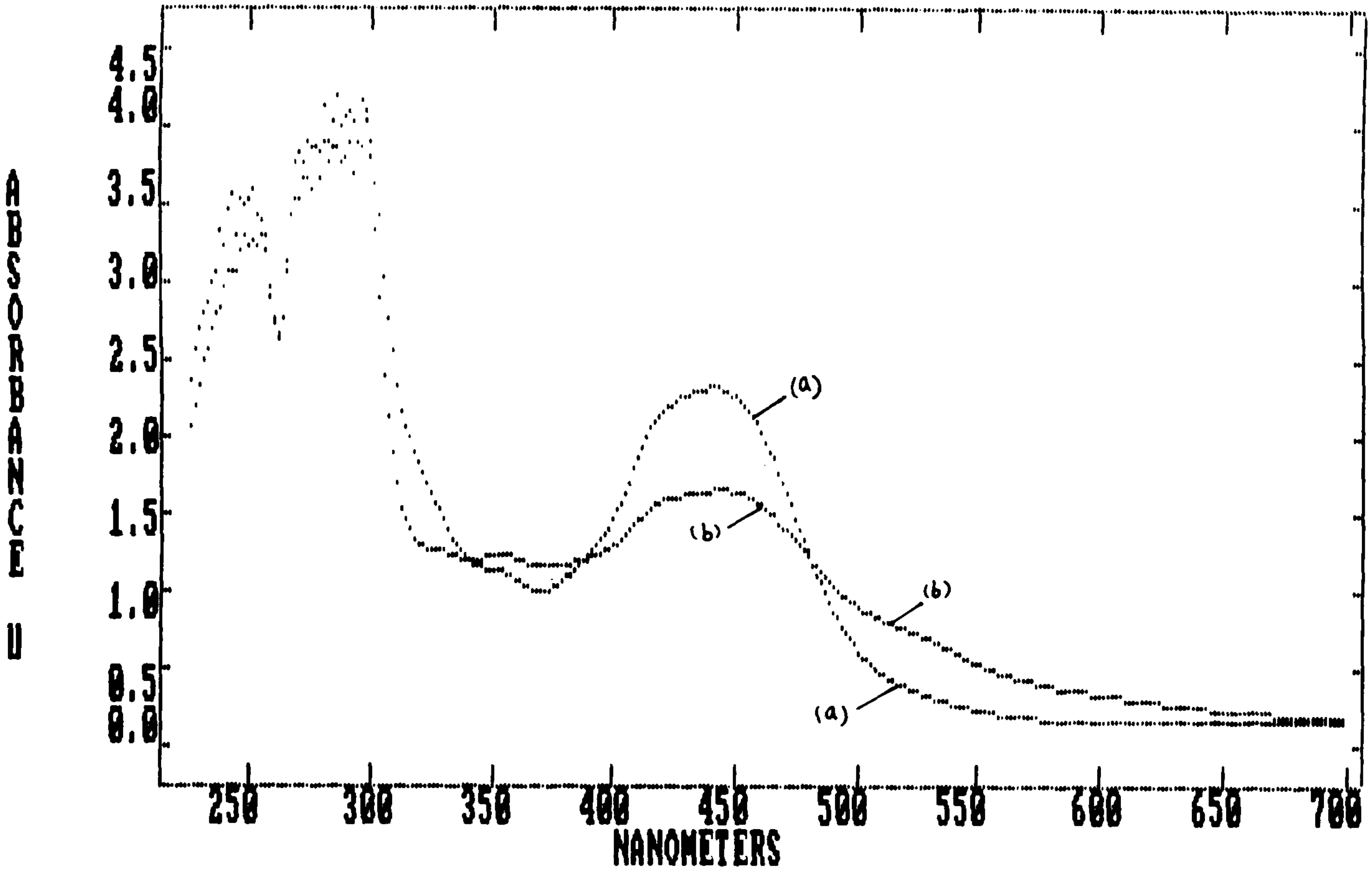
ABSORBANCE U
4.5
4.0
3.5
3.0
2.5
2.0
1.5
1.0
0.5
0.0
250
300
350
400
450
500
550
600
650
700
NANOMETERS
(a)
(b)
(b)
(a)

EPR spectra recorded periodically during photolysis of the degassed impregnated samples with and without chemisorbed NH_3 are shown in Figures 44 and 43. Both spectra show that a signal with g = 2.01 and a peak-to-peak linewidth of 23 G increases with photolysis time. This is consistent with previous work, where an EPR signal with g = 2.0086 and a peak-to-peak linewidth of 25±2G produced during the photolysis was assigned to $[Ru(bpy)_2(bpy^-)]^+$(ads).[124] Besides, the spectra also show that the rate of the product formation for NH_3 treated samples is much faster than that for NH_3 untreated samples.

(iii) Concentration Dependence of Quantum Yield

Quantum yields can be calculated from the initial rates of $Ru(bpy)_3^+$(ads) formation, dn/dt, and the absorbed intensity, I_{abs}. The latter is calculated from an average of the initial and final absorbance, A, of the complex at the excitation wavelength

$$\Phi = (dn/dt)_{t=0} / I_{abs} \qquad [33]$$

$$= (dn/dt)_{t=0} / I_0 (1-10^{-A})$$

The calculation of absolute quantum yield involves the area exposed to the light, which is difficult to measure accurately, and the intensity of the excitation light. However, this is unnecessary since we are only interested in the relative change in the quantum yield as a function of loading. Under these conditions, the relative quantum yield is given by

Figure 43. EPR signal generated during the photolysis of a degassed $Ru(bpy)_3^{2+}$(ads) sample with a 350 W Hg lamp. Microwave power = 5 mW, microwave frequency = 9.70 GHz, Gain = $8x10^5$.

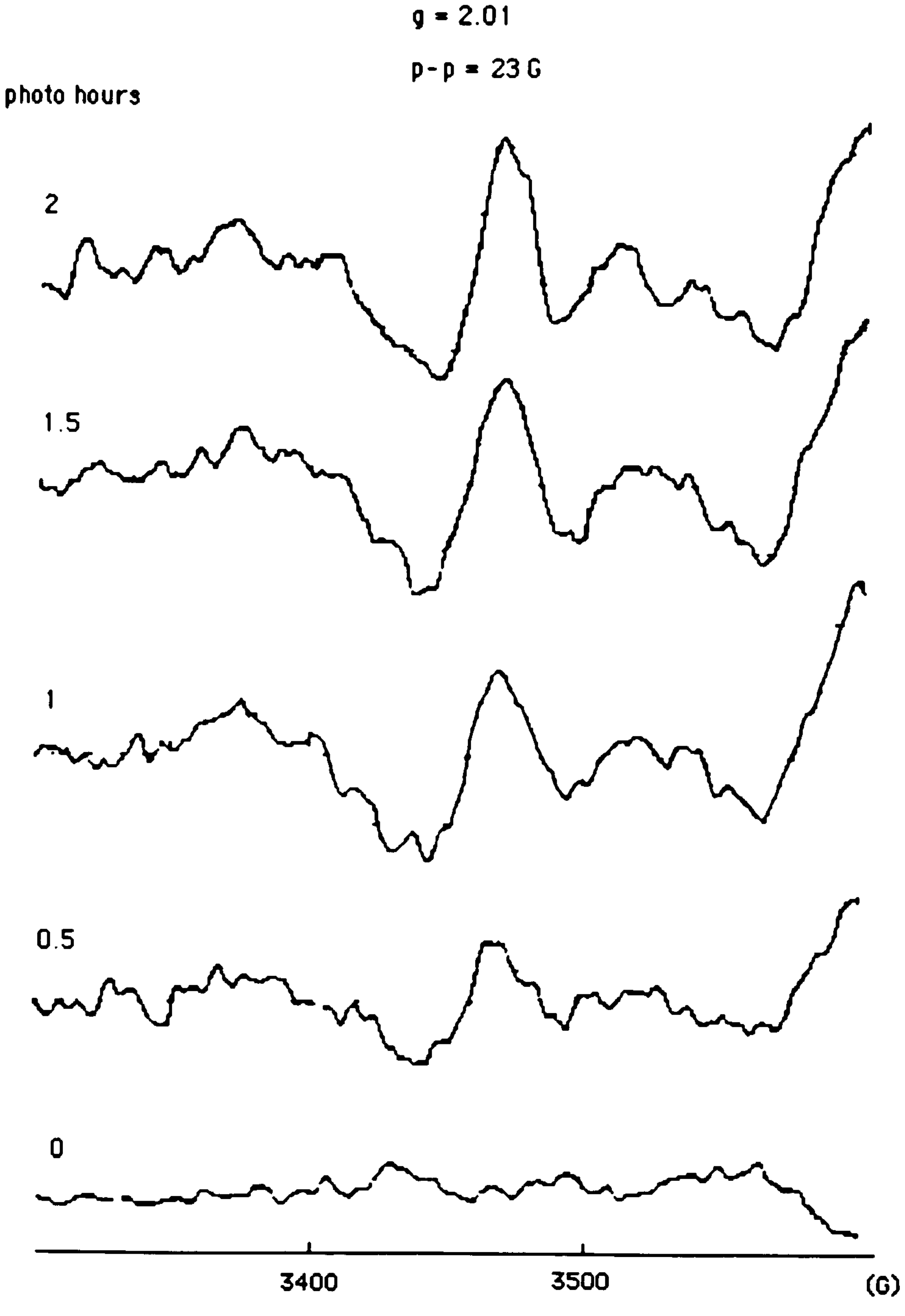
g = 2.01
p-p = 23 G
photo hours
2
1.5
1
0.5
0
3400
3500
(G)

Figure 44. EPR signal generated during the photolysis of a degassed $Ru(bpy)_3^{2+}$(ads) sample containing chemisorbed NH_3 with a 350 W Hg lamp. Microwave power = 2 mW, microwave frequency = 9.70 GHz, Gain = $8x10^5$.

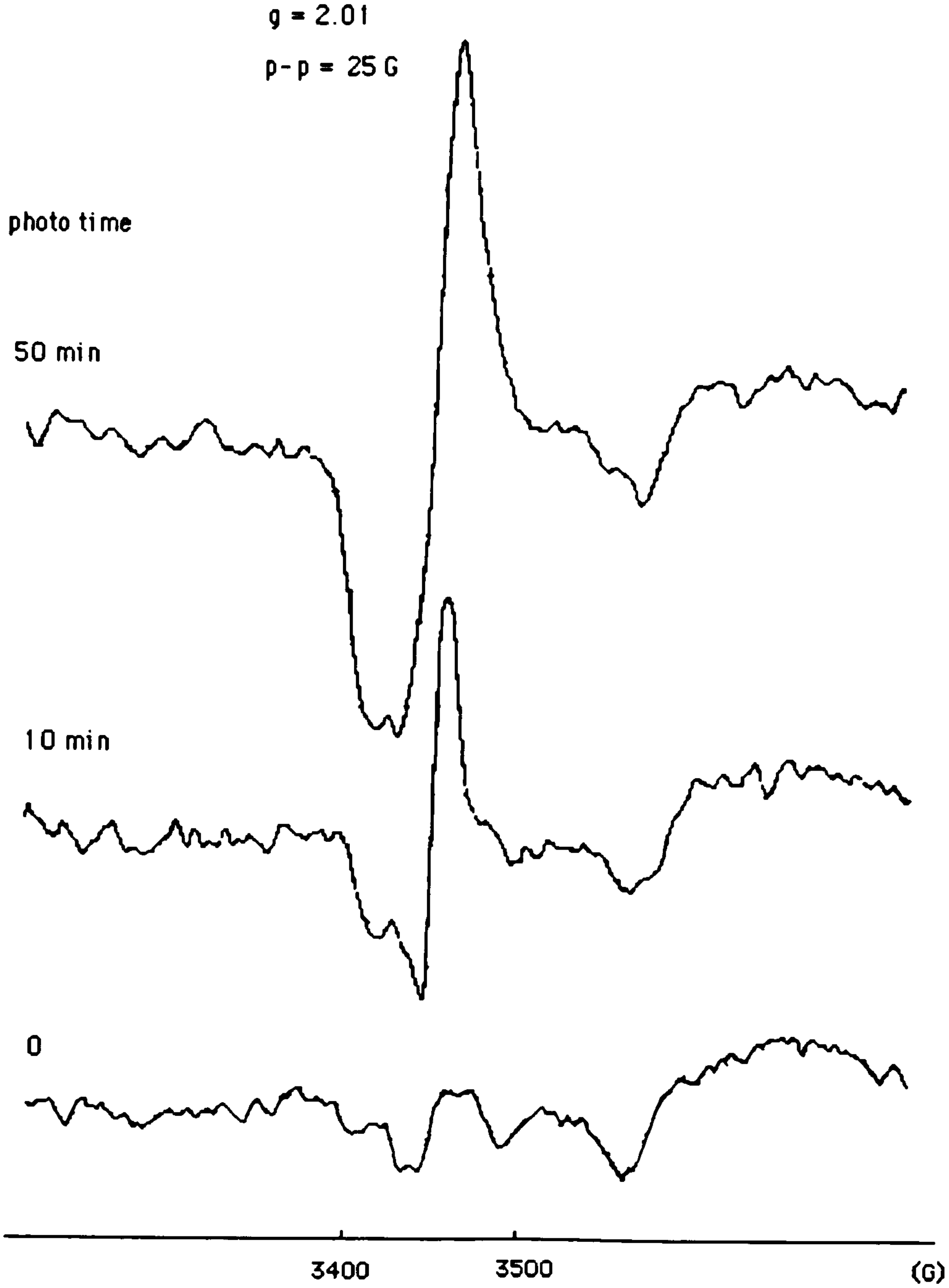
g = 2.01
p-p = 25 G
photo time
50 min
10 min
0
3400
3500
(G)

$$\begin{aligned}\Phi_1/\Phi_2 &= [(dn_1/dt)_{t=0}/(dn_2/dt)_{t=0}]\ [(1-10^{-A})_2/(1-10^{-A})_1] \qquad [34] \\ &= [(dA_{510}/dt)_{1,t=0}/(dA_{510}/dt)_{2,t=0}]\ [(1-10^{-A_{452}})_2/(1-10^{-A_{452}})_1]\end{aligned}$$

By choosing any one of the samples in a given series as a reference and taking its quantum yield arbitrarily to be 1, the relative quantum yields of the others are obtained by just measuring their absorbance at 452-nm before and after photolysis and absorbance at 510-nm as a function of photolysis time. The latter is then used to get the initial rate of absorbance change, $(dA_{510}/dt)_{t=0.}$ Figure 45 shows plots of absorbance at 510-nm vs. photolysis time for (a) a degassed sample that was not exposed to NH_3, and (b) a degassed sample with chemisorbed NH_3. The initial rate of $[Ru(bpy)_2(bpy^-)]^+$ formation, calculated from the slope of the curve at $t = 0$, is about three times larger for the latter than for the former.

Tables 7 and 8 list the relative quantum yields of disproportionation as a function of loading for (a) degassed samples that were not exposed to NH_3 (Table 7), and (b) the degassed samples with chemisorbed NH_3 (Table 8). Figures 46 and 47 are the corresponding plots of quantum yield vs. log of the moles of $Ru(bpy)_3^{2+}$/g of PVG, which show that for both sets of samples the maximum in the quantum yield occurs at a loading of $2.1\text{x}10^{-6}$ moles of $Ru(bpy)_3^{2+}$/g of PVG for NH_3 untreated samples, and at $1.8\text{x}10^{-6}$ mole of $Ru(bpy)_3^{2+}$/g of PVG for NH_3 treated samples, and decline at both lower and higher loadings. Figure 48 compares the relative values of quantum yield

Figure 45. The increase of absorbance at 510-nm vs. photolysis time for (a) degassed $Ru(bpy)_3^{2+}$(ads) (b) degassed $Ru(bpy)_3^{2+}$(ads) with chemisorbed NH_3. $\lambda_{ex} = 457.9$ nm, P = 0.1 W.

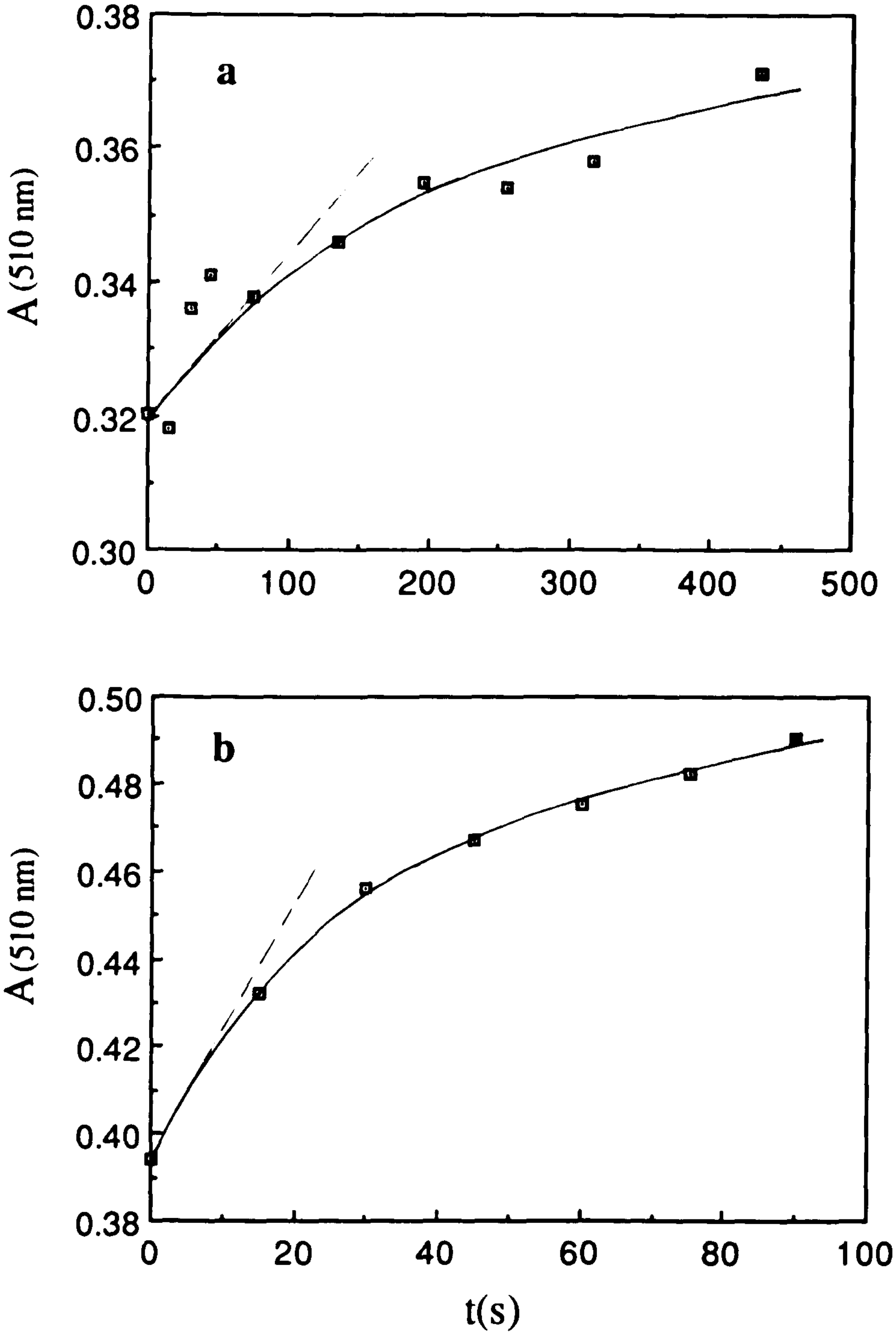
a
A (510 nm)
0.30
0.32
0.34
0.36
0.38
0
100
200
300
400
500
b
A (510 nm)
0.38
0.40
0.42
0.44
0.46
0.48
0.50
0
20
40
60
80
100
t(s)

Table 7. Quantum yields of disproportionation and other related parameters for degassed Ru(bpy)$_3^{2+}$(ads) samples vs. loading.

NO.	mole/g ($\times10^{-6}$)	A^{452}	A^{510}	$(dA^{510}/dt)_0$	$(1-A^{452})$	$\frac{(dA510/dt)_0}{(1-A452)}$	log(mole/g)	Φ
7a	0.094	.184	.024	1.94×10^{-5}	.345	5.62×10^{-5}	-7.03	.023
4b	0.55	1.281	.202	5.11×10^{-4}	.948	5.39×10^{-4}	-6.26	.219
8a	0.69	1.314	.214	9.33×10^{-4}	.951	9.81×10^{-4}	-6.16	.399
1a	0.84	1.705	.260	1.27×10^{-3}	.980	1.30×10^{-3}	-6.08	.527
1d	1.53	4.2	.474	2.1×10^{-3}	1	2.10×10^{-3}	-5.81	.854
3a	2.09	4.4	.666	2.46×10^{-3}	1	2.46×10^{-3}	-5.68	1
5a	3.21	4.3	.992	2.07×10^{-3}	1	2.07×10^{-3}	-5.49	.841
6b	3.33	5.99	1.165	2.33×10^{-3}	1	2.33×10^{-3}	-5.48	.947
5b	4.08	8.64	1.261	1.62×10^{-3}	1	1.62×10^{-3}	-5.39	.659
1b	11.3	22	2.62	8.89×10^{-4}	1	8.89×10^{-4}	-4.95	.361

Table 8. Quantum yields of disproportionation and other related parameters for degassed $Ru(bpy)_3^{2+}$(ads) samples with chemisorbed NH_3 vs. loading.

NO.	mole/g ($\times 10^{-6}$)	A^{452}	A^{510}	$(dA^{510}/dt)_0$	$(1-A^{452})$	$\frac{(dA510/dt)_0}{(1-A452)}$	log(mole/g)	Φ
7a	0.094	.221	.065	1.30×10^{-4}	.399	3.26×10^{-4}	-7.03	.055
		.206	.056	2.00×10^{-4}	.378	5.29×10^{-4}		.090
8c	0.21	.579	.109	1.20×10^{-3}	.736	1.63×10^{-3}	-6.69	.276
		.646	.128	1.53×10^{-3}	.774	1.98×10^{-3}		.336
7d	0.77	2.382	.426	2.70×10^{-3}	.996	2.71×10^{-3}	-6.11	.459
		2.463	.453	3.70×10^{-3}	.997	3.71×10^{-3}		.629
7c	1.18	4.0	.702	5.1×10^{-3}	1	5.1×10^{-3}	-5.93	.864
		3.86	.674	4.6×10^{-3}	1	4.6×10^{-3}		.780
9a	1.74	5.9	1.214	5.9×10^{-3}	1	5.9×10^{-3}	-5.76	1
			1.222	5.0×10^{-3}		5.0×10^{-3}		
			1.221	5.8×10^{-3}		5.8×10^{-3}		
6a	4.52	5.9	2.91	4×10^{-3}	1	4×10^{-3}	-5.34	.678
			2.86	4×10^{-3}		4×10^{-3}		
			2.85	4×10^{-3}		4×10^{-3}		
			2.86	4×10^{-3}		4×10^{-3}		
4a	8.20	5.9	5.9	3.2×10^{-3}	1	3.2×10^{-3}	-5.09	.542
		5.9	5.9	3.0×10^{-3}		3.0×10^{-3}		.508
2b	21.2	5.9	5.9	2.7×10^{-3}	1	2.7×10^{-3}	-4.67	.458
		5.9	5.9	1.7×10^{-3}		1.7×10^{-3}		.288
		5.9	5.9	3.3×10^{-4}		3.3×10^{-4}		.056

Figure 46. Quantum yields of disproportionation vs. log moles of $Ru(bpy)_3^{2+}$/g of PVG for degassed $Ru(bpy)_3^{2+}$(ads) samples.

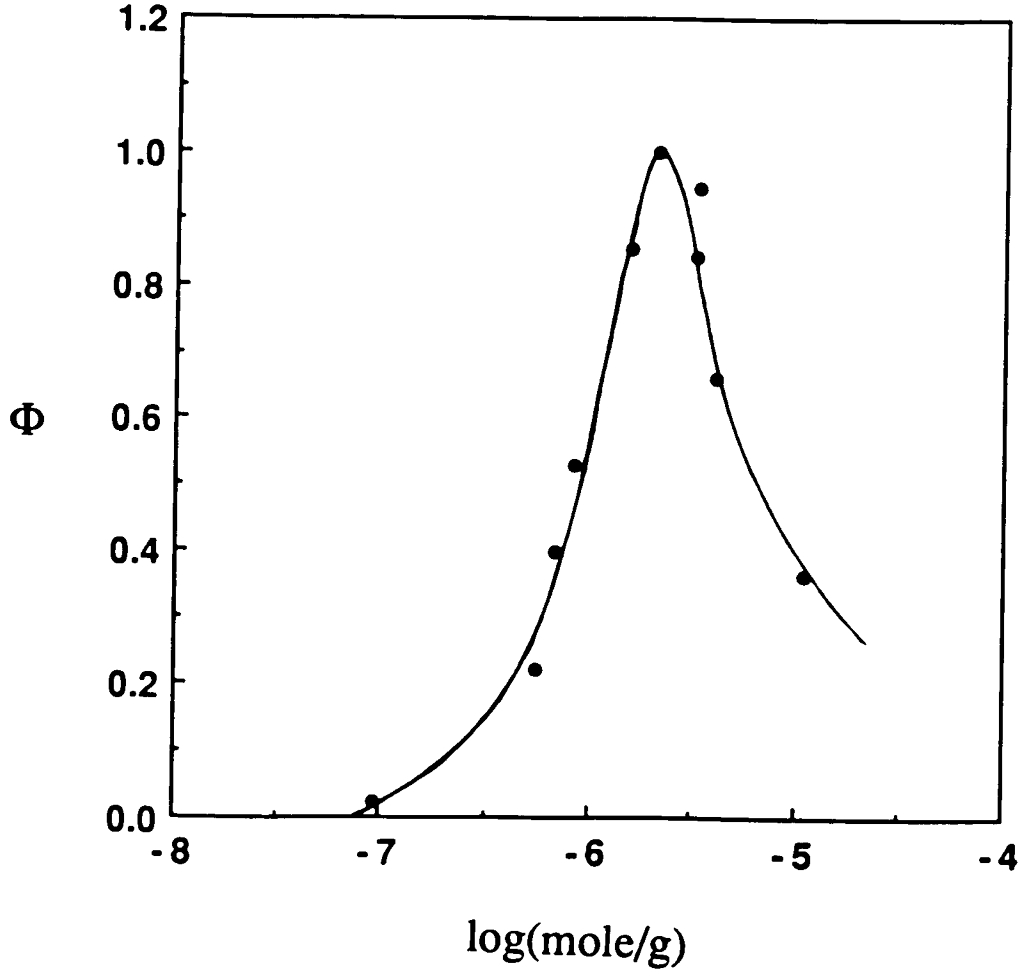
1.2
1.0
0.8
0.6
0.4
0.2
0.0
Φ
-8
-7
-6
-5
-4
log(mole/g)

Figure 47. Quantum yields of disproportionation vs. log moles of $Ru(bpy)_3^{2+}$/g of PVG for degassed $Ru(bpy)_3^{2+}$(ads) samples with chemisorbed NH_3.

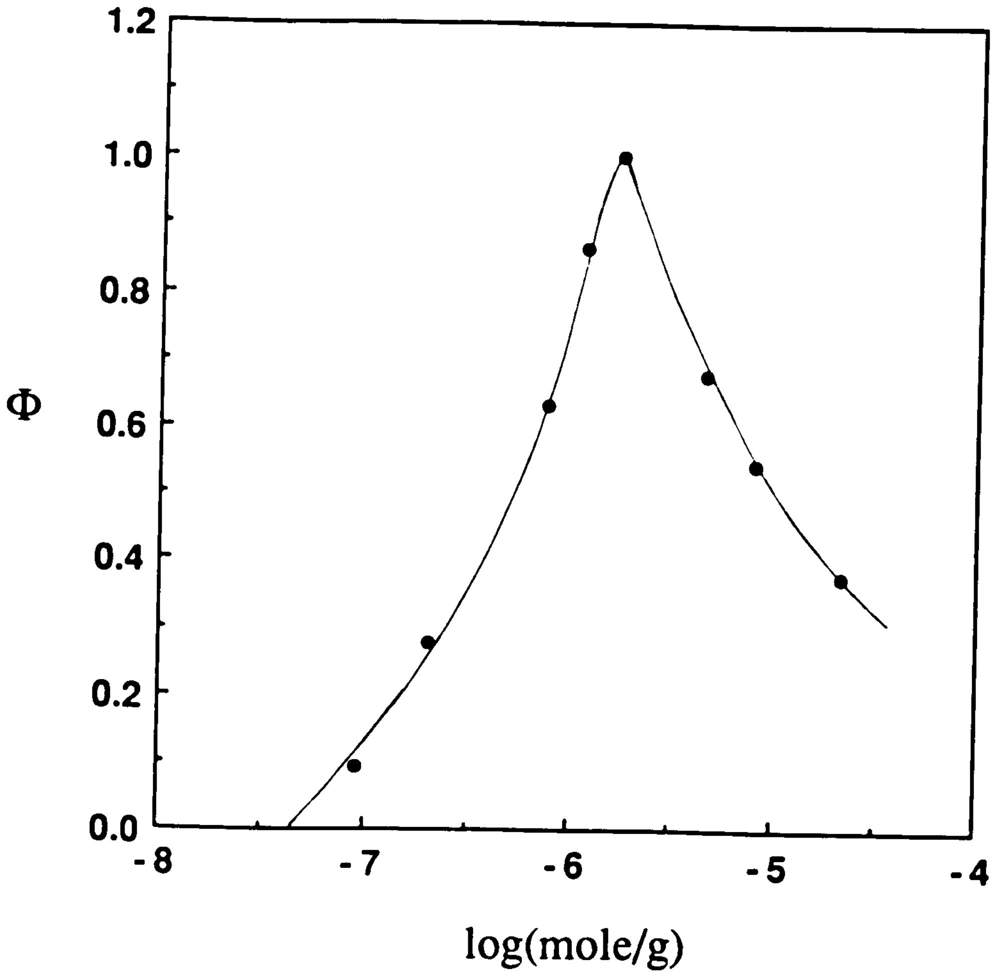
1.2
1.0
0.8
0.6
0.4
0.2
0.0
Φ
-8
-7
-6
-5
-4
log(mole/g)

Figure 48. Relative quantum yields of disproportionation vs. initial loading for (a) degassed $Ru(bpy)_3^{2+}$(ads) samples and (b) degassed $Ru(bpy)_3^{2+}$(ads) samples with chemisorbed NH_3.

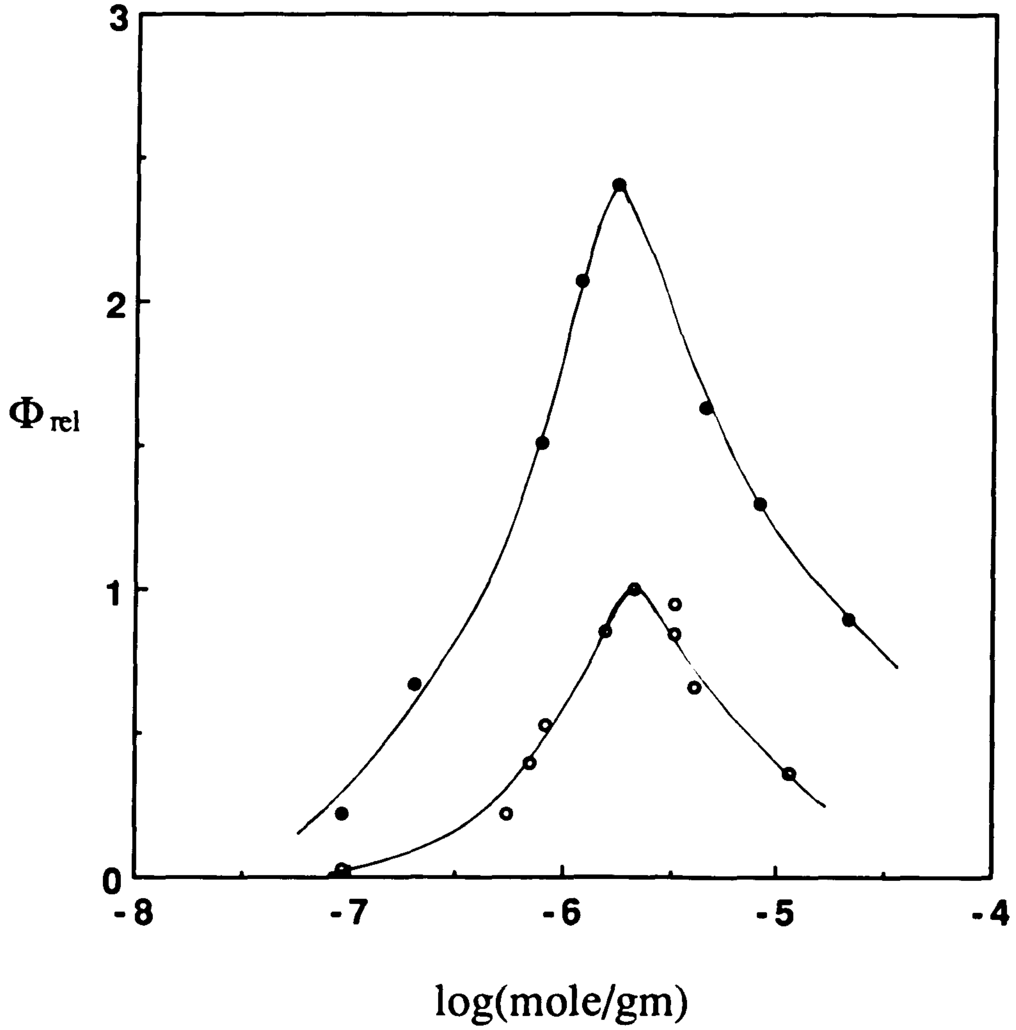
3
2
1
0
Φ rel
-8
-7
-6
-5
-4
log(mole/gm)

obtained under these two sets of conditions. With the same initial loadings, the quantum yields for NH_3 treated samples are about 3.0±0.5 times larger than those for NH_3 untreated samples.

Since previous results established that the reactants and products are fixed, Figures 46 and 47 could be interpreted in terms of the mean separation between the adsorbate ions, r,[124]

$$r = (AdpS/Nn)^{1/2} \qquad [35]$$

where n is half of the moles of $Ru(bpy)_3^{2+}(ads)$ uniformly distributed within a volume of PVG defined by geometric area of one side, A, and the penetration depth d. The parameters p and S are the density, 1.5 g/mL, and surface area, 183 m^2/g, and N is Avogadro's number. As a result, the mean separations between the adsorbate ions corresponding to the maximum quantum yield were calculated to be ca. 49 Å for NH_3 untreated samples, and ca.57 Å for NH_3 treated samples. Both are within the electron migration distance, 50±10 Å.

DISCUSSION

I. Spectroscopic Properties

$Ru(bpy)_3^{2+}$ cation exchanges onto PVG without disruption of its primary coordination sphere.[124-126] At temperatures between 5 and 90 °C, absorption and emission spectra of the adsorbed complex are similar to aqueous solution spectra (Figure 22), and bipyridine vibrations resonant with the 452-nm MLCT absorption differ by ≤ 1 cm^{-1} from the corresponding aqueous solution values (Figure 28). Nevertheless, some distortion does occur. RR spectra show a significant decline, ca. 25%, in the relative intensity of the prominent 1492 cm^{-1} band upon adsorption. Close scrutiny of the absorption spectra in the visible region (Figure 23) reveals that the band corresponding to MLCT transition in aqueous solution occurs at 452 nm with the halfwidth of 3763 cm^{-1}, while on PVG, it occurs at 444 nm with halfwidth of 4960 cm^{-1}. Also, the absorbance ratio of the bipyridine localized $\pi-\pi^*$ transition, relative to that of the MLCT transition, declines from 6.3±0.1 in aqueous solution to 5.8±0.1 for the adsorbed complex. This is considerably smaller, but in the same direction as the change that occurs when $Ru(bpy)_3^{2+}$ intercalates into hectorite, a magnesium silicate.[142] In this case, Van Damme and coworkers attribute the reduction to a distortion of the bipyridine ligands.[142] However, deviations from the fluid solution structure can occur in either the ground or excited state, or both, since the probability of light absorption is proportional to the Franck-Condon factors coupling the two states. On PVG, the spectral data indicate that the principal structural difference occurs in the excited, rather than the ground state.

Resonant Raman frequencies are a ground state property, whereas the band intensities are related to the nuclear displacements that distort the ground state configuration relative to that of the excited state.[143] The band frequencies indicate essentially equivalent ground state structures in both media. Therefore, the reduction in intensity of the 1492 cm^{-1} band, the shift of the MLCT absorption band, and the decrease in absorptivity of the bpy $\pi-\pi^*$ transition are attributed to "matrix effects" in which the rigidity of the glass curtails the distortions of the bipyridine ligand that accompany optical excitation. Consequently, the structure of the bipyridine localized $\pi-\pi^*$ state and that of the ^{1}MLCT state differ from those in aqueous solution.

II. Adsorbate Distribution and Mobility

PVG is a borosilicate glass in which the borate phase is acid leached leaving a random three-dimensional array of interconnected pores.[75] Because of this method of manufacturing, two potential adsorption sites exist; the slightly acidic silanol groups and B_2O_3 Lewis acid sites. The silanol number is on the order of 4-7/100 Å^2,[116] and XPS analyses indicate that the amount of B present in the first 50 Å of these PVG samples is 2.6±0.1%.[144] However, there is no indication that the observed temperature dependence of τ and Φ_{em} is biased by a redistribution amongst these sites. Initially, ≥99% of the $Ru(bpy)_3^{2+}$ cation exchanges onto the glass by replacing the slightly acidic silanol protons.[124] Since the maximum loading, 1.2 x 10^{-6} mol/g, corresponds to a surface coverage of 1%, a redistribution amongst the silanol and B_2O_3 sites would require some degree of adsorbate mobility, and in view of their different electron donating and withdrawing properties, would be expected to occur with some spectroscopic change. Yet, absorption spectra and the frequencies of the resonant bpy vibrations are independent of temperature, and equivalent to those in aqueous solution. In the 5 to 90 °C range, the emission polarization ratio of $Ru(bpy)_3^{2+}$(ads), 0.16±0.02, is equivalent to that in 77K hydrocarbon glasses.[126] During the excited state lifetime, $Ru(bpy)_3^{2+}$(ads) is immobile, and in the absence of a spectroscopic change or macroscopic diffusion, most likely remains bound to the silanol site onto which it originally cation exchanged.

With loadings of $\leq 10^{-6}$ mol/g, the average spacing between the adsorbed ions is ≥55 Å.[124] Since this exceeds currently known interaction distances,[141] the absence of adsorbate mobility precludes temperature-dependent self-quenching. The values of Φ_{em} and τ for $Ru(bpy)_3^{2+}$(ads) (Table 6) are also independent of initial loading, calcination conditions, and degassing procedures. Consequently, temperature dependent self quenching by either trace amounts of O_2 or some undefined impurity is also discounted. $Ru(bpy)_3^{2+}$(ads) exists as a dispersed, immobilized molecular entity, and the temperature dependence of Φ_{em} and τ reflect the temperature dependence of its excited state dynamics.

III. Temperature Dependence of Lifetime and Emission Quantum Yield

(i) Aqueous Solution

In degassed aqueous solution, the temperature dependence of $Ru(bpy)_3^{2+}$ emission lifetime, $\tau(T)$, and quantum yield, $\Phi_{em}(T)$, are given by equations 3 and 4 respectively[8]

$$\tau (T) = (k_{0r} + k_{0nr} + k_{1nr} e^{-\Delta E / kT})^{-1} \qquad [3]$$

$$\Phi_{em} (T) = k_{0r} \tau \qquad [4]$$

where k_{0r} and k_{0nr} are the rate constants for radiative and nonradiative decay of the emissive MLCT manifold. ΔE and k_{1nr} represent the activation barrier encountered in populating the dd manifold, and the rate constant of nonradiative decay from this manifold.[8] Fitting our aqueous solution data (Table 4) with equations 3 and 4 yields values of the parameters (Table 9) that are in excellent agreement with the values reported by Van Houten and Watts.[8] Aqueous solution measurements were repeated to test the reliability of our procedures, and to obtain, under as similar a set of conditions as possible, a reference to which the glass data could be compared.

(ii) Adsorbed Complex

(1) Lifetime Fitting

At the beginning of these experiments, the Van Houten-Watts' aqueous

Table 9

Parameters derived from the temperature dependence of τ and Φ_{em} of $Ru(bpy)_3^{2+}$ in aqueous solution.

ΔE = 3559 cm^{-1},[a]	3583±76 cm^{-1} [b]
k_r = 6.96×10^4 s^{-1},[a]	6.9±0.1 $\times 10^4$ s^{-1} [b]
k_{nr} = 1.222×10^6 s^{-1},[a]	1.2×10^6 s^{-1} [b]
k_1 = 10^{13} s^{-1},[a]	10^{13} s^{-1} [b]

a. Van Houten, J.; Watts, R. J. ref. 8.

b. calculated from data gathered in our experiments.

solution model was applied to describe the observed temperature dependence of τ and Φ_{em} for $Ru(bpy)_3^{2+}$(ads), i.e., both equations 3 and 4 were used to fit the temperature dependence of τ and Φ_{em} data between 5 and 85 °C for $Ru(bpy)_3^{2+}$(ads). With each loading of $Ru(bpy)_3^{2+}$(ads), lifetime vs. temperature data could be fit with the abbreviated form of equation 3 [46]

$$\tau(T) = (k_0 + k_1\, e^{-\Delta E/kT})^{-1} \qquad [8]$$

where $k_0 = k_{0r} + k_{0nr}$, and $k_1 = k_{1nr}$. Alternatively, the data could be fit with a more general expression that includes the Boltzmann weighing factor, $(1+e^{-\Delta E/kT})$[46]

$$\tau_m(T) = \left[(k_0 + k_1\, e^{-\Delta E/kT})/(1 + e^{-\Delta E/kT})\right]^{-1} \qquad [36]$$

However, the values of parameters generated from these two equations are indistinguishable. In fact, equation 36 will differ from equation 8 only if $\Delta E \leq 3kT$, where k is the Boltzmann factor. The data were also fit with the reciprocal of equation 8, i.e. τ^{-1} vs. temperature, in order to get a better idea of the uncertainty in the calculated values of the parameters. The average values of k_0, k_1 and ΔE generated from these various fittings are $3.30 \pm 0.6 \times 10^5$ s^{-1}, $3.18 \pm 0.5 \times 10^8$ s^{-1}, and 1168 ± 160 cm^{-1}, respectively. Substituting these values into equation 8, and calculating the lifetime of $^*Ru(bpy)_3^{2+}$(ads) at temperatures between 5 and 85 °C yields values that are in excellent agreement with the observed temperature dependence (Table 6 and Figure 49).

Figure 49. Measured (●) and calculated (—) (from equation 8) lifetimes vs. temperature for $Ru(bpy)_3^{2+}$(ads).

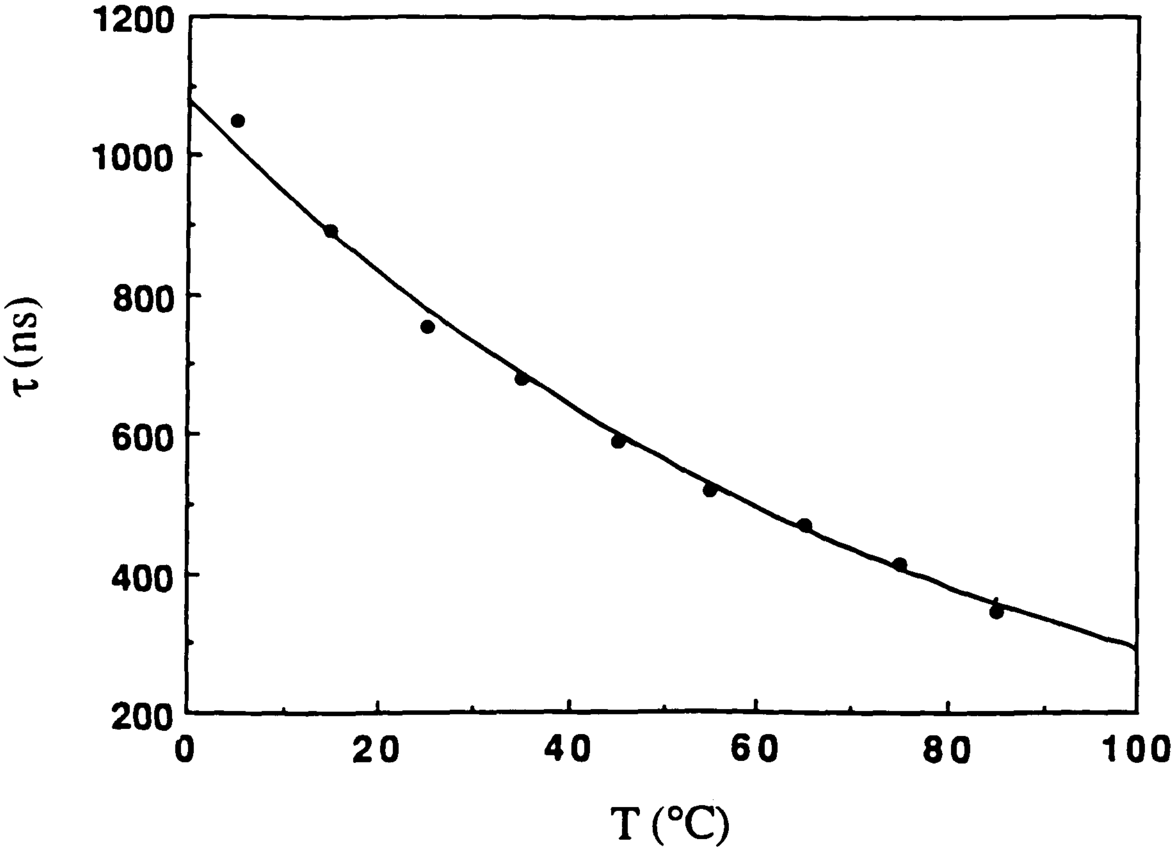
1200
1000
800
600
400
200
τ (ns)
0
20
40
60
80
100
T (°C)

In a cellulose acetate matrix and over a wider temperature range, fitting $Ru(bpy)_3^{2+}$ lifetime vs. temperature data requires a three term equation[45]

$$1/\tau = k_0 + A_1 e^{-\Delta E_1/kT} + A_2 e^{-\Delta E_2/kT} \qquad [7]$$

ΔE_1 corresponds to the energy difference between the highest and the lowest ^{3}MLCT states,[7] while ΔE_2 corresponds to the activation barrier for thermal population from the ^{3}MLCT states to a higher-lying dd state[8] or another MLCT state.[46] Equation 7 was also tested for the temperature dependence of $Ru(bpy)_3^{2+}$(ads) lifetime to see if it would also fit the data. Equation 7 fits the data very well, but it was immediately apparent that equation 7 was equivalent to equation 8 since the value of ΔE_1 obtained from equation 7 (51±14 cm^{-1}) is smaller than kT in the 5 to 90 °C range. Both equations yield equivalent activation barriers, 1168±160 cm^{-1} (equation 8) and 1136±67 cm^{-1} (equation 7); for simplicity, the former value, 1168±160 cm^{-1}, will be used.

Fitting the temperature dependence of the lifetime of $Ru(bpy)_3^{2+}$(ads) between 5 and 90 °C with equations 7, 8, and 35 establishes the following points. First, the separation of three emissive ^{3}MLCT states for $Ru(bpy)_3^{2+}$(ads) (51±14 cm^{-1}) is essentially the same as that found by Crosby and coworkers (~61 cm^{-1}) who studied $Ru(bpy)_3^{2+}$ in polymethylmethacrylate film at temperatures between 2 and 77 K.[7] Second, within the temperature range examined here (5 to 85 °C), these states are in thermal equilibrium and can be treated as an average state. And third, the decline in the lifetime of the emissive ^{3}MLCT state as temperature increases is due to the thermal population of a higher-lying nonemissive state which is located ca. 1168±160 cm^{-1} above the emissive manifold. The last result differs from that found in aqueous solution, where the thermal population of the dd manifold is responsible for the decline of lifetime at high temperature.[8] The dd state is located ca. 3600 cm^{-1} above the emissve manifold,[8] whereas the barrier found for $Ru(bpy)_3^{2+}$(ads) is only 1168±160 cm^{-1}.

(2) Emission Quantum Yield Fitting

Although the temperature dependence of the lifetime of $Ru(bpy)_3^{2+}$(ads) could be fit with equation 3, or its abbreviated form, equation 8, equation 4 failed to reproduce the observed dependence of emission quantum yield, Φ_{em}, on temperature. Inserting the values of ΔE_1 and the k's (except k_{0r}) obtained from the lifetime fitting into equation 4, the computer generated temperature dependence of Φ_{em} differs substantially from the observed dependence, as shown in Figure 50. Alternatively, if the measured temperature dependence of τ and Φ_{em} are fit with equations 3 and 4 independently, different sets of values for ΔE_1 and the k's are generated, and the difference between the sets is beyond experimental error. Neither result is acceptable. In short, the measured temperature dependence of lifetime and emission quantum yield of $Ru(bpy)_3^{2+}$(ads) could not be fit with the Van Houten-Watts' aqueous solution model. This indicates an intrinsic difference between $Ru(bpy)_3^{2+}$ in two media.

Figure 50. Measured (●) and calculated (o) emission quantum yield (from equation 4) vs. temperature for $Ru(bpy)_3^{2+}$(ads).

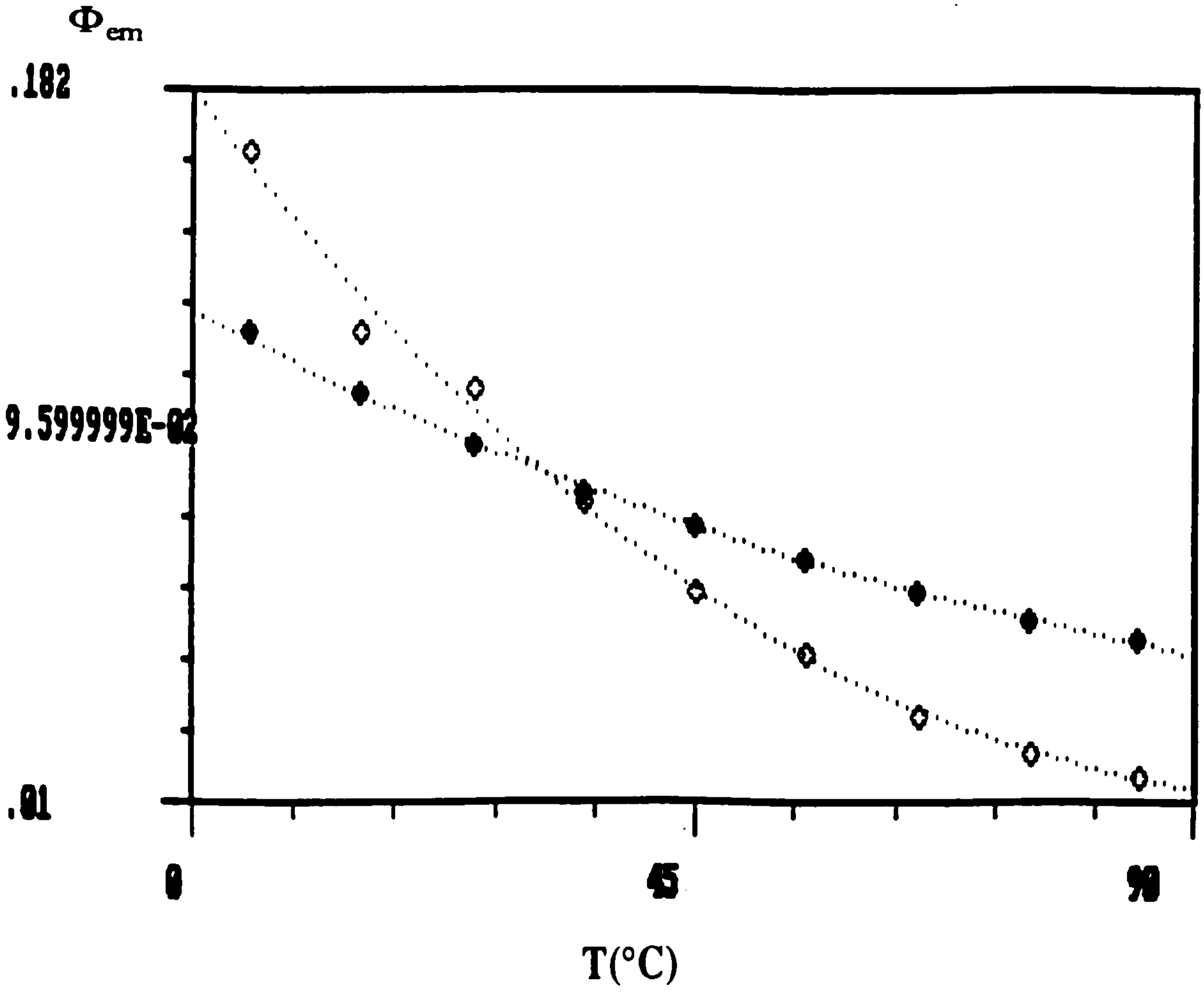
Φem
.182
9.599999E-02
.01
0
45
90
T(°C)

Comparing Figures 32 and 30 shows that the observed temperature dependence of τ and Φ_{em} of $Ru(bpy)_3^{2+}$(ads) differs from that in degassed aqueous solution. Moreover, both Van Houten and Watts' data and our data show that the calculated ratio of Φ_{em}/τ in aqueous solution is temperature independent (Figure 33a), while the ratio for $Ru(bpy)_3^{2+}$(ads) declines by ca. 42% as temperature increases from 5 to 85 °C (Figure 33b). The latter is a fundamental difference between the two media and it is this difference that leads to the failure of Watts' aqueous solution model to describe $Ru(bpy)_3^{2+}$(ads). As described in Introduction section, the general expression for Φ_{em} is given by[4,42]

$$\Phi_{em} = \eta_{isc} k_r \tau \qquad [9]$$

where η_{isc} is the efficiency of the intersystems crossing to the emissive manifold. The latter does not appear in equation 4 since Watts and Van Houten have shown that the efficiency of intersystems crossing in aqueous solution is independent of temperature and have taken its value to be unity.[8] Therefore, equation 4 yields a ratio of $\Phi_{em}/\tau = k_{0r}$ that is temperature independent. Obviously, it is not applicable to the data for $Ru(bpy)_3^{2+}$(ads). Since the interference from self-quenching or redistribution of the complex on the glass have been excluded, the temperature dependence of the Φ_{em}/τ ratio for $Ru(bpy)_3^{2+}$(ads) indicates that the product of $\eta_{isc} k_r$ is temperature dependent.

The data do not distinguish whether one or both of the parameters (η_{isc}

and k_r) of $Ru(bpy)_3{}^{2+}$(ads) are temperature dependent, but in our opinion, attributing the temperature dependence of Φ_{em}/τ to k_r is inconsistent with the very nature of a spontaneous emission process. Interposing an activation barrier in a spontaneous emission process is arbitrary, specifically in this case, where the activation barrier would have to be negative. Furthermore, spectroscopic data offer no indication that the intrinsic parameters which govern k_r change when temperature changes.

According to Einstein's law for spontaneous emission[41]

$$k_r \propto (E_{em})^3 \qquad [37]$$

where E_{em} is the emission energy. According to Demas and Crosby[28]

$$k_r = \varepsilon(s)\, K\, |M_{so}|^2 (E_T{}^3/E_s)/(E_T - E_s)^2 \qquad [38]$$

where $\varepsilon(s)$ is molar extinction coefficient for singlet state, K is a constant, M_{so} is the spin-orbit coupling constant, E_T is triplet state energy (corresponding to emission maximum) and E_s is singlet state energy (corresponding to absorption maximum). Both equations indicate that a temperature dependence of k_r would be evident as temperature dependent changes in the complex's spectroscopic parameters. To examine the possibility that k_r is temperature dependent, UV-visible and emission spectra in both media were recorded at different temperatures. As shown in Figure 24, in both media, the absorption spectra recorded at 5 °C agree in band maxima, halfwidth, and relative extinction coefficient with those recorded at

90 °C. The only evidence that k_r may change with temperature appears in the emission spectra. As shown in Figures 25 and 26, when the temperature increases from 5 to 90 °C, the emission maxima shift ≤ 7 nm to longer wavelengths in both media. However, the shifts in emission maxima, or assuming similar shifts in the 0-0 emission energies, correspond to declines of only $\leq 5\%$ in k_r over the 5 to 90 °C range. This is within the experimental error in the aqueous solution data, but insufficient to account for the 42% decline in the Φ_{em}/τ ratio for $Ru(bpy)_3^{2+}$(ads) (Figure 33b). In both media, spectroscopic data offer no indication that the intrinsic parameters which govern k_r change appreciably with temperature. Since k_r is temperature independent in aqueous solution, k_r for the adsorbed complex is also taken to be temperature independent. Consequently, the observed temperature dependence of Φ_{em}/τ ratio for $Ru(bpy)_3^{2+}$(ads) is attributed to the intersystem crossing yield, $\eta_{isc.}$

The fact that η_{isc} in aqueous solution is unity indicates that all molecules in the ^{1}MLCT state transform to ^{3}MLCT state **without** direct decay to ground state. The decline in η_{isc} with increasing temperature for $Ru(bpy)_3^{2+}$(ads) suggests that the glass matrix opens a "door" for direct relaxation from the ^{1}MLCT state to the ground state. Since this "door" is temperature dependent, it may indicate a higher-lying energy level that is connected to the ground state by a nonradiative pathway. As a result, the thermal population of this state couples the ^{1}MLCT state to the ground state.

Based on the experimental data and theoretical analysis, the principal

Figure 51. The proposed model for excited state decay processes of $Ru(bpy)_3^{2+}(ads)$.

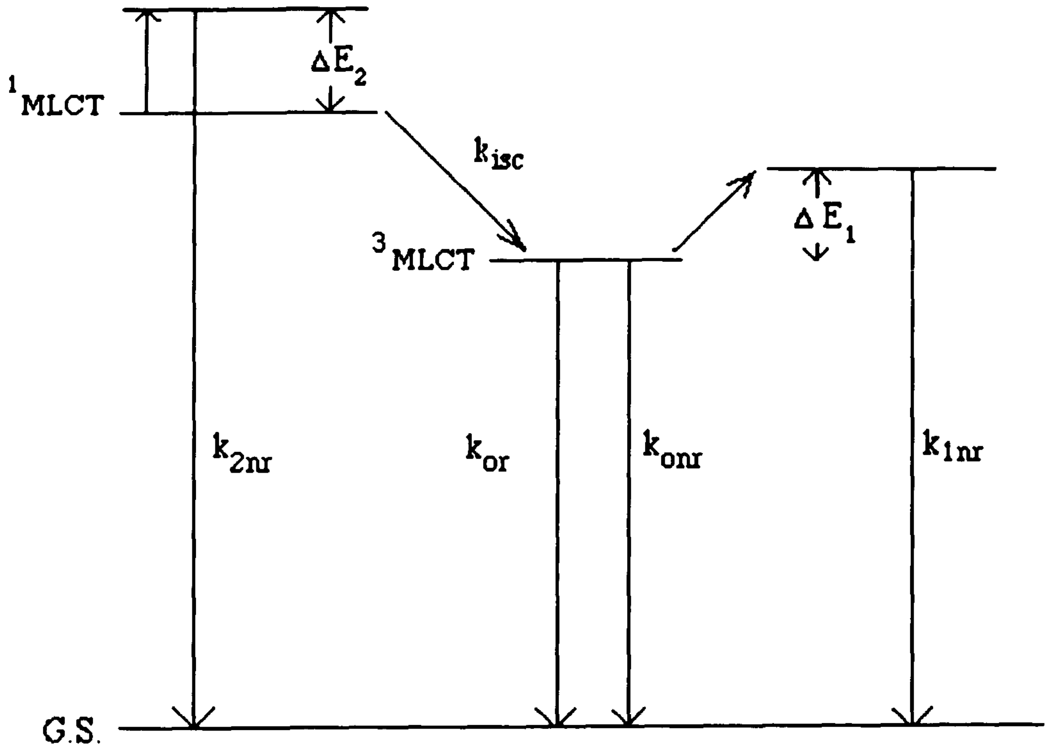
^{1}MLCT
ΔE_2
k_{isc}
^{3}MLCT
ΔE_1
k_{2nr}
k_{or}
k_{onr}
k_{1nr}
G.S.

model for $Ru(bpy)_3^{2+}$(ads) is shown in Figure 51. The left side of the figure represents the events prior to the population of emissive manifold, while the right side represents the events after the population of emissive manifold. Direct adsorption of 450-nm light produces ^{1}MLCT excited state, and at low temperature, all molecules in the ^{1}MLCT state intersystem cross to the corresponding ^{3}MLCT state. As a consequence, η_{isc} is unity at low temperature. As temperature increases, however, the molecules in ^{1}MLCT state can decay to the ground state nonradiatively via population of a higher-lying state located ΔE_2 above the ^{1}MLCT state. Consequently, the efficiency of population of emissive ^{3}MLCT state, i.e., η_{isc}, declines as temperature increases since the thermal energy allows more molecules in ^{1}MLCT to overcome the thermal activation barrier ΔE_2.

To test the model shown in Figure 51, the expression for the intersystem crossing yield, η_{isc}, as a function of temperature was derived. The intersystem crossing yield is the fraction of molecules existing in the ^{1}MLCT state that convert to the ^{3}MLCT state.[42] Assuming that the ^{1}MLCT state and the higher-lying level are in thermal equilibrium, the intersystem crossing yield is given by

$$\eta_{isc} = \Sigma\, k_{isc} / \Sigma\, k = k_{isc} / (k_{isc} + k_{2nr} e^{-\Delta E2 / kT}) \qquad [39]$$

where k_{isc} is the rate constant of intersystem crossing to the emissive manifold, k_{2nr} is the nonradiative decay rate constant from that higher-lying state, and ΔE_2 is the thermal barrier for conversion of the ^{1}MLCT state to the higher-lying state. However, it is impossible to measure η_{isc} directly. Rather, equation 39 was substituted into the relation $\Phi_{em} = \eta_{isc} k_r \tau$, and the resulting expression for Φ_{em} as a function of temperature, i.e.,

$$\Phi_{em} = \eta_{isc} k_{0r} \tau$$

$$= \frac{k_{isc}}{(k_{isc} + k_{2nr} e^{-\Delta E2/kT})} \, \frac{k_{0r}}{(k_{0r} + k_{0nr} + k_{1nr} e^{-\Delta E1/kT})} \qquad [40]$$

was tested against the observed temperature dependence of Φ_{em}. In equation 40, k_{2nr} is the rate constant for nonradiative decay from the higher-lying state, and ΔE_2 is the energy gap between the higher lying state and the ^{1}MLCT state (Figure 51). The parameters k_{0r}, k_{0nr}, k_{1nr}, and ΔE_1 are those described in equation 3. Although their values have been calculated from fitting the temperature dependence of the lifetime, in this approach, they were treated as unknowns to test the self consistency of the model. Rearranging equation 40 by grouping the rate constants together yields

$$\Phi em = \frac{T(1)}{(1 + T(2)\, e^{-T(3)\, X})\ (T(4) + T(5)\, e^{-T(6)\, X})} \qquad [41]$$

where $T(1) = k_{0r}$, $T(2) = k_{2nr}/k_{isc}$, $T(3) = \Delta E_2/k$ (k is the Boltzman constant), $T(4) = k_{0r} + k_{0nr}$, $T(5) = k_{1nr}$, $T(6) = \Delta E_1/k$ (k is the Boltzman constant). Computer fitting equation 41 to the observed temperature dependence of Φ_{em} by means of Simplex yields $T(1) = k_{0r} = 1.1 \pm 0.1 \times 10^5$ s^{-1}, $T(2) = k_{2nr}/k_{isc}$

=101±17, ΔE_2 = 1117±70 cm^{-1}, T(4) = $k_{0r} + k_{0nr}$ = 2.56±0.5x10^5 s^{-1}, T(5) = k_{1nr} = 2.36±0.8x10^8 s^{-1}, ΔE_1= 1122±100 cm^{-1}. Substituting these values into equation 41, and calculating the individual values of Φ_{em} between 5 to 85 °C results in excellent agreement with the experimental data (Table 6). The agreement is perhaps best illustrated graphically in Figure 52. Furthermore, comparing the values of parameters generated from equation 41

$k_{0r}+k_{0nr}$ = 2.56±0.5x10^5 s^{-1}, k_{1nr} = 2.36±0.8x10^8 s^{-1},
ΔE_1= 1122±100 cm^{-1},

with those calculated from the lifetime data, equation 8,

$k_{0r}+k_{0nr}$ = 3.30±0.6x10^5 s^{-1}, k_{1nr} = 3.18±0.5x10^8 s^{-1},
ΔE_1= 1168±160 cm^{-1},

establishes the self consistence of the data obtained from the two sets of independent measurements.

IV. Significance of ΔE_1 and ΔE_2

(i) Comparing the Values of Kinetic Parameters of $Ru(bpy)_3^{2+}$(ads) With Those Obtained From Aqueous Solution

Fitting the temperature-dependent lifetime data of $Ru(bpy)_3^{2+}$(ads) with equation 3, or its abbreviated form, equation 8, generates the following values of the kinetic parameters; k_0=3.30±0.6x10^5 s^{-1}, k_1 =3.18±0.5x10^8 s^{-1},

Figure 52. Measured (▲) and calculated (—) emission quantum yield (from equation 40) vs. temperature for $Ru(bpy)_3^{2+}$(ads).

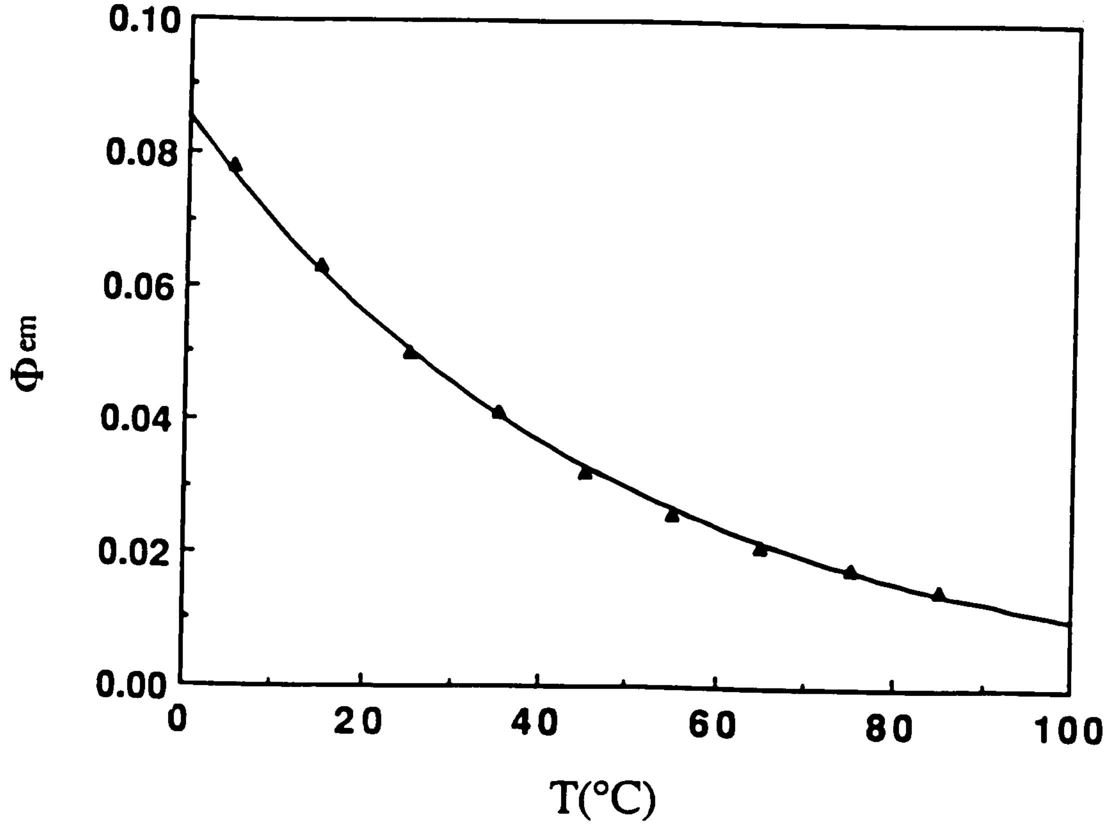

0.10
0.08
0.06
0.04
0.02
0.00
Φem
0
20
40
60
80
100
T(°C)

and $\Delta E_1=1168\pm160$ cm^{-1}. The corresponding values in aqueous solution of Ru(bpy)$_3^{2+}$ are $k_0 = 10^6$ s^{-1}, $k_1 = 10^{13}$ s^{-1}, and $\Delta E_1 = 3600\pm100$ cm^{-1}.[8] In one kinetic limit, the energy gap ΔE_1 has been interpreted as the activation barrier for the ^{3}MLCT to dd state conversion and k_1 as the rate of barrier crossing.[5] Although the energy gap between dd and ^{3}MLCT states will depend upon the solvent and the surrounding ligands, in all complexes where the dd states appear to play a significant role in dictating the temperature dependent properties of the observed luminescence, typical values of the parameters are $k_1 = 10^{12}$-10^{14} s^{-1}, and ΔE_1= 2500-4500 cm^{-1}.[45,46] The substantial difference between the values of the kinetic parameters for Ru(bpy)$_3^{2+}$ in aqueous solution and those for Ru(bpy)$_3^{2+}$(ads) indicates that cation exchanging the complex onto the glass results in a significant change in excited state behavior.

Experimental evidence is accumulating which suggests that the combination of a series of three low-lying ^{3}MLCT states and a thermally activated ^{3}MLCT->dd transition is not adequate to account for the temperature dependencies in all cases.[46] For polypyridal complexes of Os(II) in fluid solution,[47,48] as well as for a number of mixed ligand complexes of Ru(II) in fluid solution[49-51] and for Ru(II) complexes in rigid matrices at ambient temperature,[45] fitting their lifetime vs. temperature data with equation 8 yields kinetic parameters in the range of ΔE_1=300-800 cm^{-1}, and $k_1 = 10^6$-10^8 s^{-1}. Also, in each of these cases, ligand loss photochemistry, which occurs via the population of dd state, is not observed.[46] These apparent contradictions led to the suggestion that an additional, nonemissive MLCT state, rather than a dd state, participates in the relaxation processes in these complexes.[46] Evidence for such a state occurs in the polarized emission spectra of $[Ru(bpy)_3](PF_6)_2$ single crystals, where a low lying MLCT state, designated $2A_2'$, lies 650±130 cm^{-1} above the lowest MLCT state.[39] As described in the Introduction, several explanations have been suggested for why the dd state is not thermally accessible for these Ru(II) and Os(II) diimines mentioned above.[46] In rigid matrices, it is attributed to "matrix effects".[46] For example, when $Ru(bpy)_3^{2+}$ is incorporated into a cellulose acetate matrix, the values of k_1 and ΔE_1 are reduced from 10^{13} s^{-1} and 3600 cm^{-1} in fluid solution to 1.73 $x10^7$ s^{-1} and 800±120 cm^{-1}, respectively.[45] The reduction is attributed to a "matrix effects", in which the rigidity of the matrix curtails the metal-ligand distortions accompanying the transition between the states, MLCT --> dd.[46] In the more rigid environment of a cellulose acetate matrix, expansion along the metal-ligand bond axes may be so costly, energetically, that access to the dd state is no longer feasible even under ambient conditions. With the loss of the dd decay channel, nonradiative decay through another MLCT state, such as the $2A_2'$ state, is less energy demanding, and the temperature dependence of the lifetime suggests that this becomes a dominant decay pathway. Representative plots of ln $(1/\tau)$ vs. $1/T$ where decay occurs through another MLCT state (Figure 53b) differ from those in which decay occurs via the thermal population of dd state (Figure 53a).[46]

Although the values of k_1 and ΔE_1 for $Ru(bpy)_3^{2+}$(ads) obtained from lifetime fittings are very different from those in aqueous solution, they are quite similar to those obtained on cellulose acetate film (Table 10).[45] Also, the plot of ln $(1/\tau)$ vs. $1/T$ for $Ru(bpy)_3^{2+}$(ads) (Figure 54b) is similar to the typical plot for population of another MLCT state (Figure 53b). These similarities suggest the population of another MLCT state instead of the dd state for $Ru(bpy)_3^{2+}$(ads) during decay of the emissive excited states. The change of the excited state decay channel when $Ru(bpy)_3^{2+}$ is cation exchanged onto PVG can also be attributed to a "matrix effect". As in the cellulose acetate film, the rigidity of PVG matrix curtails the molecular vibration required to access the dd state. As a result, nonradiative decay is thought to occur via the less energy demanding population of the MLCT state. RR spectra recorded in these experiments do not probe the metal-ligand vibration per se, but the reduction in the intensities of the 1492 cm^{-1} vibration and the 286-nm $\pi-\pi^*$ absorption shows that the glass at least curtails ligand vibrations.

(ii) Photochemical Evidence

Population of a lower energy MLCT state, as opposed to a dd state, is also consistent with the observed photochemistry for $Ru(bpy)_3^{2+}$(ads). Since the emissive ^{3}MLCT state is photoinert, photochemistry is attributed to the population of a thermally accessible higher energy state. The contribution of a decay channel through a thermally populated dd or MLCT state to the total deactivation of emissive excited states, η, as a function of temperature, is

Figure 53. Plots of ln(1/τ) vs. 1/T which illustrate two different types of temperature-dependent behavior. (a) Thermal activation to a dd state for $Ru(bpy)_3^{2+}$ in CH_2Cl_2; (b) Thermal activation to an additional MLCT state for $[Os(bpy)_2(PPh_2Me)_2]^{2+}$. (From Ref. 5.)

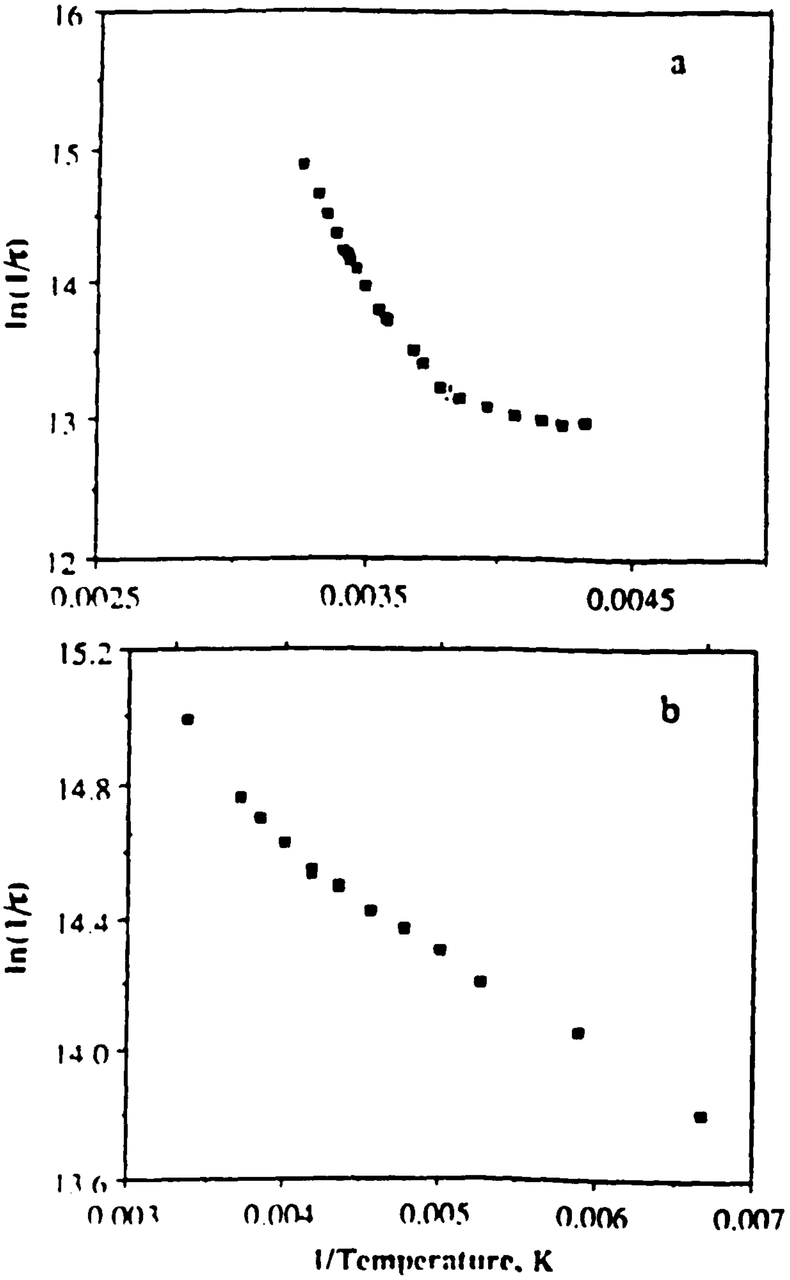
a
16
15
14
13
12
ln(1/τ)
0.0025
0.0035
0.0045
b
15.2
14.8
14.4
14.0
13.6
ln(1/τ)
0.003
0.004
0.005
0.006
0.007
1/Temperature, K

Figure 54. Plots of ln(1/τ) vs. 1/T for $Ru(bpy)_3^{2+}$ (a) in aqueous solution; (b) adsorbed onto PVG.

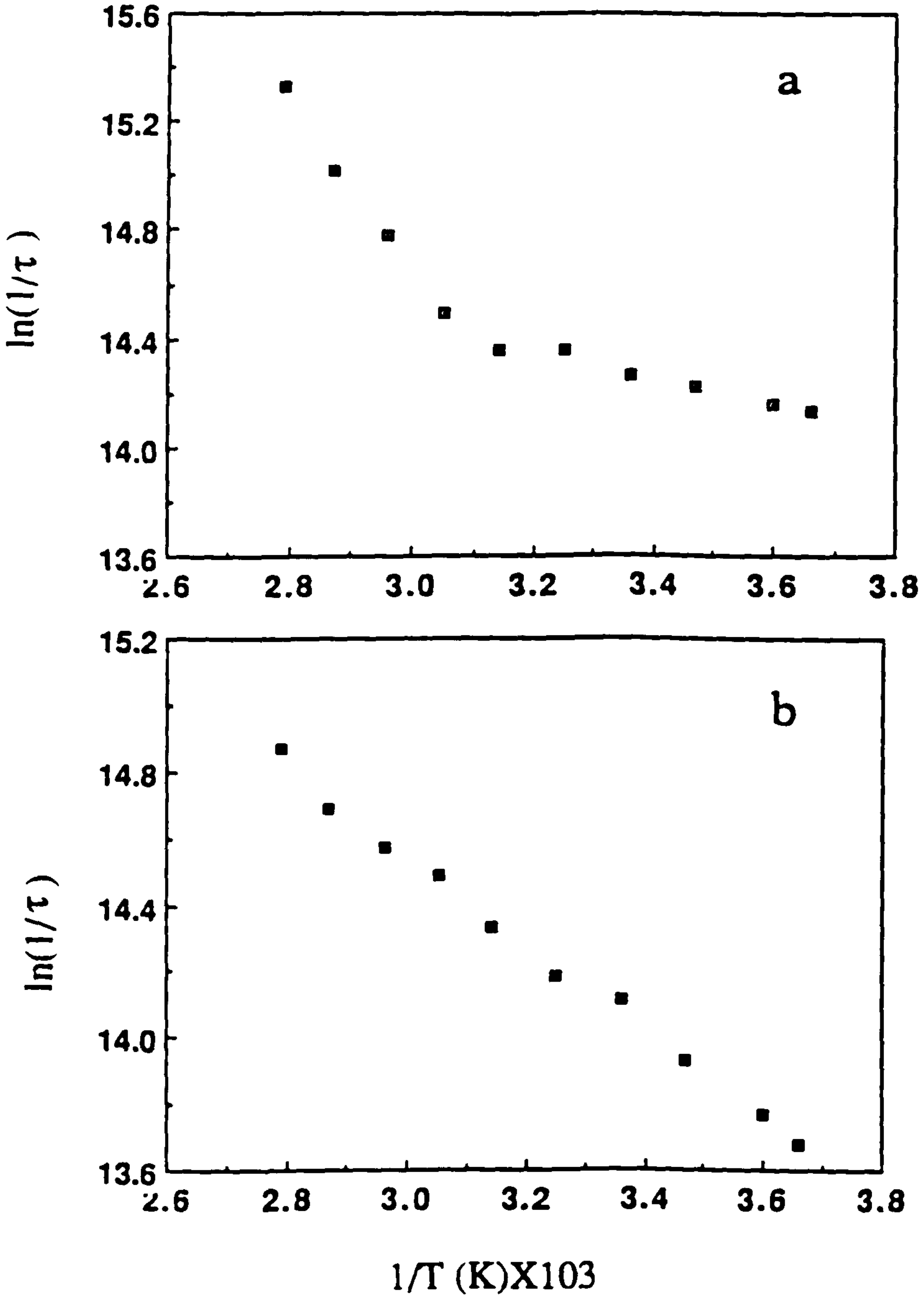
a
b
ln(1/τ)
15.6
15.2
14.8
14.4
14.0
13.6
2.6
2.8
3.0
3.2
3.4
3.6
3.8
1/T (K)X103

Table 10 **A comparison of values of parameters generated from temperature dependent lifetime fitting with equation 8 for $Ru(bpy)_3^{2+}$ on PVG, cellulose acetate film and in aqueous solution.**

Media	$k_0(s^{-1})$	$k_1\ (s^{-1})$	$\Delta E(cm^{-1})$
PVG	3.30×10^5	3.18×10^8	1168±160
cellulose acetate	2.2×10^5	1.73×10^7	800±93
H_2O	1.29×10^6	10^{13}	3600

given by[46]

$$\eta = k_1\, e^{-\Delta E/kT} / (k_0 + k_1\, e^{-\Delta E/kT}) \qquad [42]$$

where k_0 and k_1 are the total decay rate constants from the emissive state and the thermal accessible higher energy state, respectively, and ΔE is the energy difference between these two states. Calculation shows that at 83 °C, ca. 80% of the excited states of $Ru(bpy)_3^{2+}$(ads) decay from the upper level either via a nonradiative pathway or undergo photochemistry. Correlations between the orbital natures of the excited state and the observed photoreaction are now well established.[8,46] The spectral changes occurring during 350-nm photolysis of $Ru(bpy)_3^{2+}$ in aqueous solution at 83 °C (Figure 34a) establish photoinduced ligand labilization[8]

$$Ru(bpy)_3^{2+}(aq) \xrightarrow[H^+]{h\nu} [Ru(bpy)_2(H_2O)_2]^{2+}(aq) + Hbpy^+(aq) \qquad [5]$$

which is consistent with population of a dd state as opposed to a charge transfer state.[8] The dd states are formally antibonding and their population reduces the metal-ligand bond energy thereby rendering the ligand more susceptible to dissociation.[46]

Population of charge-transfer states, on the other hand, generally leads to a redox reaction in which the central metal changes its oxidation state.[8] Under essentially equivalent conditions, photolysis of $Ru(bpy)_3^{2+}$(ads) results in spectral changes (Figure 34b) suggestive of photoinduced disproportionation, i.e.[124]

$$2Ru(bpy)_3{}^{2+}(ads) \dashrightarrow Ru(bpy)_2(bpy)^{+}(ads) + Ru(bpy)_3{}^{3+}(ads) \qquad [43]$$

which is more consistent with the population of a charge-transfer state. In a rigid matrix, however, ligand labilization may not be observed because diffusional separation of the photoproducts is curtailed, and/or scavenging of the coordinatively unsaturated intermediate is not competitive with recombination. On PVG, the most likely scavenging reagent is the weakly acidic silanol groups. Cation exchanging $Ru(bpy)_3{}^{2+}$ onto the glass places two $Si\text{-}O^-$ groups in the immediate vicinity of the complex, and based on an average of 4-7 silanol groups/100 $Å^2$,[116] the planar surface area of the complex, 171 $Å^2$, places 7-12 silanol groups in the vicinity of the complex. This availability of silanol groups argues for a reduction in quantum efficiency, rather than the observed change in reaction pathway. In both aqueous solution and on PVG, disproportionation initiates via biphotonic excitation, and appears to occur via photoinduced ionization of a lower energy charge transfer state.[124,127] The data do not specify the specific state, but ionization of a charge transfer state is more likely than ionization of a metal-centered dd state. In this sense, the photochemical behavior of $Ru(bpy)_3{}^{2+}(ads)$, i.e., disproportionation, is consistent with the thermal population of an MLCT state as opposed to a dd state.

(iii) PVG Matrix Effects

When $Ru(bpy)_3{}^{2+}$ cation exchanges onto PVG, two possible matrix effects can be envisioned. One arises from the rigidity of the glass which in turn curtails the molecular vibrations required to access the dd state. As a result, nonradiative decay is thought to occur via the less energy demanding population of the MLCT state. The data gathered in these experiments do not probe the metal-ligand vibration per se, but the reduction in the intensities of the 1492 cm^{-1} vibration and the 286-nm $\pi-\pi^*$ absorption attest to a matrix effect that curtails ligand vibrations.

The other possible matrix effect is related to the reduction in molecular symmetry that occurs on adsorption onto the glass. The latter does not necessary happen on all solid matrices, and depends on the specific surface characteristics, such as surface topology and surface charge. Adsorbing $Ru(bpy)_3^{2+}$ cation, which has a molecular diameter of ca. 13 Å, onto the inner and outer surfaces of a porous substrate with average pore diameters of 100±10 Å, creates an asymmetric environment. Ideally, cation exchanging $Ru(bpy)_3^{2+}$ onto PVG reduces the molecular symmetry from D_3 to C_{2V} or C_S depending on its orientation on the glass surface (Figure 55). Lowering molecular symmetry, however, seems to have little effect on the ground state properties of $Ru(bpy)_3^{2+}$(ads). The frequencies of the bipyridine vibrations resonant with the MLCT transition for $Ru(bpy)_3^{2+}$(ads) are equivalent to those found in aqueous solution, which indicates that the ground state properties are similar in both media. This is probably due to the fact that, in the ground state, the majority of electron density is centered at the core of the complex, i.e., about the Ru^{2+} ion and the more electronegative

Figure 55. Idealized geometries of $Ru(bpy)_3^{2+}$ adsorbed onto PVG surface (the surface is negative charged: zeta potential = -26 mV).

Cs

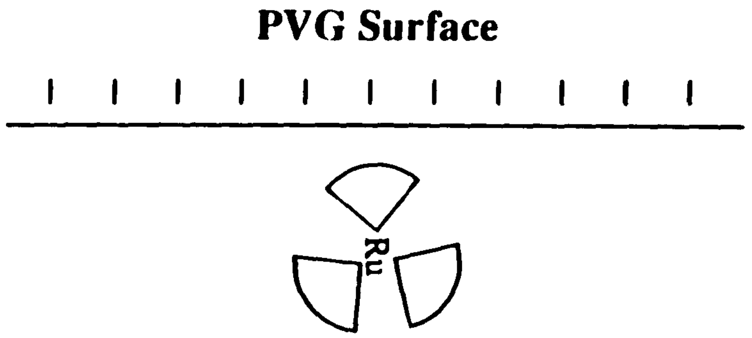

C2v

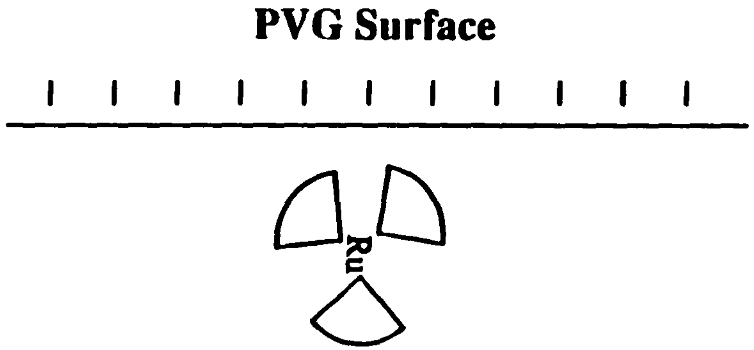

N atoms. As a result, the electron distribution is not very sensitive to the surrounding environment. However, population of the MLCT excited state, where excitation transfers electron density from the central metal to the bipyridine π^* orbital, leads to a significant change in the complex's dipole moment, and an electron configuration that is much more sensitive to the surrounding environment. As a result, the excited state is more sensitive to the surrounding environment than the ground state, and the sensitive part is principally localized on the bipyridine ligands. Although the RR spectra recorded in this experiments do not reveal the symmetry of the excited state per se, the reductions in the relative intensities of the 286-nm bipyridine $\pi-\pi^*$ transition, and the bipyridine 1492-cm^{-1} vibration resonant with the 452-nm MLCT excitation at least indicate the change of the excited state structure upon adsorption as compared with that in aqueous solution.

Now consider the consequence of an asymmetric environment on the three bipyridines ligands in the excited state. Figure 55 shows two limiting cases for cation exchanging $Ru(bpy)_3^{2+}$ onto PVG surface. The actual symmetry maybe more complicated, but the important point is that adsorption onto the anionic surface of the glass, which exhibits a zeta potential of -26 mV in water, differentiates three equivalent ligands according to their distances to the glass surface. Charge transfer to those ligands directed towards the anionic surface of the glass would be expected to require more energy than charge transfer to those directed away from the glass surface due to the electrostatic repulsion between the negative charged surface and the negative charged ligands. As a consequence, adsorption removes the degeneracy of MLCT excited states. Indeed, the fittings of both temperature dependent lifetime and emission quantum yield data for $Ru(bpy)_3^{2+}$(ads) require two additional excited sates located at ΔE_1 and ΔE_2 above the ^{3}MLCT state and ^{1}MLCT state, respectively. The coincidence of the values of ΔE_1 (1168 cm^{-1}) and ΔE_2 (1120 cm^{-1}) obtained from two independent fittings may reflect the effect of the negative charged PVG surface on the splitting of the excited state. As with many mixed-ligand complexes, where distinct metal-to-ligand change transfer absorptions are present, but emission only occurs from the lowest energy ^{3}MLCT state corresponding to a specific metal-ligand pair,[49-51,145,146] there is only one emission peak is observed for $Ru(bpy)_3^{2+}$(ads) regardless of the splitting of the ^{3}MLCT state. However, a broadening of MLCT absorption band, which corresponds to the population of the spin allowed ^{1}MLCT excited state, is observed upon the adsorption (Figure 23). The band halfwidth of MLCT transition in aqueous solution is 3763 cm^{-1}, but increases to 4960 cm^{-1} upon adsorption. This 1197 cm^{-1} broadening of the MLCT absorption peak may be indicative of the loss of ligand degeneracy and corresponding splitting of the ^{1}MLCT state upon adsorption. It should also be noted that the 1197 cm^{-1} increase in the halfwidth of MLCT transition agrees with the calculated value of ΔE_2, i.e., 1117±70 cm^{-1}.

V. Excited State Dynamics of $Ru(bpy)_3^{2+}$(ads)

Based on the above analysis, the detailed excited state energy levels of

Figure 56. The excited state energy level diagram for Ru(bpy)$_3^{2+}$(ads).

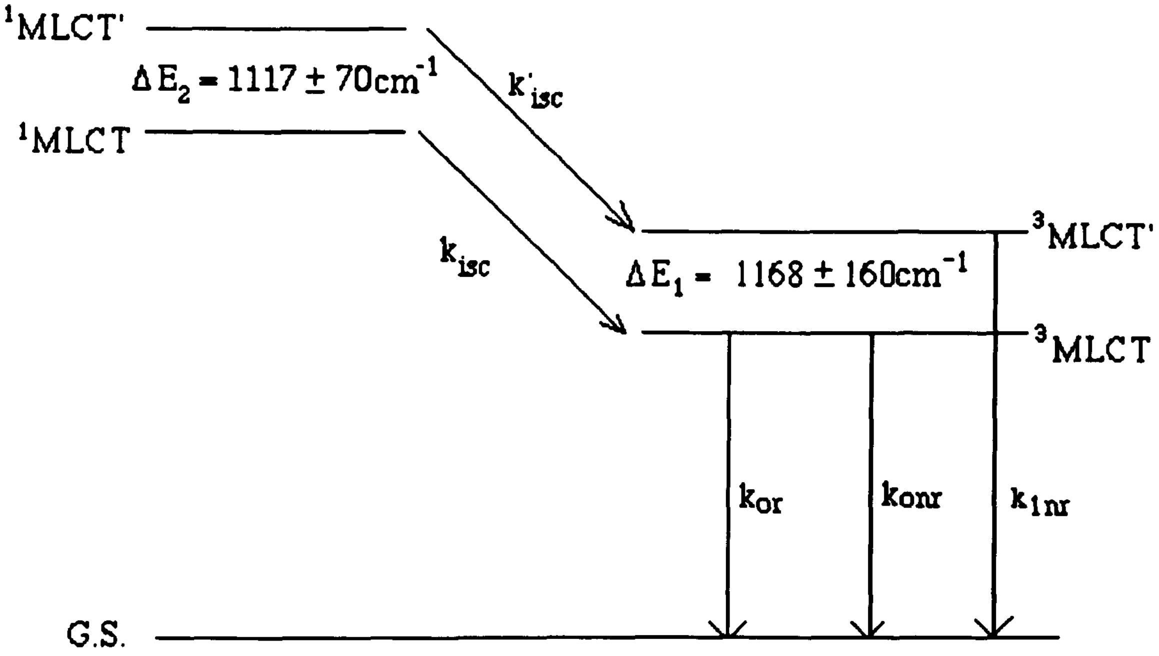

^{1}MLCT'
$\Delta E_2 = 1117 \pm 70\text{cm}^{-1}$
^{1}MLCT
k'_{isc}
k_{isc}
^{3}MLCT'
$\Delta E_1 = 1168 \pm 160\text{cm}^{-1}$
^{3}MLCT
k_{or}
k_{onr}
k_{1nr}
G.S.

$Ru(bpy)_3^{2+}$(ads) are proposed in Figure 56. To distinguish the split MLCT states, the lower energy states, which correspond to a transition to ligands directed away from the surface, are designated as the MLCT states, whereas the higher energy states, which correspond to a transition to ligands directed towards the surface, are designated as the MLCT' states. Direct absorption of 450-nm light produces the lower energy ^{1}MLCT state. At low temperatures, all molecules in ^{1}MLCT excited state intersystem cross to the corresponding triplet ^{3}MLCT excited state, which then decays to the ground state via radiative (k_{0r}), nonradiative (k_{0nr}), and/or thermal population to the high energy ^{3}MLCT' state which subsequently decays nonradiatively (k_{1nr}) to the ground state. As temperature increases, some molecules in ^{1}MLCT excited states would thermally populate the higher energy ^{1}MLCT' state. As described previously, the latter is supposed to decay to the ground state directly via a nonradiative pathway (k_{2nr}). However, according to the energy gap law,[41] that decay would be quite slow due to the large energy gap between the ^{1}MLCT' excited state and the ground state. Therefore it is reasonable to describe that nonradiative decay as the intersystem crossing process from the ^{1}MLCT' excited states to its corresponding triplet state, ^{3}MLCT' state, and the latter decays to the ground state via a rapid nonradiative pathway (k_{1nr}). To compare with the excited state dynamics of $Ru(bpy)_3^{2+}$ in aqueous solution described in the Introduction as Scheme 1, the excited state dynamics of $Ru(bpy)_3^{2+}$(ads) can be represented by the following scheme, Scheme 2,

GS ----> ^{1}MLCT

$$\begin{tikzcd} & & \mathrm{GS} + h\nu' \\ {}^{1}\mathrm{MLCT} \arrow[r] & {}^{3}\mathrm{MLCT} \arrow[ur] \arrow[dr] & \\ & & \mathrm{GS} + \mathrm{heat} \end{tikzcd}$$

$${}^{3}\mathrm{MLCT} \longrightarrow {}^{3}\mathrm{MLCT'} \longrightarrow \mathrm{GS} + \mathrm{heat}$$

$${}^{1}\mathrm{MLCT} \longrightarrow {}^{1}\mathrm{MLCT'} \longrightarrow {}^{3}\mathrm{MLCT'} \longrightarrow \mathrm{GS} + \mathrm{heat}$$

VI. Temperature Dependence of η_{isc}

In the previous discussion, the temperature dependence of the Φ_{em}/τ ratio observed for $Ru(bpy)_3^{2+}$(ads) has been attributed to the intersystem crossing yield, η_{isc}. The temperature dependence of η_{isc} is interpreted as arising from the competition of a nonradiative decay process with the intersystem crossing process ($k_{2nr}/k_{isc} = 101$) at high temperature. As discussed before, this may be a matrix effect, where adsorption creates an asymmetric environment that causes a splitting of complex's MLCT excited states. The thermal population of high energy singlet MLCT state, i.e., ^{1}MLCT' state, from the photoinduced ^{1}MLCT state leads to nonradiative decay at the expense of intersystem crossing to the emissive manifold. However, if the reduction of the molecular symmetry is the fundamental cause for the unusual excited state behavior observed in $Ru(bpy)_3^{2+}$(ads), compared with $Ru(bpy)_3^{2+}$ in aqueous solution (D_3), one would also expect to observe a similar phenomenon in Ru(II) polypyridyl compounds of lower molecular symmetry, i.e., mixed-ligand Ru(II) diimines. Indeed, in many respects the properties of $Ru(bpy)_3^{2+}$(ads) resemble those of mixed-ligand

Ru(II) diimines. For some mixed-ligand compounds, where both emission lifetime and quantum yield data are available, the ratio of Φ_{em}/τ appears to be temperature dependent. The emission lifetimes and quantum yields of $Ru(bpy)_2(diaz)^{2+}$ (diaz = 4,5-diazafluorene), for example, suggest that Φ_{em}/τ ratio approximately doubles as temperature rises from ca. 200K to 236K.[54] Schmehl and Cherry and their coworkers suggest that k_r changes with temperature, but in the absence of a spectroscopic change, the temperature dependence may reflect a change in η_{isc}. Nakamura reports that the intersystems crossing efficiency of $Ru(bpy)_2(dmby)^{2+}$ (dmby = 3,3'-dimethyl-2,2'-bipyridine) at 77K is ca. 10^2 times larger than that at 298 K.[55] In two other complexes, $Ru(bpy)_2(py)_2{}^{2+}$ and $[Ru(bpy)_2NPP]^+$ (NPP = 4-nitro-2-(2-pyridyl)phenyl), the activation barriers calculated from the emission quantum yields differ from those calculated from the lifetime data using Watts' equation[54,56]. This is also encountered in fitting $Ru(bpy)_3{}^{2+}$(ads) data using Watts' equation, and the data gathered here indicate that this difference arises from the temperature dependent Φ_{em}/τ ratio. In summary, the above data suggest that an asymmetric environment, whether it arises from different ligands, or in the case of $Ru(bpy)_3{}^{2+}$(ads), a differentiation due to adsorption, creates a situation in which the apparent intersystems crossing efficiency is temperature dependent. Clearly, the relationship between the temperature dependence of the intersystem crossing efficiency with molecular symmetry of these Ru(II) diimine compounds deserves much closer scrutiny.

VII. Comparison of k_{0r} and k_{0nr} in Both Media

As in aqueous solution, the radiative decay rate constant, k_{0r}, of $Ru(bpy)_3^{2+}$ is considered to be temperature independent.[8] The assumption appears to be quite reasonable since, by its very nature, the spontaneous emission of a photon from a higher energy excited state would be expected to be temperature independent.[42] Furthermore, spectroscopic data in both media (Figure 24) confirm that the intrinsic spectroscopic parameters (equations 37 and 38) which govern k_r are temperature independent. From both temperature dependent lifetime and quantum yield data fittings, values of k_{0r} are found to be $0.70 \pm 0.1 \times 10^5$ sec^{-1} in aqueous solution,[8] and $1.1 \pm 0.1 \times 10^5$ sec^{-1} on PVG. The similarity of the spectra of $Ru(bpy)_3^{2+}$ in two media (Figure 22) indicates that the value of k_{0r} for $Ru(bpy)_3^{2+}$(ads) would be close to that in aqueous solution. Yet, some difference is predictable because k_r is also dependent on the medium, specifically, the refractive index of the medium. Bowen and Woke[42] have derived the following expression for k_r

$$k_r = 2900\, n^2 \nu_0^2 \int \varepsilon \, d\nu \qquad [43]$$

where ν_0 and ε are spectroscopic parameters, i.e., the absorption band maximum in wavenumbers and the molar extinction coefficient, respectively. n is the refractive index of the medium. Considering the difference of the refractive index between H_2O and PVG glass, which is 1.31 in the former and 1.51 in the latter, the radiative decay rate constant k_r for $Ru(bpy)_3^{2+}$(ads) calculated from that in aqueous solution would be $0.93 \pm 0.13 \times 10^5$ sec^{-1}.

However, the total decay rate constant, or average decay rate constant from three emissive states, k_0, of $Ru(bpy)_3^{2+}$(ads), which is $3.3\pm0.5x10^5$ s^{-1}, is smaller than that in aqueous solution, where the value is $1.29\pm0.1x10^6$ s^{-1}. However, the value is similar to that found in a cellulose acetate matrix, $2.2\pm0.1x10^5$ s^{-1} (Table 10). The difference can be attributed to the rate of nonradiative decay, k_{0nr}, which is greatly reduced in rigid medium ($k_0 = k_{0r} + k_{0nr}$). The calculated value of k_{0nr} for $Ru(bpy)_3^{2+}$(ads) is $2.2\pm0.5x10^5$ s^{-1}, while that in aqueous solution is $1.2\pm0.1 \times 10^6$ s^{-1}. It is found that the rate of nonradiative decay depends strongly on the viscosity of the solvent.[41-44] For example, the rate of the nonradiative decay process is enhanced in passing from a rigid to a fluid matrix.[44] The lack of collision with solvent molecules and curtailed molecular vibrations in a rigid medium reduce the decay of excited states via nonradiative pathways relative to that in fluid solution.

VIII. The Effect of NH_3 on Disproportionation of $Ru(bpy)_3^{2+}$(ads)

Previous experiments in this laboratory have shown that a 457.9-nm photolysis of $Ru(bpy)_3^{2+}$(ads) leads to disproportionation[124]

$$2Ru(bpy)_3^{2+}(ads) \text{ ---> } Ru(bpy)_2(bpy)^{+}(ads) + Ru(bpy)_3^{3+}(ads) \qquad [43]$$

Emission polarization measurements indicate that the reaction occurs between a fixed array of immobilized adsorbates and flash photolysis data confirm the presence of a photodetached electron.[124] The quantum yield of disproportionation exhibits a parabolic dependence of the moles of $Ru(bpy)_3^{2+}$ adsorbed which suggests that disproportionation depends on the mean separation between the redox partners.[124] The maximum yield occurs at a loading of ca. $2x10^{-6}$ mole of $Ru(bpy)_3^{2+}$/g PVG, and declines to zero at both higher and lower loadings.[124] The maximum quantum efficiency occurs at a loading that corresponds to a mean separation of 50 Å between the $Ru(bpy)_3^{2+}$ ions.[124] These data led to the postulation of a surface conduction model where biphotonic excitation of $Ru(bpy)_3^{2+}$ leads to ionization

$$Ru(bpy)_3^{2+}(ads) + 2\,h\nu \dashrightarrow Ru(bpy)_3^{3+}(ads) + e^- \qquad [44]$$

and the photodetached electron migrates on the glass surface. Electron transfer occurs when the redox partners are within the electron migration distance, 50±10 Å,[129,130] and the products are stable when the mean separation between the immobilized products exceeds that necessary for the thermal back reaction, 13 Å.[124]

To account for the delay in $[Ru(bpy)_2(bpy^-)]^+(ads)$ appearance and the observation of the photodetached electrons on the glass, it is assumed that a significant number of photodetached electrons reside on the PVG surface for a finite period of time.[124] This is thought to occur by means of the population of intermediate surface acceptor sites, S,

$$e^- + S \dashrightarrow S^- \qquad [45]$$

These surface acceptor sites are thought to be shallow energy wells from which the photodetached electrons can be thermally activated but, nevertheless, present an energy barrier that prevents immediate recombination.[124] The temperature dependence of quantum yield measurements indicates that the activation energy of electron transfer on the glass surface is ≤ 6.87±0.11 kcal/mol, which is taken as the average depth of these surface acceptor sites.[126] However, the identity of these surface acceptor sites has not been established, and experiments were undertaken to explore one possibility; B_2O_3 Lewis acid sites.

Porous Vycor glass is a borosilicate glass. On cooling of the melt, the boron oxide phase separates from the silicon oxide phase. The cooled glass is then acid leached to remove the boron oxide phase to obtain the porous glass used in these experiments. However, some boron in the from of B_2O_3 Lewis acid sites remains in the glass. Although XPS analysis of the glasses used in these experiments indicate that the amount of B present in the first 50 Å of these PVG samples is 2.6±0.1%,[143] the majority is on the surfaces of the pore structure where electron transfer occurs.[123] Consequently, one possibility is that these electron deficient B_2O_3 Lewis acid sites act as potential surface acceptor sites, which accept electron density and then release it upon thermal excitation.

Cant and Little have shown that exposing PVG to NH_3 results in NH_3 physisorbing onto the glass by hydrogen bonding to the SiOH group, and chemisorbing onto the B_2O_3 sites.[117] The latter occurs by a chemical reaction in which NH_3 reacts with the B_2O_3 to form a H_3N-B_2O_3 donor-acceptor complex.[117] As a result, the chemisorbed NH_3 is more strongly held on the glass, and the two forms can be distinguished by their desorption temperatures. Disorption of the physisorbed NH_3 requires temperatures of ≤ 50 °C whereas desorption of chemisorbed NH_3 requires temperatures of ≥ 200 °C.[117] Consequently, adsorption of NH_3 followed by desorption of the physisorbed NH_3 offers a means of specifically tying up the Lewis acids sites, and, by so doing, reducing or eliminating their Lewis acid, electron acceptor properties.

FTIR spectra (Figures 35-40) recorded as functions of time, for unimpregnated and $Ru(bpy)_3^{2+}$ impregnated PVG samples exposed to NH_3 and then evacuated at room temperature, showed that a 30 minute exposure to 760 torr of NH_3 followed by ≥ 4 hours of evacuation at room temperature removes all the gas phase NH_3 and the physisorbed NH_3, but not the chemisorbed NH_3. This established the experimental conditions under which the effect of binding NH_3 to the surface B_2O_3 sites on the disproportionation of $Ru(bpy)_3^{2+}$(ads) could be examined.

A 457.9-nm photolysis of $Ru(bpy)_3^{2+}$(ads) in vacuo results in a decline in absorbance at 452nm and corresponding increases in 350 and 510 nm (Figure 41). The latter is indicative of $[Ru(bpy)_2(bpy^-)]^+$(ads), and stoichiometric measurements indicate that for one mole of $[Ru(bpy)_2(bpy^-)]^+$ formed, 2.1±0.6 moles of $Ru(bpy)_3^{2+}$(ads) are reacted. Equivalent results occur when $Ru(bpy)_3^{2+}$(ads) is photolyzed in the presence of chemisorbed NH_3. UV-visible spectra recorded before and after photolysis (Figure 42) exhibit a decline in absorbance at 450-nm with a concurrent increase at 510-nm. Calculation of the reaction stoichiometry from these absorbance changes using the corresponding molar extinction coefficients yields that for every one mole of $[Ru(bpy)_2(bpy^-)]^+$ formed, 2.1±0.6 moles of $Ru(bpy)_3^{2+}$(ads) are reacted.This is consistent with the result for NH_3-untreated samples, and indicates an equivalent photochemistry both in the presence and absence of NH_3.

The quantum yield of disproportionation of $Ru(bpy)_3^{2+}$(ads) in the presence of chemisorbed NH_3 is also dependent on initial loading, and exhibits a similar parabolic dependence on the moles of $Ru(bpy)_3^{2+}$(ads) (Figure 47). For NH_3 treated samples, the maximum yield occurs at ca.1.8×10^{-6} moles of $Ru(bpy)_3^{2+}$/g of PVG (Figure 47), which corresponds to a mean separation between the adsorbates of 57 Å. For NH_3 untreated samples, the maximum yield occurs at ca. 2.1×10^{-6} moles of $Ru(bpy)_3^{2+}$/g of PVG (Figure 46), which corresponds to a mean separation of 49 Å. Both are within electron migration distance on surface, 50 ±10 Å.[129,130]

However, EPR (Figures 43 and 44) and UV-visible (Figures 41 and 42) spectra recorded as a function of photolysis time indicate that the rate of disproportionation is much faster for NH_3 treated samples than for untreated samples. Figures 45 shows that the initial rate of formation of $[Ru(bpy)_2(bpy^-)]^+$ at 510-nm for an NH_3 treated sample is about three times faster than that for an untreated sample, in spite of the fact that both samples have the same initial loadings. As a result, the quantum yields calculated from the initial rate are also 2-3 times larger than those obtained in untreated samples (Figure 48). These results are not surprising considering the electron deficient character of these surface Lewis acid, B_2O_3 sites. They are thought to be the shallow energy well to trap the photodetached electrons and prevent them from immediate combination with another $Ru(bpy)_3^{2+}$(ads). The activation energy of electron migration on the surface is found to be $\leq$ 6.87±0.11 kcal/mol.[126] Eliminating or reducing the energy barrier by reacting surface B_2O_3 sites with NH_3 seems to lead photodetached electrons to migrate longer on surface (57 Å, compared with 49 Å for unexposed samples). As a consequence, the probability of reducing another $Ru(bpy)_3^{2+}$(ads) is larger, and the rate of disproportionation increases. However, it is believed that the population of the surface acceptor sites is essential for the electron transfer reaction on the glass surface,[124] and the data gathered in these experiments indicate that B_2O_3 sites actually hinder electron migration on surface. From this point of view, it seems that B_2O_3 sites are not involved in the electron migration process.

REFERENCES

1. Gafney, H.D.; Adamson, A.W. *J. Am. Chem. Soc.* **1972,** 94, 8238.

2. Sutin, N.; Creutz, C. *Advaan. Chem. Ser.* **1978,** 168, 1.

3. Kalyanasundaram, K. *Coor. Chem. Rev.* **1982,** 46, 159.

4. Juris, A.; Balzani, V.; Barigelletti, F.; Campagna, S.; Belser, P.; Von Zelewsky, A. *Coor. Chem. Rev.* **1988,** 84, 85.

5. Barigelletti, F.; De Cola, F.; Juris, A. *Gazzetta Chimica Italiana*, **1990,** 120, 545.

6. Harrigan. R. W.; Hager, G. D.; Crosby, G. A. *Chem. Phys. Lett.* **1973,** 21, 487.

7. Hager, G.D.; Crosby, G. A. *J. Am. Chem. Soc.* **1975,** 97, 7031.

8. Van Houten, J.; Watts, R. J. *J. Am. Chem. Soc.* **1976,** 98, 4853.

9. Balzani, V.; Bolletta, F.; Gandolfi, M.T.; Maestri, M. *Top. Curr. Chem.* **1978,** 75, 1.

10. Marcus, R. A.; Sutin. N. *Biochem. Biophys. Acta.* **1985,** 811, 265.

11. Kavarnos, G. J.; Turro, N. J. *Chem. Rev.* **1986,** 86, 401.

12. *New J. Chem.*, **1987**, 11.

13. Norris, J.R. Jr.; Meisel, D. Eds., *"Photochemical Energy Conversion"* Elsevier: New York, **1989**.

14. Incavo, J. A.; Dutta, P. K. *J. Phys. Chem.* **1990,** 94, 3075.

15. Kuykendall, V.G.; Thomas, J. K. *J. Phys. Chem.* **1990,** 94, 4224.

16. Friedman, A. E.; Chambron, J.; Sauvage, J.; Turro, N. J.; Barton, J.K. *J. Am. Chem. Soc.* **1990,** 112, 4960.

17. Turro, N. J.; Barton, J. K.; Tomalia, D. A. *Acc. Chem. Res.*, **1991,** 24, 332.

18. Heinlein, A. *Pure. Appl. Chem.* **1984,** 56, 1212.

19. Kalyanasundaram, K.; Gratzel, M. *Photochem. Photobiol.* **1984,** 40, 807.

20. Creutz, C.; Sutin, N. *Proc. Natl. Acad. Sci. USA,* **1975,** 72, 2858.

21. Porter, G. *Proc. R. Soc. London Ser.* **(A1978),** 362, 281.

22. Kirch, M.; Lehn, J-M.; Sauvage, J. P. *Helv. Chim. Acta.* **1979,** 62, 1345.

23. Brown, G. M.; Gray, H. B.; Brunschwig, B. S.; Creutz, C.; Sutin, N. *J. Am. Chem. Soc.* **1979,** 101, 1298; **1981,** 103, 2141.

24. Maveric, A. W.; Gray, H. B. *Pure. Appl. Chem.* **1980,** 52, 2339.

25. Connolly, J. Ed., *"Photochemical Conversion and Storage of Solar Energy"*, Academic Press: New York, **1981.**

26. Gratzel, M. *"Energy Resources Through Photochemical Catalysis"*, Academic Press: New York, **1983.**

27. Sutin, N. *J. Photochem.* **1979,** 10, 19.

28. Demas, J. N.; Crosby, G. A. *J. Am. Chem. Soc.* **1971,** 93, 2841.

29. Harrigan, R. W.; Crosby, G. A. *J. Chem. Phys.* **1973,** 50, 3468.

30. Hipps, K. W. *Inorg. Chem.* **1980,** 19, 1390.

31. Motten, A. G.; Dearmond, M. K.; Hauck, K.W. *Chem. Phys. Lett.* **1981,** 79, 541.

32. Sutin, N. *J. Am. Chem. Soc.* **1980,** 102, 1309.

33. Dallinger, R. F.; Woodruff, W. H. *J. Am. Chem. Soc.* **1979,** 101, 4391.

34. Bradley, P. G.; Kress, N.; Hornberger, B. A.; Dallinger, R. F.; Woodruff, W. H. *J. Am. Chem. Soc.* **1981,** 103, 7441.

35. Feruson, J.; Krausz, E. R.; Maeder, M. *J. Phys. Chem.* **1985,** 89, 1852.

36. Kitamura, N.; Kim, H-B.; Kawanishi, Y.; Obata, R.; Tazuke, S. *J. Phys. Chem.* **1986,** 90, 1488.

37. Ferguson, J.; Krausz, E. *Chem. Phys. Letts.* **1986**, 127, 551.

38. Ferguson, J.; Krausz, E. *J. Phys. Chem.* **1987**, 91, 3161.

39. Yersin, H.; Gallhuber, E. *J. Am. Chem. Soc.* **1984**, 106, 6582.

40. Krauze, E. *Chem. Phys. Lett.* **1985**, 116, 501.

41. Kober, E. M.; Caspar, J. V.; Lumpkin, R. S.; Meyer, T. J. *J. Phys. Chem.* **1986**, 90, 3722.

42. Parker, C. A. *"Photoluminescence of Solution"*, Elsevier Publishing Company: Amsterdam-London-New York, **1968**.

43. Barigelletti, F.; Juris, A.; Balzani, V.; Belser, P.; Von Zelewsky, A. *J. Phys. Chem.* **1987**, 91, 1095.

44. Caspar, J. V.; Meyer, T. J. *J. Am. Chem. Soc.* **1983**, 105, 5583.

45. Allsopp, S. R.; Cox, A.; Kemp, T. J.; Reed, W. J. *J. Chem. Soc., Faraday Trans. 1*, **1978**, 74, 1275.

46. Lumpkin, R. S.; Kober, E. M.; Worl, L. A.; Murtaza, Z.; Meyer, T. J. *J. Phys. Chem.* **1990**, 94, 239.

47. Meyer, T. J. *Pure. Appl. Chem.* **1986**, 50, 1293.

48. Sullivan, B. P.; Allen, G. H.; Meyer, T. J. *J. Chem. Soc., Chem. Commun.*, **1981**, 793.

49. Juris, A.; Barigelletti, F.; Balzani, V.; Belser, P.; Von Zelewsky, A. *Inorg. Chem.* **1985**, 24, 202.

50. Barigelletti, F.; Juris, A.; Balzani, V.; Belser, P.; Von Zelewsky, A. *Inorg. Chem.* **1983**, 22, 3335.

51. Barigelletti, F.; Belser, P.; Von Zelewsky, A.; Juris, A.; Balzani, V.; *J. Phys. Chem.* **1985**, 89, 3680.

52. Figgis, B. N. *"Introduction to Ligand Fields"*, Interscience: New York, **1966**.

53. Demas, J. N.; Taylor, D. G. *Inorg. Chem.* **1979**, 18, 3177.

54. Wacholtz, W. M.; Auerbach, R. A.; Schmehl, R.H.; Ollino, M.; Cherry, W. R. *Inorg. Chem.* **1985**, 24, 1758.

55. Nakamura, K. *Bull. Chem. Soc. Jpn.* **1982**, 55, 2697.

56. Reveco, P.; Schmehl, R. M.; Cherry, W. R.; Fronczek, F. R.; Selbin, J. *Inorg. Chem.* **1985**, 24, 4078.

57. Bock, C. R.; Meyer, T. J. *J. Am. Chem. Soc.* **1974**, 96, 7410.

58. Bock, C. R.; Meyer, T. J.; Whitten, D. G. *J. Am. Chem. Soc.* **1975**, 97, 2909.

59. Sutin, N. *J. Photochem.* **1979**, 10, 19.

60. Brunschwig, B.S.; Sutin, N. *Chem.Phys. Lett.* **1981**, 77, 63.

61. Natarajan, P.; Endicott, J. F. *J. Phys. Chem.* **1973**, 77, 1823.

62. Demas, J. N.; Adamson, A. W. *J. Am. Chem. Soc.* **1973**, 95, 6864.

63. Juris, A.; Gandolfi, M. T.; Manfrin, M. F.; Balzani, V. *J. Am. Chem. Soc.* **1976**, 98, 1047.

64. Yong, R. C.; Keen, F. R.; Meyer, T. J. *J. Am. Chem. Soc.* **1977**, 99, 2468.

65. Hazelton, M. A.; Lin, C. T.; Schwartz, H.; Sutin, N. *J. Am. Chem. Soc.* **1978**, 100, 2382.

66. Brunschwig, B. S.; Sutin, N. *Chem. Phys. Lett.* **1981**, 77, 63.

67. Boletta, F.; Maestri, M.; Moggi, L.; Balzani, V. *J. Chem. Soc. Chem. Commun.*. **1975**, 901.

68. Mandel, K.; Hoffman, M.Z. *J. Phys. Chem.* **1984**, 88, 5632.

69. Ebbesen, T. W.; Ohgushi, M. *Photochem. Photobiol.* **1983**, 38, 251.

70.Prasad, D. R.; Mandel, K.; Hoffman, M.Z. *Coor. Chem. Rev.* **1985**, 64, 175.

71. Jones, G.; Malba, V. *J. Org. Chem.* **1985**, 50, 5776.

72. Harriman, A.; West, M. A., Eds. " *Photogeneration of Hydrogen*" Academic Press: New York, **1982**.

73. Chan, S. F.; Chou, M.; Matsubara, T.; Sutin, N. *J. Am. Chem. Soc.* **1981**, 103, 369.

74. Xu, J.; Porter, G. B. *Can. J. Chem.* **1982**, 60, 2856.

75. Gafney, H. D. *Coor. Chem. Rev.* **1990**, 104, 113.

76. Somorjai, G. A. " *Chemistry in Two Dimensions: Surfaces*" Cornell University Press, Ithaca, New York, **1981**.

77. Fendler, J. *J. Phys. Chem.* **1985**, 89, 2730.

78.Gerischer, H. *Pure. Appl. Chem.* **1980**, 52, 2649.

79. Gratzel, M. *Acc.Chem. Res.* **1981**, 14, 376.

80. Calvin, M. *Photochem. Photobiol.* **1983**, 37, 349.

81. Whitten, D. G.; Russell, J. C.; Schmel, R. H. *Tetrahedron.* **1982**, 38, 2455.

82. Kitamura, N.; Tazuke, S. *Pure. Appl. Chem.* **1984**, 56, 1269.

83. Qnayle, W. H.; Lunsford, J. K. *Inorg. Chem.* **1981**, 20, 97.

84. Infelta, P. P.; Gratzel, M.; Thomas, J. K. *J. Phys. Chem.* **1974**, 78, 1906.

85. Infelta, P. P.; Gratzel, M.; Thomas, J. K. *J. Am. Chem. Soc.* **1980**, 108, 1479.

86. Ford, W. E.; Otvos, J. W.; Calvin, M. *Nature (London)* **1978**, 274, 507.

87. Gershfelt, N.L. *Annu. Rev. Phys. Chem.* **1976**, 27, 346.

88. Wheeler, J.; Thomas, J.K. *J. Phys. Chem.* **1982**, 86, 4540.

89. Baxendale, J. H.; Rodgers, M. A. *Chem. Phys. Lett.* **1980**, 72, 424.

90. Furlong, D. N. *Aust. J. Chem.* **1982**, 35, 911.

91. Kurimura, Y.; Katzumata, K. *Bull. Chem. Soc.Jpn.* **1982**, 55, 2560.

92. Abdo, S.; Canesson, P.; Cruz, M.; Fripiat, J.J.; Van Damme, H. *J. Phys. Chem.* **1981**, 85, 797.

93. Milosavijevic, B. H.; Thomas, J. K. *J. Phys. Chem.* **1983**, 87, 616.

94. Milosavijevic, B. H.; Thomas, J. K. *J. Chem. Soc. Faraday Trans. 1.* **1985**, 81, 735.

95. Szentirmay, M. N.; Prieto, N. E.; Martin, C. R. *J. Phys. Chem.* **1985**, 89, 3017.

96. Furlong, N.D.; Tricot, Y. M.; Swift, J. D.; Sasse, W. *Aust. J. Chem.* **1984**, 37, 703.

97. Tunneli, M.S.; Fendler, J.H. *J. Am. Chem. Soc.* **1981**,103, 2507.

98. Willner, I.; Otors, J.W.; Calvin, M. *J. Am. Chem. Soc.* **1981**, 103, 3203.

99. Ege, D.; Ghosh, P. K.; White, J. R.; Eqney, J. F.; Bard, A. J. *J. Am. Chem. Soc.* **1985**, 107, 5644.

100. De Laguardia, R. A.; Thomas, J. K. *J. Phys. Chem.* **1983**, 87, 990; 3550.

101. Albery, W. J.; Barlett, P.N.; Wilde, C. P.; Darwent, J. R. *J. Am. Chem. Soc.* **1985**, 107, 1854.

102. Habti, A.; Keravis, D.; Levitz, P.; Van Damme, H. *J. Chem. Soc. Faraday Trans. 2* **1984**, 80, 67.

103. Thomas, J. K. *Chem. Rev.* **1980**, 80, 283; *J. Phys. Chem.* **1987**, 91, 267.

104. Krueger, J. S.; Mayer, J. E.; Mallouk, T. E. *J. Am. Chem. Soc.* **1988**, 110, 8232.

105. Li, Z.; Lai, C.; Mallouk, T.E. *Inorg. Chem.* **1989**, 28, 178.

106. Vlachopoulos, N.; Liska, P.; Augustynski, J.; Gratzel, M. *J. Am. Chem. Soc.* **1988**, 110, 1216.

107. Lehn, J.M.; Sauvage, J.P.; Ziessel, R. *Nouv. J. Chim.* **1980**, 4, 623.

108. Clark, W. D.; Sutin, N. *J. Am. Chem. Soc.* **1977**, 99, 4676.

109. Novak, A. J. *Appl. Phys. Lett.* **1977**, 30, 567.

110. Shi, W. Ph. D. Thesis, City Univ. of New York, **1986**.

111. Chandrasekaran, K.; Thomas, J. K. *J. Chem. Soc. Faraday Trans. 1* **1984**, 80, 1163.

112. Spitler, M.T.; Calvin, M. *J. Chem. Phys.* **1977**, 66, 4294.

113. Duoghong, D.; Borgarello, E.; Gratzel, M. *J. Am. Chem. Soc.* **1981**, 103, 4685.

114. Hannay, N. B. *"Solid State Chemistry"* Prentice-Hall, Englewood Cliffs, New Jersy, **1967**.

115. Mendoza, E. A. Ph. D. Thesis, City Univ. of New York, **1992**.

116. Snyder, L. R.; Ward, J. W. *J. Phys. Chem.* **1966**, 70, 3941.

117. Cant, N. W.; Little, L. H. *Can. J. Chem.* **1964**, 42, 802; **1965**, 43, 1252.

118. Darsillo, M. S.; Paquette, M. S.; Gafney, H. D. *J. Am. Chem. Soc.* **1987**, 109, 3275.

119. Basu, A.; Perettie, D. J.; Clark, J. B.; Gafney, H. D. *J. Phys. Chem.* **1983**, 87, 4532.

120. Goonatilakie, H. W.; Ph. D. Thesis, City Univ. of New York, 1986.

121. Iler, R. K. *"The Chemistry of Silica"*, Wiley-Interscience, New York, **1979**.

122. Sidorov, A. N. *Opt. Spektrosk.* (Akad. Nauk SSSR, Otd. Fiz.-Mat. Nauk), **1960**, 8, 424 (English translation).

123. Hair, M. L.; Chapman, I. D. *J. Am. Cera. Soc.* **1966**, 49, 651.

124. (a) Kennelly, T., Ph. D. Thesis, City Univ. of New York, 1980; (b) Kennelly, T.; Gafney, H.D.; Braun, M. *J. Am. Chem. Soc.* **1985**, 107, 4431.

125. (a) Wolfgang, S., Ph. D. Thesis, City Univ. of New York, 1983; (b)

Wolfgang, S.; Gafney, H.D. *J. Phys. Chem.* **1983**, 87, 5393.

126. Fan, J; Shi, W.; Tysoe, S.; Strekas, T.C.; Gafney, H. D. *J. Phys. Chem.* **1989**, 93, 373.

127. Meisel, D.; Matheson, M. S.; Mulac, W. A.; Rabani, J. *J. Phys. Chem.* **1977**, 81, 1449.

128. Mulazzani, Q. G.; Emmi, S.; Fuochi, P. G.; Hoffman. M. Z.; Veturi, M. *J. Am. Chem. Soc.* **1978**, 100, 981.

129. Wong, P. K. *Photochem. Photobiol.* **1974**, 19, 391.

130. Wong, P.K.; Allen, A. D. *J. Phys. Chem.* **1970**, 74, 774.

131. Palmer, R. A.; Piper, T. S. *Inor. Chem.* **1966**, 5, 864.

132. Mallick, P. K.; Danzer, G. D.; Strommen, D. P.; Kincaid, J. R. *J. Phys. Chem.* **1988**, 92, 5628.

133. Poizat, O.; Sourisseau, C. *J. Phys. Chem.* **1984**, 88, 3007.

134. Konig, E.; Lindner, E. *Spectrochimica Acta.* **1972**, 28A, 1393.

135. (a) Morgan, J. *"Introduction to Geometrical and Physical Optics"*, McGraw-Hill, New York, **1953**; (b) Robertson, J. K. *"Introduction to Optics: Geometrical and Physical"*, 4th ed., Van Nostrand, New York, **1954**.

136. Calvert, J. G.; Pitts, J. N. Jr. *"Photochemistry"*, John Wiley & Sons, New York, **1966**.

137. Bryant, G. M.; Fergusson, J.E.; Powell, H.K.J. *Auat. J. Chem.*, **1971**, 24, 257.

138. Wolkow, E., Ph.D. Thesis, City Univ. of New York, **1992**.

139. Demas, J. N. *"Excited State Lifetime Measurements"*, Academic Press, New York London, **1983**.

140. Demas, J. N.; Crosby, G. A. *J. Phys. Chem.* **1971**, 75, 991.

141. Miller, J. R.; Hartman, K. W.; Abrash, S. *J. Am. Chem. Soc.* **1982**, 104, 4286.

142. Krenske, D.; Abdo, S.; Van Damme, H.; Cruz, M,; Fripiat, J. J. *J. Phys. Chem.* **1980**, 84, 2447; **1981**, 85, 797.

143. Washel, A. *Annu. Rev. Biophys. Bioeng.* **1977**, 6, 273.

144. Mendoza, E. A.; Wolkow, E.; Sunil, D.; Wong, P.; Sokolov, J.; Rafailovich, M. H.; den Boer, M.; Gafney, H. D. *Langmuir*, in press.

145. Barigelletti, F.; Juris, A.; Balzani, V.; Belser, P.; von Zelewsky, A. *J. Phys. Chem.* **1986**, 90, 5190

146. Caspar, J. V.; Meyer, T. J. *Inorg. Chem.* **1983**, 22, 2444.